SMALL SIGNAL STABILITY CONSTRAINED DISTRIBUTION SYSTEM RECONFIGURATION

Ph.D. THESIS

by

JYOTI SHUKLA

DEPARTMENT OF ELECTRICAL ENGINEERING
INDIAN INSTITUTE OF TECHNOLOGY ROORKEE
ROORKEE -247667, INDIA
APRIL, 2019

SMALL SIGNAL STABILITY CONSTRAINED DISTRIBUTION SYSTEM RECONFIGURATION

A THESIS

Submitted in partial fulfilment of the requirements for the award of the degree

of

DOCTOR OF PHILOSOPHY

in

ELECTRICAL ENGINEERING

by

JYOTI SHUKLA

DEPARTMENT OF ELECTRICAL ENGINEERING
INDIAN INSTITUTE OF TECHNOLOGY ROORKEE
ROORKEE -247667, INDIA
APRIL, 2019

INDIAN INSTITUTE OF TECHNOLOGY ROORKEE
ROORKEE

CANDIDATE'S DECLARATION

I hereby certify that the work which is being presented in this thesis entitled **"SMALL SIGNAL STABILITY CONSTRAINED DISTRIBUTION SYSTEM RECONFIGURATION"** in partial fulfilment of the requirements for the award of the Degree of Doctor of Philosophy and submitted in the Department of Electrical Engineering of the Indian Institute of Technology Roorkee, Roorkee is an authentic record of my own work carried out during the period from July, 2013 to April, 2019 under the supervision of Dr. Biswarup Das, Professor, Department of Electrical Engineering, Indian Institute of Technology Roorkee.

The matter presented in this thesis has not been submitted by me for the award of any other degree of this or any other Institution.

(JYOTI SHUKLA)

This is to certify that the above statement made by the candidate is correct to the best of my knowledge.

(Biswarup Das)
Supervisor

Dated:

The Ph. D. Viva-Voce Examination of Jyoti Shukla, Research Scholar, has been held on……..

Chairman, SRC **Signature of External Examiner**

This is to certify that the student has made all the corrections in this thesis.

Signature of Supervisor (s) **Head of the Department**
Date:

Abstract

In modern age, the demand of electricity is ever-increasing due to rapid urbanization and industrialization. To satisfy this ever increasing demand for electricity, power systems are operating close to their operational limits. This situation has led to higher system losses and poor voltage regulation. Studies indicate that approximately 1013 $\%$ of the total power generated is lost as I^2R losses at the distribution level, which in turn, causes increase in the cost of energy and poor voltage profile along the distribution feeder. Therefore, the requirement for reliable and sufficient power supply is becoming more and more intensive. In order to improve the reliability of a radial distribution system, the configuration of the network should be optimal to maximize the operational benefits. For improving the performance of the distribution system (DS), reconfiguration of DS has been studied and implemented throughout the world for more than two decades. In the face of varying loads, power loss in a distributed network will not be minimum for a fixed network configuration. In addition, due to the rapid expansion of distribution networks, the voltage stability of distribution systems has become an important issue. Hence, there is a need for reconfiguration of the network from time to time. In distribution system reconfiguration (DSR), the topology of the DS is altered by the operation of tie-line and sectionalising switches to achieve operational improvements. Further, distributed generation (DG) will play an important and crucial role in emerging DS. Increasing DG deployment in DS causes a significant impact on the power flow, voltage profile, power losses and stability. However, due to increasing deployment of DG units in a DS, the power flow pattern in a DS can change significantly, which can cause operational problem in an otherwise optimally reconfigured (without any DG) system. Therefore, it is necessary to undertake reconfiguration of a DS in the presence of DGs.

The literature published in last one decade has proposed several optimization methods in the presence of DGs for achieving new optimized system configuration. However, in the literature, only steady state behaviour of DGs are included so far. When the system configuration changes (with the DGs installed at some fixed buses), the impedance between the DGs may change which may lead a stable system into unstable mode or vice versa. Therefore, while undertaking DSR in the presence of DGs, stability aspect of DS should also be considered. DSR without stability consideration may lead to an unstable configuration of DS in the presence of renewable energy

sources (RES) based DG such as wind power and solar photovoltaics based DGs. In view of this, the first contribution of this thesis is multiobjective DSR with stability consideration in which the objectives are to reduce the system real power losses and to maximize the voltage stability with minimum number of switching number operations while simultaneously maintaining the dynamic stability of the system. Further, different operating limits of the DS have also been considered in the formulation. Initially, the main emphasis is on the small signal stability of the synchronous machine based DGs under deterministic environment of the distribution system. However, the deterministic nature of the DS may lead to inadequate configuration of DS due to varying load demands and intermittencies associated with DGs. Therefore, the formulated DSR problem has been further solved taking into account the uncertain load demands and generation from renewable energy sources. These uncertain quantities have been represented by appropriate probability density functions (PDF). Further, impact of integration of PV-DGs, small hydro power plant (SHPP) DGs and DFIGs has been considered on reconfiguration. To accurately evaluate the small signal stability of RES-DGs, detailed models of DGs (SHPP-DGs, PV-DGs and DFIGs) have been included in this formulated DSR problem. Further, the generations from SHPP-DGs, PV-DGs and DFIGs are strongly correlated to the generation from the adjacent SHPP-DGs, PV-DGs and DFIGs respectively due to similar water availability, solar irradiance and wind speed at that area. As a result, correlations among RES-DGs have been taken into account in the formulated DSR.

To investigate the change in stability with the increased penetration of the DGs, the eigen value analysis of the DS has been carried out. Further, it is a commonly recognized fact that load modeling has a major impact on the DSR. Therefore, proper and adequate load modelling is also required for DSR. In this thesis, voltage dependent loads in the form of load combinations (constant power, constant impedance and constant current loads) have been considered during DSR. Furthermore, a methodology for determining the proper switching sequence has been presented in this thesis.

In the literature, different techniques such as mathematical programming based algorithm, heuristic rule-base approach, meta heuristic approach and hybrid methods have been presented to solve the DSR problem. However, in many meta-heuristic approaches, multiobjective DSR problem is converted into single objective optimization problem by using weighting factors. The values of the weighting factors generally depend on the relative importance of the objective functions (as perceived by the system operator). Therefore, tuning of weighting factors are requried for

every network. To mitigate this problem, a large number of multiobjective evolutionary algorithms (MOEAs) have been proposed in the literature. These techniques find a set of Pareto optimal solutions. Most widely used Pareto optimal solution technique is non dominated genetic algorithm-II (NSGA-II). However, crowding distance calculation as a diversity measure in NSGA-II can be highly time-consuming for more than three objectives. To overcome these difficulties, Knee point driven point algorithm (KnEA) has been utilized for DSR. The main difference between KnEA and other multi-objective EAs (MOEAs) such as NSGA-II is that KnEA uses knee points as a secondary selection criterion additionally with the principle of non-dominated sorting to enhance the search ability of MOEAs. Knee points of non-dominated fronts in the current population are preferred for selection to maximise the hypervolume that helps in maintaining better balance between the convergence of the method and the diversity in the population. In this methodology, an adaptive strategy is utilized for identifying the knee points in the present population without prior knowledge about the number of knee points in the true pareto front to accelerate the convergence and promote diversity.

Acknowledgements

In the name of God, the infinitely Good, the All Merciful

I take this opportunity to express my sincere gratitude towards my august guide Prof. Biswaroop Das in the Department of Electrical Engineering, Indian Institute of Engineering, Roorkee for their proficient and enthusiastic guidance, academic advice moral support, continuous encouragement, priceless guidance, endless patience and immense help throughout the research work and believing in me all throughout the research work and believing in me all throughout the journey. I am fortunate to have guide with profound individualities, humanistic and warm personal approach, love and care which has given me the strength to carry out this research work. Their excellent and aesthetic oriented guidance has helped immensely in shaping up this thesis. I humbly acknowledge a lifetime gratitude to my mentor. I express my deep sense of gratitude to Dr. Vinay Pant, Electrical Engineering Department, Indian Institute of Technology, Roorkee, for providing excellent computing facility in the department for the research work. I also express my indebtedness to Dr. Vinay Pant, Chariman, Department Research Committee, Electrical Engineering Department, Dr. N. P. Padhy, of Electrical Engineering Department and Dr. Kusumdeep of Mathematics Department for being the members of my research committee and sparing their valuable time in reviewing and critically examining the whole work. I am thankful to the technical staff of Power System Simulation Lab, for their timely cooperation and needful help. My journey in Roorkee is blessed with many friends: Mr. Dratha Novalio, Mr. Akhilesh Mathur, Neha Kumari, Rinalini Lohan and Tejeswara Rao for their technical and personal support rendered throughout the completion of research work during my stay at Roorkee. I am indebted to my parents for their sincere prayers, constant encouragement and everlasting blessings. They have been the main driving force in this endeavour for which no words of thanks would be sufficient. My heartiest gratitude goes to my sister, Dr. Dipti Shukla and my brother, Dr. Gaurav Shukla, for their constant support and encouragement. I gratefully acknowledge the inspiration and unflagging support of my mother- in-law, Mrs. Nikita Sharma for their constant support, encouragement and sharing my family responsibilities during my stay at Roorkee. I am also thankful to my brother-in-law, Ankush Vashistha and sister-in-law, Shubha Sharma, for continuous motivation provided by them. Above all, I am lucky to have such a caring husband, Ankur Vashistha. I am immensely thankful to him for shouldering responsibilities,

which lets me, concentrate on my research work and for the excellent cooperation during the whole stage of my work. His loving, caring and sacrificing attitude has been the inspiring and driving force in this endeavour and hence no words of thanks are enough. I am thankful to my daughter Ira Vashistha for giving me happiness with her smiles during the last seven months of my research. I also wish to express my deep sense of gratitude to all persons who with their encouraging words, constructive criticism and suggestions have contributed directly or indirectly in a significant way towards the completion of this work. I owe deep sense of gratitude to all prevailing spirit whose divine light provided me the perseverance, guidance, inspiration, faith, strength and energy to carry on even when time was tough for me.

Jyoti Shukla

Roorkee, April 2019

Contents

List of Tables

List of Figures

List of Abbreviations

CDF Cumulative distribution function.

DFIG Doubly-Fed Induction Generator.

DG Distributed Generation.

DS Distribution System.

DSR Distribution system reconfiguration.

DSTATCOM Distribution Static Synchronous Compensator.

DW Weighted distance.

ENS Effective non-dominated ranking.

Fig. Figure.

GA Genetic Algorithm.

KnEA Knee point driven evolutionary algorithm.

kVA kilo Volt Ampere.

kW kilo Watt.

kWh kilo Watt hour.

LHS Left hand side.

MINLP Mixed Integer Non Linear Programming.

MOEAs Multiobjective evolutionary algorithms.

MPPT Maximum power point tracking.

MVA Mega Volt Ampere.

NSGA-II Non-dominated sorting genetic algorithm-II.

NSW Number of switching.

PDF Probability density function.

PEM Point estimation method.

PT Penalty term.

pu per unit.

PV Photovoltaic.

RES Renewable energy based sources.

SDSR Stochastic distribution system reconfiguration.

SG Synchronous Generator.

SHPP Small hydro power plant.

SSSA Small signal stability analysis.

VDL Voltage-dependent loads.

VSI Voltage stability index.

WPG Wind power generation.

ZIP Combination of constant-impedance (Z), constant-current (I) and constant power (P) loads.

Chapter 1

Introduction

Overview

The consumption oriented civilization, rapid urbanization and industrialization are creating ever-growing demand for electricity in the world economy. In order to meet the supply-demand gap, the power industry is oriented towards competitive business environment. To harness competitive advantage, pressure to reduce costs has increased, leading to operation of power systems close to their limits. Therefore, efforts are required to supply electricity as efficiently as possible. Distribution system reconfiguration (DSR) represents an attractive approach to improve the operating conditions of the overall system as it can be implemented at minimal cost to the utility.

DSR is a process of changing the topological structure of a system by altering the status of switches in such a way that an optimal operation of the system (in some sense) can be obtained. The DSR generally includes the following objectives:
1) Reduction of power loss,
2) Improvement in voltage security margin,
3) Enhancement of reliability,
5) Reduction of line maintenance costs,
6) Improvement in power quality,
7) Load balancing.

Further, nowdays, there is a significant increase in penetration of renewable energy sources (RES) at the distribution level. These RES based DGs have the major operational, economic and environment benefits such as
1) Reduced power losses,
2) Improved voltage profile,
3) Reduced harmful emission and greenhouse gases,
4) Reduced operational costs of some DG technologies, e.g. solar and wind,

5) Reliability and security enhancement.

Because of these advantages, more and more DGs are being integrated into the DS which in turn, affect the operation and planning of distribution networks significantly. Recognising this need, several works [1] in the literature have addressed this issue.

1.1 Literature Survey

The solution algorithms for DSR can be broadly classified in four categories: (i) mathematical programming based algorithm, (ii) heuristic approach, (iii) meta heuristic approach (iv) hybrid method and other methods.

1.1.1 Mathematical programming based algorithm

In [2], a mixed-integer two-stage robust optimization model and a master-slave algorithm are presented to solve the DSR with the aim of minimising the total active power losses under uncertain load and generation. However, this method requires significant computational time to achieve the optimal solution especially when the system size is large. In [3], mixed-integer conic programming and mixed-integer linear programming (MILP) formulations are used to obtain the optimal configured network in the presence of DGs for minimizing the system power losses. The computational efficiencies of these two algorithm are also compared. However, as outlined in this paper, both approaches require appreciable computational time (more than 25 minutes) to reach an acceptable level of optimality gap. In [4], the DSR problem in the presence of DGs is modeled as a mixed integer linear programming (MILP) problem in which all quadratic terms of objective function, expressions of injected currents and constraints are linearized to achieve the optimal or near optimal solution. However, this work has not considered the constraint on the number of switching operations. In [5], DSR is formulated as a mixed integer nonlinear programming (MINLP) problem in order to minimize system losses in the presence of DGs. One of the main challenges in DSR is binary representation of the status of the switches. Therefore, these nonlinear problems require significant computational time especially when the system size is large.

1.1.2 Heuristic method

The work presented in [6] adopted a heuristic algorithm based on sensitivity indexes to find the best structure of the network with least energy losses. The load variation is also considered in this

study through the system load curves. In [7], a knowledge-based search algorithm is presented to find the best locations of the distributed generators (DGs) for reducing power loss and improving reliability using DSR. In [8], [9], a two-stage solution approach, based on heuristics and sensitivities is adopted for real power loss minimization. Further, in [9], DSR is implemented on balanced and unbalanced distribution systems. A heuristic algorithm presented in [10] focused on minimizing the real power loss considering the demand variation through the system load curves. In [11], the distribution network is divided into groups of busses using a fast heuristic technique in order to achieve the best DSR for power loss minimization. However this work is limited to loss reduction. The real-time reconfiguration methodology based on a heuristic method is presented in [12]. The considered objective functions are: minimization of normalized expected loss of energy, expected system average interruption frequency index and expected value of energy not supplied while Analytic Hierarchy Process (AHP) method is implemented to determine the best switching sequence. Although these approaches can solve the problem with less computational burden, the results are only approximate solutions and attain local optimal points. These search techniques also do not necessarily guarantee global optimization.

1.1.3 Meta heuristic method

In [13], Harmony Search Algorithm (HSA) has been used for simultaneous network reconfiguration and DG installation. However, this work considered only power loss reduction. An efficient two-step reconfiguration for minimisation of active power loss with enhancement of loadability limit is presented in [14] by implementing an improved HSA. DSR methodology based on ant colony algorithm (ACA) is presented in [15] for power loss reduction and maximization of load balance factor among feeders in the presence of DGs. However, both objective functions are not optimized simultaneously. The methodology inspired by the immune network theory is presented in [16], [17] with the aim of minimising the cost of energy losses. Further, the work on DSR presented in [16], considered variable load demand. The genetic algorithm (GA) with special crossover and mutation operators is presented in [18] for simultaneous reconfiguration and optimal allocation of capacitor in order to reduce power loss. In [19], cuckoo search algorithm (CSA) is implemented for DSR with the aim of minimizing power loss and voltage stability deviation index. However, the number of switching (NSW) operations has not been considered in [13]- [19].

The work reported in [20], [21] considered different models of DGs and proposed the application of decimal coded quantum particle swarm optimization (DQPSO) method to find the best possible configuration for minimizing the power loss. In [22], a binary PSO based search algorithm is employed to find the optimal network configuration for reliability enhancement and the power loss minimization. An enhanced gravitational search algorithm is implemented in [23] for minimizing power loss, operational cost and energy not supplied (ENS) index during reconfiguration with DGs. In [24], fireworks algorithm is proposed to solve the reconfiguration problem alongwith DG placement problem in which the locations of DGs are determined using voltage stability index (VSI). This work is limited to power loss minimization and voltage deviation minimization. However, switching cost is not considered in this work. In [25], a meta-heuristic Artificial Immune System (AIS) is implemented for DSR with the aim of minimising the power loss considering uncertainties in the power generation of wind based distributed generation (DG). A new modified HSA for reconfiguring the system with DGs to minimise the cost of generated electric energy, real power loss, energy not supplied and average interruption frequency index is presented in [26] under a stochastic framework. The methodology of DSR presented in [27] focused on minimizing various objectives such as real power loss, voltage deviation of the buses, total cost of power and emission produced by the grid and DGs (Fuel cells) using the methodology based on teacher learning algorithm (TLA). The work on DSR reported in [28] made use of modified Bee Algorithm for reducing total active power losses, System Average Interruption Frequency Index (SAIFI) and cost of produced power considering the variability in active and reactive loads and DG power generation. In [29], a Modified Firefly Algorithm (MFA) is implemented for DSR with the aim of minimising the total active power losses, the total emission produced and the total cost related to the grid and DGs. However, the NSW operations have not been considered in [25]- [29] and the 2m point estimation method (PEM) has been utilized to model the uncertainty in [25]- [29]. In [30], the risk-based reconfiguration is presented for minimizing the cost of power loss and switching cost in presence of reward/penalty scheme with the consideration of load and generation uncertainty. These uncertainties are modelled as scenarios with different probabilities. In [31], scenario based stochastic multiobjective framework is presented for DSR to minimize total power losses, voltage deviation and total cost with the consideration of uncertainties related to DGs and load demand. In this work, adaptive modified particle swarm optimisation (AMPSO) is implemented

deterministically for each of the scenarios. The work on DSR reported in [32] is aimed at reducing the seasonal energy losses and switching operation costs considering the variability in active and reactive loads and DG output power. An adaptive PSO with fuzzy set theory for reconfiguring the system with DGs (wind power generation (WPG) and fuel cells) to minimise the cost of generated electric energy, real power loss, bus voltage deviation and emission produced is discussed in [33]. In this paper, 2m+1 PEM is utilized to consider the uncertainties in the power demand and the output of wind power generator (WPG). In [34], an approach based on strength pareto evolutionary algorithm 2 (SPEA2) is applied considering temporal loads and outputs of renewable DGs to achieve minimization of real power loss and annual operation costs (installation, maintenance, and active power loss costs).

1.1.4 Hybrid method and other methods

The ACA with fuzzy sets is presented in [35] for simultaneous reconfiguration and optimal allocation of distribution static compensator (DSTATCOM) and DG in order to improve load balancing among feeders, bus voltage profile and also to reduce power loss. In [36], a novel approach based on energy efficiency performance indices is presented to achieve an energy efficient configuration in the presence of DGs. In this study, various load combinations are used to examine the impact of load behaviour on reconfiguration. In [37], a hybrid fuzzy-bee algorithm approach along with the improved analytical (IA) method is presented for simultaneous network reconfiguration and DG allocation. However, in this work also, the constraint on number of switching operations has not been considered. In [38], a Self adaptive modified TLA with fuzzy set theory is presented for DSR to minimise the cost of generated electric energy, real power loss, bus voltage deviation and emission produced by substation. A method based on heuristic rules and fuzzy multi-objective approach is presented in [39], [40]. On the other hand, the algorithm adopted in [41] is based on the fuzzy multiobjective approach and the maxmin principle. The objective function considered in [39]- [41] are to balance load among the feeders and to minimize the real power loss, node voltage deviation and branch current constraint violation. Further, in [40], different types of loads are considered during reconfiguration. A decentralized multi agent system is presented in [42] to solve the reconfiguration and service restoration problem for minimizing congestion in the lines and power losses. In [43], an efficient topology processor is presented for handling the switching operations with the

help of the network topology-related attributes which represent the physical nature of the DS components. In [44], a modified Honey Bee Mating Optimization (MHBMO) algorithm with fuzzy clustering technique is presented with the consideration of the renewable energy based sources (RESs). An algorithm based on Hybrid Big Bang-Big Crunch (HBB-BC) with fuzzy set theory is presented in [45]. The objective functions considered in [44], [45] are minimization of power loss, total cost, emissions, and the maximization of the voltage stability index (VSI). In [46], an artificial neural network (ANN)-based reconfiguration method is presented for loss minimization. The developed ANN model is based on the multilayer perceptron network and the training of the ANN is carried out by the back propagation algorithm to determine the optimum switching status for loss minimization. A two-stage solution methodology based on branch exchange operations for loss reduction is presented in [47]. An exhaustive search based method [48] is presented to solve DSR considering voltage dependence of loads. However, this technique is not applicable for large-sized DS.

In spite of several positive benefits, the incorporation of renewable energy sources based DGs (RES-DGs) have negative impact on the systems. Integration of RES-DGs may adversely affect the system stability due to the high level of intermittency and unpredictability associated with them. Due to increasing deployment of distributed generation (DG) units in a DS, it is necessary to investigate stability issues of distribution system. Several studies have been carried out to analyze the impact of penetration level of DG on the stability behavior of the power system. The impact of DGs on dynamic behaviour of the power system and active damping enhancement is discussed in [49]. Probabilistic small-signal stability of the power system with the grid connected wind turbine generation is carried out in [50] using analytical approach. In [51], the impact of synchronous machine based and DFIG based DGs on the small signal stability of distribution system is discussed. In [52], [53] the impact of the stochastic PV generation on the dynamic stability of grid-connected PV systems is investigated by using a probabilistic small-signal analysis approach. Further, the impact of system parameters i.e. control gains and line impedance on the stochastic stability of the system is also analyzed in [52]. A mathematical model of grid connected photovoltaic (PV)-diesel engine (DE) system feeding dynamic loads is developed to analyze the stability with the increased penetration of the PV power in [54]. In [55], a power system stability analysis method considering Wiener noise (concerning the changes brought by wind power fluctuation and

wind speed uncertainty) is presented. In this work, a stochastic stability degree index is defined to quantify the effect of stochastic parameters on system stability. An analytical method based on multi-point linearization technique is presented in [56] considering the stochastic fluctuations of multiple grid-connected wind farms to assess the voltage stability and small-signal stability of an AC/DC power system. In [57], probabilistic small signal stability assessment is carried out to investigate the impact of the WPG uncertainty and it is shown that the system stability significantly deteriorates with high level of wind penetration. The dynamic behavior of PV-DG and the whole distribution system with PV integration is modeled and investigated in [58]. Based on the small-signal model of the power system, this work has examined the impact of the PV generation on the damping performance of local-mode oscillations. Further, the intermittent generation from PV-DGs also alters the network flows significantly [58]- [59], thereby again affecting the system stability. In [60], the effect of high penetration of PV-DGs is investigated on the small signal stability of a power system. The system inertia reduces with the integration of PV-DGs, which, in turn, will have detrimental impact on system stability.

Hence, in the literature, small signal stability of distribution system is considered as an important probabilistic stability index for maintaining system security

1.2 Contribution of the author

As discussed, in all the literature related to distribution system reconfiguration in the presence of DGs, only steady state behaviour of DGs has been considered in reconfiguration problem. Similarly, configuration of system is assumed to be fixed during the stability analysis [49]- [60]. However, as the topology of the network changes (having the DGs installed at some fixed buses) during DSR, the stability of DS may change (as compared to the stability of the system in the original configuration). The impedance between DGs has significant effect on small signal stability of DS. The reconfiguration in DS may alter the impedance between the DGs which may lead an unstable system into stable mode or vice versa. Therefore, in this thesis, while undertaking DSR in the presence of DGs, stability aspect of DS has been considered.

In this thesis, DSR is formulated as a multi-objective and multi-constrained optimisation problem. Following objective functions and constraints have been considered in this thesis.

Objective functions

1. Minimization of power loss.
2. Maximization of voltage stability margin.
3. Minimization of number of switching operations.
4. Maximization of the system stability.

Constraints

1. Line current carrying limits.
2. Bus voltage constraints.
3. Preservation of radial configuration of the system.
4. No interruption of loads.

For another formulation the fourth objective has been considered as a constraint to ensure stability. To solve this constrained multi-objective optimization problem, knee point driven evolutionary algorithm (KnEA), is applied. In contrast to the non-dominated sorting genetic algorithm-II (NSGA-II) based approach, preference is given to the knee points among non dominated solutions in selection and tournament mating. Therefore it maintains better balance between the convergence of the method and the diversity in the population. The performance of KnEA has been validated on three different distribution systems. Further, to include the uncertainty of load and generation, a two-stage KnEA-PE approach, consisting of a knee point driven method and 3-point estimation method, has been utilized to solve this small signal stability constrained distribution system reconfiguration problem. Moreover, the uncertain parameters have been assumed to have a considerable level of correlation to each other, in addition to their uncertainties. The proposed KnEA-PE approach has been modified to handle correlation among uncertain variables. In DSR scheme, renewable energy sources such as SHPP, DFIG, and PV-DGs have been taken into account and their detailed models have been included for small signal stability analysis. Moreover, uncertainties of renewable generation affect the DSR strategy and therefore, the effect of variation of solar power and wind power penetration on stability constrained DSR is also investigated.

Traditionally, in most of the reported reconfiguration work, mainly constant power or constant impedance loads have been considered [4]- [61], [12]- [33]. However, practically, distribution system loads comprise of different types of loads, such as residential, commercial, and industrial. For these kind of loads, the active and reactive powers consumed by any load are generally dependent

on the voltage across it. To account for these voltage-dependent loads (VDLs), several works have considered VDLs during the DSR [36], [48] and [62]. In [36], [48] and [62], reconfiguration process has been carried out assuming fixed values of the input quantities (output power of DGs, active and reactive power loads). In reality, however, all these quantities may contain uncertainties due to intermittencies associated with the power output of the DGs and inaccuracies in the forecasted nominal values of the real and reactive power loads in the system. DSR problem has been formulated and solved with voltage dependent loads (combination of constant power, constant current and constant impedance) considering load and generation uncertainties.

In the DSR problem, the concern is not only to find a new network configuration that optimize the system performance but also to find an optimal switching sequence to achieve this optimal configuration. There have been few studies focusing on determination of switching sequence [12], [63] but these studies have not taken into account the above mentioned objectives and constraints. Hence, a methodology for determining proper switching sequence is also described taking into account the uncertainties of correlated loads and DGs.

To summarize, the major contributions of this thesis are as follows:

- The small signal stability aspect of a DS in the presence of DGs has been considered during DSR.

- For considering the uncertainty of load and generation, a two-stage KnEA-PE approach, consisting of a knee point driven method and 3-point estimation method, has been utilized to solve this small signal stability constrained DSR problem. Moreover, the uncertain parameters may have a considerable level of correlation with each other, in addition to their uncertainties. The developed method is also capable of handling the correlated variables.

- Further, the uncertainty and correlation between the system input variables such as the load and generation from SHPP, wind, and solar power plants have been taken into account in DSR scheme. Detailed DG modeling (appropriate mathematical models) of different types (solar cell, wind turbines, and small hydro plant) have been included in the stability constrained DSR scheme. Effect of varying level of power generation from RES-DGs on DSR has been investigated.

- The formulated DSR problem has been solved with voltage dependent loads (combination of constant power, constant current, and constant impedance loads) considering load and generation uncertainties.

- A methodology for determining the proper switching sequence is developed to achieve optimal configuration from the original configuration.

1.2.1 Organisation of the thesis

The aim of this thesis is to develop an optimum DSR methodology while ensuring the stability and other operational constraints of the DS. The organisation of this thesis is as follows:

- The present chapter introduces the DSR, presents a brief state of art review and author's contribution in this thesis.

- In Chapter 2, multi-objective DSR problem with small signal stability consideration, has been formulated. To solve this DSR problem efficiently, a knee point driven evolutionary algorithm (KnEA) has been implemented. Three test distribution systems i.e. IEEE 33-bus, 69-bus and 119-bus radial distribution systems have been considered to demonstrate the feasibility and effectiveness of the KnEA algorithm, However, the formulated optimization problem in this chapter assumes that both load and generation conditions are accurately known. The obtained results have also been compared with those obtained by the multi-objective NSGA-II based method.

- In Chapter 3, the uncertainties in both load and generation conditions have been considered in the DSR problem. Besides the uncertainties, the effect of correlations between loads and between power outputs of DGs has been considered in stability constrained DSR of DS. A two-stage KnEA-PE method has been utilized to solve this DSR problem. Again, the effectiveness of the presented methodology has been investigated on IEEE 33-bus, 69-bus and 119-bus radial distribution systems with SHPP type of DGs.

- In Chapter 4, the small-signal stability constrained DSR with probabilistic uncertainties in correlated photovoltaic, SHPP type of DGs and loads has been presented. The solution of the formulated problem ensures that the obtained configuration always remains dynamically stable along with other operational constraints (voltage and current constraints) with increased

penetration of photovoltaic generation. As in the previous chapter, the two-stage KnEA-PE method has been implemented on the three test systems to validate its effectiveness.

- In Chapter 5, integration of DFIG has been considered along with SHPP-DGs and PV-DGs in DSR. Probabilistic DSR with stability consideration has been carried out with different penetration level of wind power generation.

- In Chapter 6, voltage dependent loads have been considered (in all the previous chapters, constant power loads have been used). To represent the voltage dependent loads, polynomial model of the load has been used. Simulation studies have been carried out on all the three systems to investigate the comparative performances. Appropriate switching sequence has been determined (for optimal reconfiguration obtained with voltage dependent loads). Detailed studies have been carried out on all the three systems to compare the obtained results with those obtained with constant power load corresponding to uncertain load and power generation from DGs.

- In Chapter 7, major conclusions of this work are given and a few suggestions for future work in this field of study are also provided.

Chapter 2

Consideration of small signal stability in DSR in the presence of distributed generation

This chapter presents a methodology for distribution system reconfiguration (DSR) in the presence of DGs with objectives of minimizing real power loss, switching operations as well as maximizing the voltage stability margin while maintaining the constraints of bus voltage, branch current carrying capacity and radiality of distribution system. Further, the small signal stability of the distribution system in the presence of DGs has also been considered in this formulation. To obtain the pareto-optimal solutions of this constrained multi-objective optimization problem, knee point driven evolutionary algorithm (KnEA), is applied. The method has been tested on IEEE 33-bus, 69-bus and 119-bus radial distribution systems to demonstrate its feasibility and effectiveness. The obtained results have also been compared with those obtained by the multi-objective NSGA-II based method.

2.1 Introduction

For improving the performance of the distribution system (DS), feeder reconfiguration of DS in the presence of DGs has been studied and implemented throughout the world for more than two decades as reported in the previous chapter. Due to increasing deployment of DG units in a DS, the power flow pattern in a DS changes significantly, which can cause operational problem in an otherwise "optimally reconfigured (without any DG)" system. Further, the stability of the DS is also affected with the incorporation of DGs in the DS. Therefore, it is necessary to undertake feeder reconfiguration studies of a DS in the presence of DGs. In this chapter, objective functions, constraints for DSR and small signal stability model of synchronous based DGs and the whole distribution system with DG integration are presented. Further, it is also assumed that the DGs installed in the DS are not equipped with power system stabilizers (PSS) and therefore, the stability of the system is entirely dependent on the system operating condition (topology and loading condi-

tion) and there is no scope for improving the system stability by utilising any auxiliary controller. The basic goal of this work is to devise an optimum DSR methodology while ensuring the small signal stability of the DS.

2.2 Problem Formulation

In this work, the DSR problem is formulated as a multi objective optimization problem (MOOP) subject to various network operational constraints. The objective functions considered in this work are described in detail below.

2.2.1 Objective Functions

Minimization of system real power loss

Let B_L denote the set of branches that contains all closed switches in a distribution system. Further, let $(k, k+1) \in B_L$ denote a distribution feeder connecting two buses, k and $k+1$, as shown in Fig. 2.1. The resistance and reactance of this feeder are denoted by R_k and X_k respectively. The first objective is minimization of the total real power loss in the system as given by,

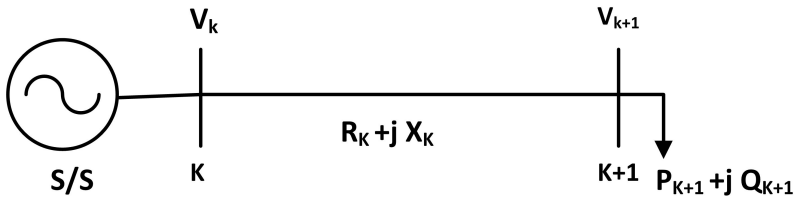

Figure 2.1: Single line diagram of distribution feeder

$$\min f_1(\boldsymbol{X}) = \min \sum_{(k,k+1)\in B_L} \frac{R_k.(P_k^2 + Q_k^2)}{|V_k|^2} \tag{2.1}$$

In eqn. (2.1), P_k and Q_k are the real and reactive power flowing out of bus k respectively and V_k is the complex voltage at bus k as shown in Fig. 2.1. Further, $\boldsymbol{X}$ denotes the vector of decision variables. The details of this vector $\boldsymbol{X}$ is given in Section 2.2.4.

Maximization of voltage stability margin

The second objective is maximization of the steady-state voltage stability margin. In the literature, various voltage stability indices have been proposed for assessing the voltage stability of a radial

distribution system. Among these indices, a fast indicator namely, L-index [19], has been used in this work. The L-index of $(k+1)^{th}$ bus (denoted as L_{k+1}) and the voltage stability index ΔL_{k+1} can be expressed as follows [19]:

$$L_{k+1} = |V_k|^4 - 4(P_{k+1}X_k - Q_{k+1}R_k)^2 - 4(P_{k+1}R_k + Q_{k+1}X_k)|V_k|^2 \tag{2.2}$$

$$\Delta L_{k+1} = (1 - L_{k+1}) \tag{2.3}$$

where P_{k+1} and Q_{k+1} are the total real and reactive power load fed from the $(k+1)^{th}$ bus respectively. The bus that has minimum L-index value is the most critical bus and may cause voltage instability of the entire system. The maximum of all ΔL-indices (corresponding to all buses in the system), given in equation (2.3), indicates the proximity of the system to voltage collapse.

$$\Delta L = \max(\Delta L_2, \Delta L_3, \Delta L_4, ...\Delta L_N) \tag{2.4}$$

In equation (2.4), N denotes the total number of buses in the system, with bus 1 being the substation bus. Therefore, to maximize the voltage stability margin, the corresponding function is

$$\min f_2(\boldsymbol{X}) = \min(\Delta L) \tag{2.5}$$

A smaller value of ΔL (voltage stability index) indicates an improved voltage stability margin.

Minimization of number of switching operation

The third objective is minimization of the number of switching operations due to operational costs and network management considerations. For this purpose, Manhattan distance [64] is used to calculate the number of switching operations (NSW) as given below:

$$NSW = \sum_{k=1}^{N_s} |s_k^c - s_k^o| \tag{2.6}$$

where N_s is the total number of switches, s_k^c and s_k^o denotes the status of k^{th} switch in the current and initial configuration respectively. It is to be noted that $s_k^p = 0(1)$ denotes the open (closed) switch status respectively, where $p = c, o$. Thus, this objective is implemented as

$$\min f_3(\boldsymbol{X}) = \min(NSW) \tag{2.7}$$

Maximization of the system stability

The distribution system should remain dynamically stable (i.e. in the sense of small signal stability). To analyse the stability of the system, the differential and algebraic equations (DAE) of the distribution system are linearized around the current operating point to obtain the system state ma-

trix and subsequently the eigenvalues of the system state matrix are calculated. If all eigenvalues have negative real part, then the system is considered to be dynamically stable. Further, the damping ratios of the eigenvalues indicate how fast the oscillations will decay after any disturbance. If the damping ratios are large and positive, then oscillations will decay faster. On the other hand, if the damping ratios are small, then oscillations will decay slowly. Therefore, to improve the dynamic stability of the network, the damping ratio of eigenvalues should be maximised. To ensure this, the chosen objective in this work is maximization of the least damping ratio of the network. The details of the small signal stability analysis of the distribution system in the presence of DGs are given below.

Let there be 'm_g' synchronous machine based DGs in the system. Also, let E be the set of DG buses, which is given by $\mathbf{E} = \{e(1), e(2)...e(i)...e(m_g)\}$, with $e(i)$ denoting the bus number at which i^{th} DG is connected . Further, $2 \leq e(i) \leq N$, and $e(i) \neq s$, for $i = 1, 2...m_g$, where s denotes the substation bus. The i^{th} DG is assumed to be equipped with a fast exciter, and can be modeled by the following set of nonlinear differential equations [65]:

$$\dot{\delta}_i = \omega_i - \omega_s \tag{2.8}$$

$$\dot{\omega}_i = \frac{T_{Mi}}{M_i} - \frac{E'_{qi} I_{qi}}{M_i} - \frac{(X_{qi} - X'_{di})}{M_i} I_{di} I_{qi} - \frac{D_i(\omega_i - \omega_s)}{M_i} \tag{2.9}$$

$$\dot{E'_{qi}} = -\frac{E'_{qi}}{T'_{doi}} - \frac{(X_{di} - X'_{di})}{T'_{doi}} I_{di} - \frac{E'_{fdi}}{T'_{doi}} \tag{2.10}$$

$$\dot{E_{fdi}} = -\frac{E'_{fdi}}{T'_{Ai}} - \frac{(X_{di} - X'_{di})}{T_{Ai}} I_{di} - \frac{K_{Ai}}{T_{Ai}} (V_{ref,i} - V_{e(i)}) \tag{2.11}$$

where $M_i = 2 * H_i$, H_i is inertia constant, ω_i is angular frequency, ω_s is synchronous speed of rotor, δ_i represents generator torque angle, T_{Mi} is mechanical torque, T'_{doi} is d-axis open-circuit time constant, E'_{fdi} is field voltage, T_{Ai} is amplifier time constant, K_{Ai} is amplifier gain, D_i is damping ratio, I_{di} and I_{qi} are the d and q-axis currents respectively, X_{di} and X_{qi} are the d and q-axis synchronous reactances respectively, X'_{di} is d-axis transient reactance, $V_{ref,i}$ is reference voltage and E'_{qi} is equivalent internal q-axis voltage of i^{th} DG and $V_{e(i)}$ is the voltage magnitude of the bus $e(i)$ corresponding to i^{th} DG. Stator algebraic equations corresponding to i^{th} DG ($1 \leq i \leq m_g$) can be written as [65]

$$V_{e(i)} \sin(\delta_i - \theta_{e(i)}) + R_{si} I_{di} - X_{qi} I_{qi} = 0 \tag{2.12}$$

$$E'_{qi} - V_{e(i)}\cos(\delta_i - \theta_{e(i)}) - R_{si}I_{qi} - X'_{di}I_{di} = 0 \tag{2.13}$$

where R_{si} is stator resistance of i^{th} DG and $\theta_{e(i)}$ is angle of the voltage of bus $e(i)$. The power balance equations at the substation bus are given as

$$\sum_{k=1}^{N} V_s V_k Y_{sk}\cos(\theta_s - \theta_k - \alpha_{sk}) = P_s \tag{2.14}$$

$$\sum_{k=1}^{N} V_s V_k Y_{sk}\sin(\theta_s - \theta_k - \alpha_{sk}) = Q_s \tag{2.15}$$

where P_s and Q_s are substation real and reactive powers respectively, Y_{sk} and α_{sk} is magnitude and angle of the $(s,k)^{th}$ element of the bus admittance matrix respectively. It is to be noted that in this work, bus 1 has been taken as the substation bus (i.e. s=1). Further, V_k and θ_k denote the voltage magnitude and angle of the k^{th} bus respectively. The algebraic power flow equations at bus $e(i)$ corresponding to i^{th} DG can be written as [65]

$$\begin{aligned}\sum_{k=1}^{N} V_{e(i)}V_k Y_{e(i)k}\cos(\theta_{e(i)} - \theta_k - \alpha_{e(i)k}) - PL_{e(i)} + I_{di}V_{e(i)}\sin(\delta_i - \theta_{e(i)}) \\ +I_{qi}V_{e(i)}\cos(\delta_i - \theta_{e(i)}) = 0\end{aligned} \tag{2.16}$$

$$\begin{aligned}\sum_{k=1}^{N} V_{e(i)}V_k Y_{e(i)k}\sin(\theta_{e(i)} - \theta_k - \alpha_{e(i)k}) - QL_{e(i)} + I_{di}V_{e(i)}\cos(\delta_i - \theta_{e(i)}) \\ -I_{qi}V_{e(i)}\sin(\delta_i - \theta_{e(i)}) = 0\end{aligned} \tag{2.17}$$

where $PL_{e(i)}$ and $QL_{e(i)}$ are real and reactive load at bus $e(i)$ respectively. The real and reactive power balance equations at all the buses other than the DG buses can be written as [65]

$$\sum_{k=1}^{N} V_l V_k Y_{lk}\cos(\theta_l - \theta_k - \alpha_{lk}) - P_{Ll} = 0 \tag{2.18}$$

$$\sum_{k=1}^{N} V_l V_k Y_{lk}\sin(\theta_l - \theta_k - \alpha_{lk}) - Q_{Ll} = 0 \tag{2.19}$$

$$l = 2, 3.....N, \quad l \notin E$$

By linearizing the differential equations (2.8)-(2.19), following expressions are obtained:

$$\frac{d\Delta\delta_i}{dt} = \Delta\omega_i \tag{2.20}$$

$$\frac{d\Delta\omega_i}{dt} = \frac{\Delta T_{Mi}}{M_i} - \frac{\Delta E'_{qi} I_{qi}}{M_i} - \frac{E'_{qi}\Delta I_{qi}}{M_i} - \frac{(X_{qi} - X'_{di})}{M_i} I_{di}\Delta I_{qi} - \frac{(X_{qi} - X'_{di})}{M_i} I_{qi}\Delta I_{di} - \frac{D_i(\Delta\omega_i)}{M_i} - \frac{(\omega_i - \omega_s)\Delta D_i}{M_i} \tag{2.21}$$

$$\frac{d\Delta E'_{qi}}{dt} = -\frac{\Delta E'_{qi}}{T'_{doi}} - \frac{(X_{di} - X'_{di})}{T'_{doi}}\Delta I_{di} - \frac{\Delta E'_{fdi}}{T'_{doi}} \tag{2.22}$$

$$\frac{d\Delta E_{fdi}}{dt} = -\frac{\Delta E'_{fdi}}{T'_{Ai}} - \frac{(X_{di} - X'_{di})}{M_i}\Delta I_{di} - \frac{K_{Ai}}{T_{Ai}}(\Delta V_{ref,i}) + \frac{K_{Ai}}{T_{Ai}}(\Delta V_{e(i)}) \tag{2.23}$$

Collecting equations (2.20) - (2.23) for all DGs together and writing them in matrix form, we get,

$$\mathbf{\Delta\dot{x}} = \mathbf{A}\Delta\mathbf{x} + \mathbf{B}_1\Delta\mathbf{I}_g + \mathbf{B}_2\Delta\mathbf{Z}_G + \mathbf{E}\Delta\mathbf{u} \tag{2.24}$$

where

$\mathbf{x} = [\mathbf{x}_1^T \quad \mathbf{x}_2^T \ldots \mathbf{x}_i^T \ldots \mathbf{x}_{m_g}^T]^T, \qquad \mathbf{x}_i = [\delta_i \quad \omega_i \quad E'_{qi} \quad E_{fdi}]^T$

$\mathbf{I}_g = [\mathbf{I}_{g1}^T \quad \mathbf{I}_{g2}^T \ldots \mathbf{I}_{gi}^T \ldots \mathbf{I}_{gm_g}^T]^T, \qquad \mathbf{I}_{gi} = [I_{di} \quad I_{qi}]^T$

$\mathbf{u} = [\mathbf{u}_1^T \quad \mathbf{u}_2^T \ldots \mathbf{u}_i^T \ldots \mathbf{u}_{m_g}^T]^T, \qquad \mathbf{u_i} = [T_{Mi} \quad V_{ref_i}]^T$

$\mathbf{Z}_G = [V_{e(1)} \quad V_{e(2)} \ldots V_{e(m_g)} \quad \theta_{e(1)} \quad \theta_{e(2)} \ldots \theta_{e(m_g)}]^T$

where $\mathbf{x_i}$ is the vector of state variables and $\mathbf{u_i}$ is the vector of input variables of i^{th} DG. The linearization of stator algebraic equations yields,

$$\Delta V_{e(i)}\sin(\delta_i - \theta_{e(i)}) + V_{e(i)}\cos(\delta_i - \theta_{e(i)})\Delta\delta_i - V_{e(i)}\cos(\delta_i - \theta_{e(i)})\Delta\theta_{e(i)} + R_{si}\Delta I_{di} - X_{qi}\Delta I_{qi} = 0 \tag{2.25}$$

$$\Delta E'_{qi} - \cos(\delta_i - \theta_{e(i)})\Delta V_{e(i)} + V_{e(i)}\sin(\delta_i - \theta_{e(i)})\Delta\delta_i - V_{e(i)}\sin(\delta_i - \theta_{e(i)})\Delta\theta_{e(i)} - R_{si}\Delta I_{qi} - X'_{di}\Delta I_{di} = 0 \tag{2.26}$$

Collecting equations (2.25)-(2.26), for all DGs together and writing them in matrix form,

$$\mathbf{0} = \mathbf{A}_1\Delta\mathbf{x} + \mathbf{B}_2\Delta\mathbf{I}_g + \mathbf{B}_3\Delta\mathbf{Z}_G \tag{2.27}$$

The linearized power balance equations at the substation bus are given as

$$\Delta P_s = \sum_{k=1}^{N} V_s Y_{sk}\cos(\theta_s - \theta_k - \alpha_{sk})\Delta V_k + \sum_{k=1}^{N} V_s V_k Y_{sk}\sin(\theta_s - \theta_k - \alpha_{sk})\Delta\theta_k + \Delta V_{e(i)} \sum_{\substack{k=1 \\ k\neq e(i)}}^{N} V_k Y_{se(i)}\cos(\theta_s - \theta_e(i) - \alpha_{sk}) + \sum_{\substack{k=1 \\ k\neq e(i)}}^{N} V_{e(i)} V_k Y_{se(i)}\sin(\theta_s - \theta_e(i) - \alpha_{sk})\Delta\theta_{e(i)} \tag{2.28}$$

$$\Delta Q_s = \sum_{k=1}^{N} V_s Y_{sk} \sin(\theta_s - \theta_k - \alpha_{sk})\Delta V_k - \sum_{k=1}^{N} V_s V_k Y_{sk} \cos(\theta_s - \theta_k - \alpha_{sk})\Delta\theta_k + \Delta V_{e(i)}$$
$$\sum_{\substack{k=1 \\ k\neq e(i)}}^{N} V_k Y_{se(i)} \sin(\theta_s - \theta_e(i) - \alpha_{sk}) - \sum_{\substack{k=1 \\ k\neq e(i)}}^{N} V_{e(i)} V_k Y_{se(i)} \sin(\theta_s - \theta_e(i) - \alpha_{sk})\Delta\theta_{e(i)} \quad (2.29)$$

Rewriting equations (2.28) and (2.29), in matrix form, we obtain,

$$\mathbf{0} = \mathbf{D}_3\Delta\mathbf{Z}_G + \mathbf{D}_4\Delta\mathbf{Z}_l + \mathbf{D}_5\Delta\mathbf{S} \quad (2.30)$$

$\mathbf{Z}_l = [V_2 \quad V_3 \ldots V_e \ldots V_N \quad \theta_2 \quad \theta_3 \ldots \theta_e \ldots \theta_N]^T \qquad 2 \leq e \leq N; e \notin E$

$\mathbf{S} = [P_s \quad Q_s]^T = [P_1 \quad Q_1]^T$

The linearized algebraic power flow equations at bus $e(i)$ corresponding to i^{th} DG can be written as,

$$\sum_{\substack{k=1 \\ k\neq e(i)}}^{N} V_k Y_{e(i)k} \cos(\theta_{e(i)} - \theta_k - \alpha_{e(i)k})\Delta V_{e(i)} + I_{qi} \cos(\delta_i - \theta_{e(i)})\Delta V_{e(i)} + I_{di} \sin(\delta_i - \theta_{e(i)})\Delta V_{e(i)} +$$
$$\sum_{k=1}^{N} V_{e(i)} Y_{e(i)k} \cos(\theta_{e(i)} - \theta_k - \alpha_{e(i)k})\Delta V_k + \sum_{k=1}^{N} V_{e(i)} V_k Y_{e(i)k} \sin(\theta_{e(i)} - \theta_k - \alpha_{e(i)k})\Delta\theta_k -$$
$$\sum_{\substack{k=1 \\ k\neq e(i)}}^{N} V_{e(i)} V_k Y_{e(i)k} \sin(\theta_{e(i)} - \theta_k - \alpha_{e(i)k})\Delta\theta_{e(i)} - I_{di} V_{e(i)} \cos(\delta_i - \theta_{e(i)})\Delta\theta_{e(i)} + I_{qi} V_{e(i)} \sin(\delta_i - \theta_{e(i)})\Delta\theta_{e(i)}$$
$$- \Delta PL_{e(i)} - \Delta I_{di} V_{e(i)} \sin(\delta_i - \theta_{e(i)}) + I_{di} V_{e(i)} \cos(\delta_i - \theta_{e(i)})\Delta\delta_i + \Delta I_{qi} V_{e(i)} \cos(\delta_i - \theta_{e(i)}) +$$
$$I_{qi} V_{e(i)} \sin(\delta_i - \theta_{e(i)})\Delta\delta_i = 0 \quad (2.31)$$

$$\sum_{\substack{k=1 \\ k\neq e(i)}}^{N} V_k Y_{e(i)k} \sin(\theta_{e(i)} - \theta_k - \alpha_{e(i)k})\Delta V_{e(i)} - I_{qi} \sin(\delta_i - \theta_{e(i)})\Delta V_{e(i)} + I_{di} \cos(\delta_i - \theta_{e(i)})\Delta V_{e(i)} +$$
$$\sum_{k=1}^{N} V_{e(i)} V_k Y_{e(i)k} \sin(\theta_{e(i)} - \theta_k - \alpha_{e(i)k})\Delta V_k - \sum_{k=1}^{N} V_{e(i)} V_k Y_{e(i)k} \cos(\theta_{e(i)} - \theta_k - \alpha_{e(i)k})\Delta\theta_k -$$
$$\sum_{\substack{k=1 \\ k\neq e(i)}}^{N} V_{e(i)} V_k Y_{e(i)k} \cos(\theta_{e(i)} - \theta_k - \alpha_{e(i)k})\Delta\theta_{e(i)} + I_{di} V_{e(i)} \sin(\delta_i - \theta_{e(i)})\Delta\theta_{g(i)} + I_{qi} V_{e(i)} \cos(\delta_i - \theta_{e(i)})\Delta\theta_{e(i)}$$
$$- \Delta QL_{e(i)} + \Delta I_{di} V_{e(i)} \cos(\delta_i - \theta_{e(i)}) - I_{di} V_{e(i)} \sin(\delta_i - \theta_{e(i)})\Delta\delta_i - V_{g(i)} \sin(\delta_i - \theta_{e(i)})\Delta I_{qi} +$$
$$I_{qi} V_{e(i)} \cos(\delta_i - \theta_{e(i)})\Delta\delta_i = 0 \quad (2.32)$$

Collecting equations (2.31)- (2.32) for all DGs together and writing them in matrix form, one obtains,

$$\mathbf{0} = \mathbf{C}_1\Delta\mathbf{x} + \mathbf{C}_2\Delta\mathbf{I}_g + \mathbf{C}_3\Delta\mathbf{Z}_G + \mathbf{C}_4\Delta\mathbf{Z}_l \tag{2.33}$$

The lineraized real and reactive power balance equations at all the buses other than the DG buses can be written as

$$\sum_{k=1}^{N} V_l Y_{lk}\cos(\theta_l - \theta_k - \alpha_{lk})\Delta V_k + \sum_{\substack{k=1\\k\neq l}}^{N} V_l Y_{lk}\cos(\theta_l - \theta_k - \alpha_{lk})\Delta V_l +$$
$$\sum_{k=1}^{N} V_l V_k Y_{lk}\sin(\theta_l - \theta_k - \alpha_{lk})\Delta\theta_k - \sum_{\substack{k=1\\k\neq j}}^{N} V_l V_k Y_{jk}\sin(\theta_l - \theta_k - \alpha_{lk})\Delta\theta_l = \Delta P_{Ll} \tag{2.34}$$

$$\sum_{k=1}^{N} V_l V_k Y_{lk}\sin(\theta_l - \theta_k - \alpha_{lk})\Delta V_k + \sum_{\substack{k=1\\k\neq j}}^{N} V_l V_k Y_{lk}\sin(\theta_l - \theta_k - \alpha_{lk})\Delta V_l +$$
$$\sum_{k=1}^{N} V_l V_k Y_{lk}\cos(\theta_l - \theta_k - \alpha_{lk})\Delta\theta_k + \sum_{\substack{k=1\\k\neq l}}^{N} V_l V_k Y_{lk}\cos(\theta_l - \theta_k - \alpha_{lk})\Delta\theta_l = \Delta Q_{Ll} \tag{2.35}$$

Collecting equations (2.34)- (2.35) for all buses together and writing them in matrix form, one gets,

$$\mathbf{0} = \mathbf{D}_1\Delta\mathbf{Z}_G + \mathbf{D}_2\Delta\mathbf{Z}_l \tag{2.36}$$

Equations (2.27), (2.30), (2.33) and (2.36) can be written in the following form:

$$\begin{bmatrix} \boldsymbol{\Delta}\mathbf{I}_g \\ \boldsymbol{\Delta}\mathbf{Z}_G \\ \boldsymbol{\Delta}\mathbf{Z}_l \\ \boldsymbol{\Delta}\mathbf{S} \end{bmatrix} = \begin{bmatrix} \mathbf{B_2} & \mathbf{B_3} & \mathbf{0} & \mathbf{0} \\ \mathbf{C_2} & \mathbf{C_3} & \mathbf{C_4} & \mathbf{0} \\ \mathbf{0} & \mathbf{D_1} & \mathbf{D_2} & \mathbf{0} \\ \mathbf{0} & \mathbf{D_3} & \mathbf{D_4} & \mathbf{D_5} \end{bmatrix}^{-1} \begin{bmatrix} -\mathbf{A_1} \\ -\mathbf{C_1} \\ \mathbf{0} \\ \mathbf{0} \end{bmatrix} \Big[\boldsymbol{\Delta}\mathbf{x}\Big] \tag{2.37}$$

By extracting rows corresponding to $\boldsymbol{\Delta}\mathbf{I}_g$ and $\boldsymbol{\Delta}\mathbf{Z}_G$ from equation (2.37) in term of $\boldsymbol{\Delta}\mathbf{x}$ and substituting it into equation (2.24), we get,

$$\boldsymbol{\Delta}\dot{\mathbf{x}} = \mathbf{A}_{sys}\Delta\mathbf{x} + \mathbf{E}\Delta\mathbf{u} \tag{2.38}$$

where $\mathbf{A}_{sys}$ represents the system state matrix. The eigenvalues of $\mathbf{A}_{sys}$ provide the information

regarding small signal stability of the system. The damping ratio of i^{th} eigenvalue is given by,

$$D_i = -\frac{\alpha_i}{\sqrt{(\alpha_i)^2 + (\beta_i)^2}} \tag{2.39}$$

where α_i and β_i are the real and imaginary part of i^{th} eigenvalue respectively, $i = 1, 2, ...od$, od being the order of the square A_{sys} matrix. As discussed earlier, the objective in this work is to maximize the least damping ratio of the system. Mathematically, this can be represented as,

$$\max f_4(\boldsymbol{X}) = \max(D) = \min(-D) \tag{2.40}$$

$$\text{where, } D = \min(D_1, D_2, ...D_{od})$$

The above multi-objective optimization problem is solved subjected to various operational constraints as discussed below.

2.2.2 Limits and Constraints

The reconfiguration problem is subjected to the following constraints:

Distribution line current carrying limits

The current in each branch should not violate the maximum current carrying capacity of that branch.

$$|I_{k,k+1}| \leq |I^{max}_{k,k+1}| \quad k \in B_L \tag{2.41}$$

where $|I_{k,k+1}|$ denotes the per unit magnitude of complex current flowing in the branch $(k, k+1)$ and $|I^{max}_{k,k+1}|$ is the maximum permissible per unit magnitude of current flowing in that line.

Bus voltage constraints

Bus voltages of the system should not violate the permissible operational limits.

$$V_k^{min} \leq V_k \leq V_k^{max} \tag{2.42}$$

Where V_k^{max} and V_k^{min} are maximum and minimum permissible per unit voltage magnitude of k^{th} bus, respectively.

To accommodate the current and voltage constraint violations, a penalty term (PT) is added to all the objective functions. The penalty term is given by,

$$PT = \lambda_1[\textstyle\sum_{k \in C_{VL}}(V_k - V_k^{min})^2 + \sum_{k \in C_{VU}}(V_k - V_k^{max})^2] + \lambda_2[\sum_{k \in C_{IU}}(I_{k,k+1} - I^{max}_{k,k+1})^2]$$

where λ_1 and λ_2 are the penalty factors, C_{VL} is the set of all buses with minimum voltage limit

violation, C_{VU} is the set of all buses with maximum voltage limit violation and C_{IU} is the set of all lines with maximum current limit violation. It is to be noted that $C_{VL} \cap C_{VU} = \emptyset$, where $\emptyset$ is the null set. Appropriate values of λ_1 and λ_2 are selected so that inferior solutions are eliminated at an early stage.

Preservation of radial configuration of the network

At the time of reconfiguration, the radiality of the network should be maintained. During reconfiguration all loops are identified in the system and one switch should be opened from each loop to preserve the radiality of the system.

No interruption of load points

All load points have to be energized after reconfiguration.

Therefore in a nutshell, the multi-objective constrained optimization problem is described by the objective functions given in equations (2.1), (2.5), (2.7), (2.40) and the constraints given in Section 2.2.2.

2.2.3 Alternative form of DSR problem

Now, it is to be noted that, the objective function f_4 maximizes the damping ratio, but it does not ensure the dynamic stability of the reconfigured system. To ensure the stability, the objective function f_4 should be replaced with the constraint that the real parts of all the eigenvalues should be negative. Mathematically, this can be described as in equation (2.43) below.

$$Re(\lambda_i) < 0 \tag{2.43}$$

Therefore, in this case, the multi-objective constrained DSR problem is described by the objective functions in equations. (2.1), (2.5), (2.7) and the constraints given in Subsection 2.2.2 and in equation (2.43). It is to be noted that in this case also, the violations of voltage and current constraints are taken into account following the procedure described in Subsection 2.2.2.

2.2.4 Decision variables

In a radial distribution system, closing a tie switch will form a loop. Each loop has several branches. In order to maintain the radial topology of the network, a sectionalizing switch must be opened in a loop. For representing the optimal network topology, only the positions of the open switches are required to be known. If the number of tie switches is T_s, then the dimension of the solution vector

is equal to T_s. Therefore, in this method, the decision variables are coded using integer numbers as:

$$\boldsymbol{X} = [B_1, B_2, ...B_{T_s}] \tag{2.44}$$

where B_i is the serial number of the switch (either tie or sectionalizing) which should be opened in the i^{th} loop obtained after closing the tie switch in the loop. As an illustration, consider the 33-bus distribution system shown in Fig. 2.2.

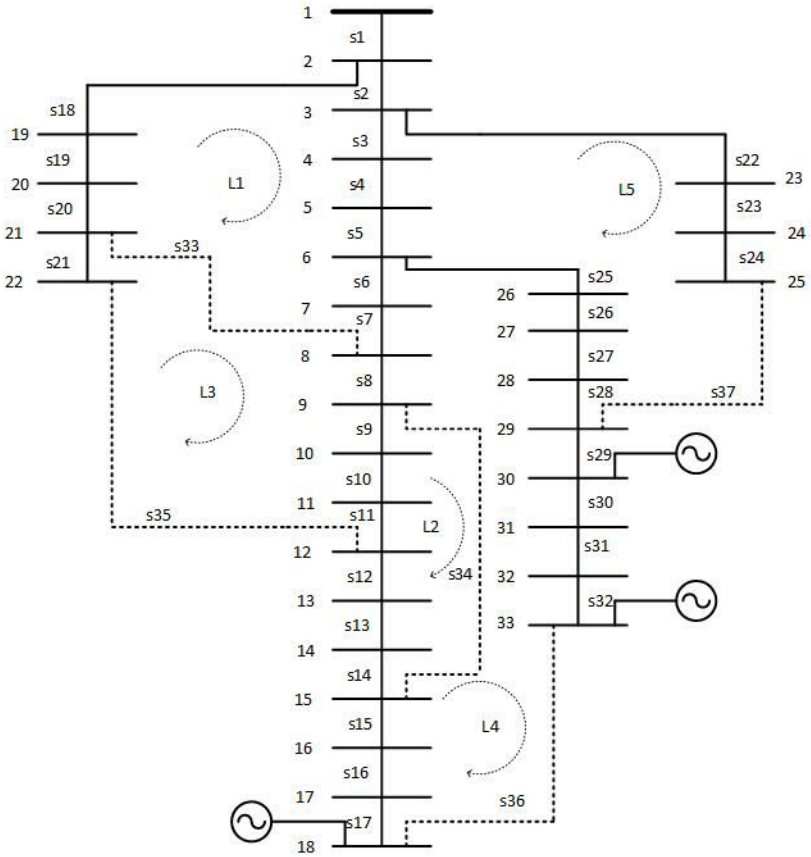

Figure 2.2: 33-bus radial distribution system.

In this system (and in all the other systems considered in this work), it is assumed that each branch contains a sectionalising switch. Further, in Fig. 2.2, the numerals 1, 2, 3 etc. denote the bus numbers whereas the branches (switches) are numbered as $s1, s2, s3$...etc. This system contains five tie switches numbered as $s33, s34, s35, s36$, and $s37$, thereby forming five loops as depicted in Fig. 2.2. The details of these five loops are given in Table 2.1.

Table 2.1: Details of the loops for 33-bus system

Loop number	Tie switch	Switches in the loop (L)	Assigned numbers to switches in loop
L1	s33	s7,s6,s5,s4,s3,s2,s18,s19,s20,s33	1-10
L2	s34	s9,s10,s11,s12,s13,s14,s34	1-7
L3	s35	s11,s10,s9,s8,s7,s6,s5,s4,s3,s2,s21,s20,s19,s18,s35	1-15
L4	s36	s6,s7,s8,s9,s10,s11,s12,s13,s14,s15,s16,s17,s25,s26,s27,s28,s29,s30,s31,s32,s36	1-21
L5	s37	s3,s4,s5,s22,s23,s24,s25,s26,s27,s28,s37	1-11

With reference to Table 2.1, if $\boldsymbol{X} = [10\ \ 7\ \ 15\ \ 21\ \ 11]$, then the switch number $s33, s34, s35, s36,$ and $s37$ are to be opened. In other words, this solution vector denotes the configuration in which all the tie line switched are "OFF". On the other hand, the solution vector $\boldsymbol{X} = [4\ \ 3\ \ 4\ \ 1\ \ 5]$ indicates that switch no. $s4, s11, s8, s6$ and $s23$ are to be opened. Clearly, the advantage of the decimal coding system is the reduction of the search space. In binary coding system, a total of 2^{32} combinations have to be checked (switch no. s1 is excluded from the search space as it should be always closed). On the other hand, in decimal coding system, a total of $10 \times 7 \times 15 \times 21 \times 11 = 242550$ combinations only have to be checked, thereby achieving a substantial reduction in the search space.

2.3 Application of KnEA algorithm for DSR

The basic anatomy of KnEA [66] is identical to that of NSGA-II [67]. The main difference between KnEA and other multiobjective evolutionary algorithms (MOEAs) such as NSGA-II is that KnEA uses knee points as a secondary selection criterion additionally along with the principle of nondominated sorting to augment the search ability of MOEAs. Knee points of nondominated fronts in the current population are preferred for selection to maximize the hypervolume that helps in maintaining better balance between convergence and diversity of MOEAs.

The basic steps of KnEA for DSR are explained as follows.

2.3.1 Initialize the problem and algorithm parameters.

A random parent population of size N_p is generated. In this step, algorithm parameters are also initialized which are the rate of knee points in population (T), set of knee points (k), adaptive pa-

rameters such as ratio of the size of the neighborhood to the span of each objective in nondominated fronts (r), and ratio of knee points to all nondominated solutions (t).

2.3.2 Check the system radiality constraint.

To determine the radiality of the system, a graph theory based approach is followed. Any radial distribution network supplied by a single substation ($N_s = 1$), can be represented as a graph G(N, S) that contains a set of nodes, $N = \{b_1, b_2, ...b_N\}$, and edges, $S = \{s_1, s_2....s_{N-N_s}\}$. Based on this analogy, the radility of the distribution network is determined as follows:

step 1: Initialize the sets of visited branches (D) and energized nodes (N_1) with reference node s_1 (substation node) and its two vertices (b_1, b_2) respectively. Further, also initialize looping or isolation index (LI) and the number of energized branches (EB). Set $D \leftarrow \{s_1\}$ ($s_1 \in S$) and $N_1 \leftarrow \{b_1, b_2\}$ ($b_1, b_2 \in N$), $EB = 0$, $LI = 0$ and $k = 1$.

step 2: While $EB \leq N - N_s$ and $LI = 0$.

step 3: Set $n = 1$.

step 4: Do

step 5: Check $s_n \notin D$ (selected edge should not belong to already visited branch set). Subsequently, select the pairs of vertices (b_2, b_3) connected by edge s_n such that $N_2 \leftarrow \{b_2, b_3\}$ ($b_2, b_3 \in N$ and $s_n \in S$).

5.1: check $N_2 \cap N_1 = C = \{c | c \in N_1$ and $c \in N_2\}$.

5.2: if $|C| = 1$ ($|C|$ denotes the cardinality of set C) then $N_1 \leftarrow N_1 \cup \{b_2, b_3\}$, $D \leftarrow D \cup \{s_n\}$, $n \leftarrow n + 1$ and $N_2 = \emptyset$.

elseif $|C| = 2$ then $LI = 1$.

else $n = n + 1$.

Any switch connected to substation node through a single path, has exactly one common node between energized nodes (N_1) and nodes of edge under consideration (N_2). The presence of two common nodes indicates presence of loop.

step 6: until $n \leq (N - N_s)$.

step 7: if k=1 then $EB = |D|$.

else check $EB \neq |D|$ then $EB = |D|$ otherwise $LI = 1$.

step 8: $k = k + 1$.

step 9: end while.

If the number of all energized branches is equal to $N - N_s$ then the configuration of the network is radial. In case of more than one substation (say two substations), application of "shortest path algorithm" identifies whether any direct path exists between the substations or not. If any direct path exists, then the radiality of the system is not preserved and the solution is discarded. In case no direct path exists, then the entire system is divided into two disjoint parts, in which each disjoint part is supplied from a single substation. Subsequently, for checking the radility of each disjoint part, the algorithm described above can be applied. This same philosophy can easily be extended for N_s ($N_s > 2$) number of substations in the system.

2.3.3 Reproduction

After evaluating the parent population, generation of offspring population is carried out in two steps.

(i) Selection. The selection of individuals is performed using binary tournament mating strategy described as follows.

1) From the population, select two individuals randomly.

2) Compare the selected individuals based on non-dominated ranking, knee point criterion and weighted distance. The solution with better rank is selected if both individuals belong to different fronts. If both the solutions have same rank, the algorithm checks for knee point. If one of the solutions is a knee point, then that solution is chosen. If both solutions are knee points or none of them is a knee point, then the solution with higher weighted distance is selected. Front ranks for solutions are decided using effective nondominated ranking as described in Section 2.3.4 and the weighted distance (DW) for each solution x in a population is calculated based on the h-nearest neighbors. The corresponding expressions are as given below [66]

$$DW(x) = \sum_{i=1}^{h} w_{xi} dis_{xxi} \tag{2.45}$$

$$w_{xi} = \frac{r_{xi}}{\sum_{i=1}^{h} r_{xi}} \tag{2.46}$$

$$r_{xi} = \frac{1}{|dis_{xxi} - \frac{1}{h}\sum_{i=1}^{h} dis_{xxi}|} \tag{2.47}$$

where xi denotes the i^{th} nearest neighbor of x in the population, w_{xi} is the weight of xi, dis_{xxi}

is the Euclidean distance between x and xi. Further, r_{xi} represents the rank of distance dis_{xxi} among all the distances dis_{xxj}, $1 \leq j \leq h$ and h is number of nearest neighbors of solution x.

3) Include the better individual out of the two options into the intermediate pool.

4) Repeat the procedure (Np/2) times.

(ii) Genetic operator (Crossover/Mutation). Generate offspring population with the application of genetic operators (i.e. mutation and crossover) on the selected individuals in the intermediate pool with a given crossover/ mutation rate. For the DSR problem, one or several switches are exchanged between two parent decision variable vectors for a given distribution system, as discussed below. Let $\mathbf{X}_1$ and $\mathbf{X}_2$ be two decision variable vectors in the intermediate pool for 33-bus distribution system. Given any $\mathbf{E}' = \mathbf{X}_2 - \mathbf{X}_1$, there exists an edge $\mathbf{E} = \mathbf{X}_1 - \mathbf{X}_2$ such that $(\mathbf{X}_1 - \{\mathbf{E}\}) \cup \{\mathbf{E}'\}$ is also a tree. Let, for example,

$\mathbf{X}_1 = \{s7 \quad s33 \quad s12 \quad s25 \quad s31\}$

$\mathbf{X}_2 = \{s33 \quad s9 \quad s13 \quad s25 \quad s34\}$

where elements of $\mathbf{X}_1$ and $\mathbf{X}_2$ are switches to be opened from different loops with, $\mathbf{E} = \{s7\, s12\, s31\}$ and $\mathbf{E}' = \{s9\ s13\ s34\}$. Two crossover points in $\mathbf{X}_1$ (assume 1st and 3rd crossover points) are selected randomly. In $\mathbf{X}_1$, $s7$ and $s12$ are at first and third crossover points, respectively. If a selected switch corresponding to the chosen crossover point, does not belong to E, then no feasible switch exists in $\mathbf{X}_2$ for exchange. In that case, next crossover point is selected. As $s7 \in \mathbf{E}$, then closing it makes a loop that can be denoted by $L = \{s2, s3, s4, s5, s6, s7, s8, s9, s10, s11, s18, s19, s20, s21, s35\}$. The exchange branch set in $\mathbf{X}_2$ is obtained as $L \bigcap \mathbf{X}_2 = \{s9\}$. Therefore the first mapping set is $\{s7, s9\}$. This mapping set implies that branches $s7$ and $s9$ are exchanged between $\mathbf{X}_1$ and $\mathbf{X}_2$. Same procedure is repeated to determine the second mapping set corresponding to the second crossover point. Loop formed by closing $s12$ is $L' = \{s9, s10, s11, s12, s13, s14, s34\}$. The common branch set between L' and $\mathbf{X}_2$ is $\{s9, s13\}$. As $s9$ is already in the first mapping set, the second mapping set is $\{s12, s13\}$. As a result, the generated two offspring solutions are $\{s9, s33, s13, s25, s31\}$ and $\{s33, s7, s12, s25, s34\}$. To maintain genetic diversity in the subsequent generations, mutation operation is also performed. For this purpose, one branch is chosen randomly in the selected decision variable vector and by closing this branch, a single loop is created. To maintain radiality, a new branch is randomly selected in the formed loop to be opened.

2.3.4 Effective non-dominated ranking (ENS).

The solutions in the population are sorted based on the values of the first objective in an ascending order before ENS [68] is implemented. Fronts are assigned to the solutions of this sorted population from staring solution to last one, individually. A solution x_n will never dominate solution x_m, if $m < n$. In that case only two possibilities exist: either x_m dominates x_n, or x_m and x_n do not dominate each other. Therefore, a solution is compared to those which are already added to the fronts to decide its front. A solution x_n is compared to all solutions of first front (F1) to determine whether any solution of F1 dominates x_n or not. If no such solution exists then x_n is placed in front F1. Otherwise x_n is compared with the solutions assigned to second front (F2). If any solution in front F2 does not dominate x_n, x_n is assigned to front F2 . If x_n is not assigned to any of the existing fronts then a new front is created and assigned to x_n and the above procedure is repeated for each solution vector.

2.3.5 An adaptive strategy to identify Knee Points.

The distance measure of a solution to the extreme hyperplane (obtained by the extreme values of objective functions) is applied to identify multi objective knee points in case of optimization problem. A solution with maximum distance in its neighborhood is characterized as a knee point. The identified knee points are affected by the size of neighborhood of the solutions. Let R^j_{gi} denotes the neighborhood of j^{th} objective function in i^{th} non-dominated front corresponding to g^{th} generation. The size of R^j_{gi} is updated using the following expression [66]:

$$R^j_{gi} = (f^{max_j}_{gi} - f^{minj}_{gi}).r_{gi} \qquad j = 2, 3.....M, \quad i = 1, ..N_f \tag{2.48}$$

Where $r_{gi} = r_{(g-1)i} * \exp(-\frac{1-t_{(g-1)i}/T}{M})$, $t_{gi} = |k_i|/$(size of non-dominated front (Fi)), $|k_i|$ is knee points of i^{th} nondominated front, $f^{max_j}_{gi}$ and $f^{min_j}_{gi}$ are the maximum and minimum values for j^{th} objective function of i^{th} nondominated front respectively at the g^{th} generation, $0 < T < 1$ is a threshold value that controls ratio of knee points to the number of nondominated solutions in every solution front, N_f is number of formed nondominated fronts and M is the number of objective functions. Further, r_{gi} and t_{gi} denote the values of $'r'$ and $'t'$ corresponding to i^{th} non-dominated front at generation $'g'$.

2.3.6 Environmental selection (Creation of next generation).

KnEA utilizes the Pareto dominance as the primary criterion and knee points as the secondary criterion in the environmental selection. The parent population for next generation X_{k+1} is selected from the combined populations by including the solutions of different front according to their rank (front with better rank is considered first). If size of the last included front makes the current population size larger than N_p, then knee points of last included front are preferred to be discarded to make the size of X_{k+1} exactly equal to N_p. If the current population size of X_{k+1} is n, then $(n - N_p)$ solutions which have the minimum distances to the hyperplane, are discarded to make size of X_{k+1} exactly equal to N_p.

2.3.7 Check Termination Criterion.

The procedure described in Sections 2.3.2 to 2.3.6 are repeated until maximum number of iteration is reached or the nondominated solution set remains same for consecutive five iterations.

The application of the knee point-driven MOEA algorithm (KnEA) for distribution system reconfiguration problem is presented as described below.

1: For the distribution test system, read the bus and line data.

2: Set generation count $g = 1$ and algorithm parameters T, r_o, t_o and set of knee points.

3: Initialize random parent population X_o of size N_p (i.e. N_p is the number of solutions in X_o) that fulfills the radiality constraint.

4: Run the load flow and evaluate the objective functions f_1, f_2, f_3 and f_4 for each individual of X_o. It is to be noted that when alternative form of DSR problem (described in Section 2.2.3) is followed, objective functions f_1, f_2 and f_3 only are evaluated. Discard all the solutions which are unstable from the solution space by the addition of large penalty factor values to all the objective functions (for alternative form of DSR problem). Assign $X_g = X_o$, where X_g denotes the parent population at any g^{th} generation.

5: Perform ENS and binary tournament mating selection, mutation and crossover on the strings in the parent population X_g and form new individuals as offspring population Y_g. Check for the radiality and other constraints and subsequently evaluate the strings in Y_g.

6: Create a combined population $R_g = X_g \cup Y_g$.

7: Determine the non dominated front and identify the knee points, based on the distances from

extreme hyperplane for combined population as described in Section 2.3.4 and 2.3.5 respectively.

8: Select the parent population X_{g+1} for next generation as described in Section 2.3.6.

9: Increment the generation count $g = g + 1$.

10: Steps 4 to 9 are repeated until termination criterion is met. Else go to step 11.

11: Choose the best solution among the N_p solution vectors using the approach as discussed below.

2.3.8 Selection of final solution

After one of the above-mentioned termination criteria is met, then the best solution from the set of Pareto-optimal solutions is obtained by summing all the normalized values of the objective functions. In case of minimization, the objective functions associated with each solution in the set of Pareto-optimal solutions are normalized using the following expressions [69].

$$\tilde{T}_{k,j} = \frac{f_{k,j} - f_j^{min}}{f_j^{max} - f_j^{min}} \tag{2.49}$$

where f_j^{max} and f_j^{min} are the maximum and minimum values for j^{th} objective function respectively, and $f_{k,j}$ is the k^{th} solution of the non-dominated set corresponding to the j^{th} objective function. As can be seen from equation (2.49), $\tilde{T}_{k,j}$ is the normalized value of k^{th} solution of non-dominated set corresponding to the j^{th} objective function. Lastly the minimum sum of normalized objective functions is selected as the final solution $F(s)$ as;

$$F(s) = \min_k \sum_{j=1}^{M} \tilde{T}_{k,j} \quad j = 1 \cdots M, \quad k = 1 \cdots N_p \tag{2.50}$$

where M is the number of objective functions.

2.4 APPLICATION OF NSGA-II ALGORITHM FOR DSR

NSGA-II uses the principle of nondominated sorting, natural evolution and population genetics to search a set of solutions for multiobjective optimization and arrive at the Pareto front. The basic steps of NSGA-II [67] for DSR is explained as follows.

Step 1: For the distribution test system, read the bus and line data.

Step 2: Set generation count $k = 1$.

Step 3: Initialization. Generate a random parent population X_o of size N_p (i.e. N_p is the number of solutions in X_o) that fulfills the radiality constraint.

Step 4: Evaluation of objective functions. Run the load flow and calculate the values of the objective functions f_1, f_2, f_3 and f_4 for each individual of X_o. Assign $X_k = X_o$, where X_k denotes the

parent population at any k^{th} generation.

Step 5: Non-dominated ranking. Before application of genetic algorithm (GA) operator, the strings in the parent population X_o are sorted based on the nondomination. The solutions in X_o, which do not constraint-dominate each other but constraint-dominate all other solutions of X_o, are placed in the first front. In order to find the individuals in the next non-dominated front, the solutions of the first front are discounted temporarily and the above procedure is repeated. Subsequently, these generated fronts are assigned their corresponding ranks. Thus, rank 1 is assigned to first front, rank 2 is assigned to second front, and so on.

Step 6: Crowding distance computation. After the completion of non-dominated sorting, the crowding distance is calculated for each individual.

Step 7: Selection. The selection of individuals is carried out using crowded tournament operator for the application of GA operators as follows.

a) From the population X_k, select two individuals randomly.

b) Compare the selected individuals based on rank and crowding distance. The solution with better rank is selected if both individuals belong to different fronts. If both the solutions have same rank, then the solution with higher crowding distance is selected.

c) Include the better individual out of the two options into the intermediate pool.

d) Repeat the procedure $(Np/2)$ times. This operator helps to keep diversity in the population.

Step 8: Generate offspring population Y_k with the application of GA operators (i.e. mutation and crossover) on the selected individuals in the intermediate pool. Evaluate the strings in Y_k as described in step 4, where Y_k denotes the offspring population at k^{th} generation.

Step 10: Create a combined population $R_k = X_k \cup Y_k$.

Step 11: On the basis of non-domination, the individuals of population are sorted and ranked into different front and crowding distance is calculated for each individual of combined population as described in step 4 and step 5 respectively.

Step 12: The parent population X_{k+1} for next generation is created by including the solutions of different front according to their rank (front with better rank is considered first). Initially, If size of first front is smaller than Np, then all the solutions of the first front set are included in X_{k+1}. Subsequently the rest of the nondominated fronts in order of their ranks are continued to be included in X_{k+1} until size of X_{k+1} becomes more than N_p. If the current population size of X_{k+1} is n, then

Table 2.2: Capacity and installation node of DG for various distribution system

System	Bus number	Capacity (MW)
33-bus system	18	0.100
	30	0.150
	33	1.100
69-bus system	63	0.55
	64	0.75
	65	1.20
119-bus system	55	2.50
	72	2.00
	78	1.50
	119	1.00

$(n - Np)$ solutions are discarded to make size of X_{k+1} exactly equal to Np. To select the individuals to be discarded, the last included front is sorted based on crowding distance. Subsequently, the solutions having least $(n - Np)$ values of crowding distance are discarded from X_{k+1}.

Step 13: Increment the generation count $k = k + 1$.

Step 14: Steps 7 to 13 are repeated until maximum iteration is reached. Else go to step 15.

Step 15: Choose the best compromising solution among the N solutions using the approach as described in Section 2.3.8.

2.5 Case study results

The formulation and the solution methodology described in the last two sections have been applied to IEEE 33-bus, 69-bus and 119-bus radial distribution systems. For all three systems, the branch data and bus data are given in Appendix A. All the simulations studies have been carried out in MATLAB [70] environment considering the nominal load level of the system. The minimum and maximum bus voltage limits considered are 0.90 pu and 1.05 pu respectively. Table 2.2 shows the assumed capacities and the installation nodes of DGs for all the above three test systems. In this work, DGs are assumed to work at 0.85 power factor (lagging). All the parameters of the synchronous based DGs are listed in Tables B.1, B.2 and B.3 in the Appendix B. It is to be noted that in this work, only reconfiguration of distribution system problem is considered and hence the location and size of each DG in the network are assumed to be known. To show the

effectiveness of the reconfiguration, parameters of generators (exciter gain and time constant) [71], the capacities and the locations of the DG have been chosen in such a way so that the system is unstable in its initial configuration. To investigate the performance of KnEA, the results have been compared with those obtained by using 'NSGA-II'. In both methods, the values of the mutation and crossover probability and the population size are kept same for any particular distribution system. The parameters chosen for simulation of all three test systems are $T = 0.5$, $r_o = 1$ and $t_o = 0$ and the justification for selecting these parameters is given in Section 2.5.4. Further, the values of the penalty factors have been chosen as $\lambda_1 = \lambda_2 = 10$. In this work, the DSR problem has been solved for the following two cases:

Case A. Stability issue is considered as an objective function (as discussed in Section 2.2.1).

Case B. Stability issue is considered as a constraint (as discussed in Section 2.2.3).

The detailed results for all the three test systems are discussed below.

2.5.1 Test System 1

In IEEE 33-bus system, the total real and reactive loads are 3.7 MW and 2.3 MVAr [15], respectively. The following parameters have been adopted for the system: population size = 50; generation = 20; crossover probability = 0.9; mutation probability = 0.18. Table 2.3 shows the comparative results for both the cases.

Table 2.3: Result of 33-bus distribution system

Method	Open switches	Power loss(kW)	Voltage stability index	Switching number	%Damping ratio**	Stability status	cpu time (s)
Case A							
Initial case	s33,s34,s35, s36,s37	68.661	0.18457	0	-0.0363	unstable	
KnEA	s7,s9,s29,s35, s37	49.70	0.0918	6	1.01	stable	19.293
NSGA-II	s6,s11,s29, s35,s37	50.04	0.10302	6	0.81	stable	27.525
Case B							
KnEA	s8,s11,s14, s33,s37	45.90	0.08748	6	0.957	stable	17.122
NSGA-II	s7,s11,s29, s35,s37	49.228	0.08566	6	0.779	stable	23.491

** Damping ratio of electromechanical oscillation mode is expressed in term of percentage ($\%D = 100 * D$).

This table shows that reconfiguration with DG reduces power loss, improves damping ratio of electromechanical oscillation modes as well as voltage stability margin with acceptable number of switching operations. From this table, it is observed that the initial system with DGs (before reconfiguration) is unstable, which is made stable through reconfiguration. For both cases A and B, KnEA as well as NSGA-II algorithms are able to stabilise the system, although the damping ratios obtained by KnEA algorithm are better than those obtained by NSGA-II algorithm in both the cases. Further, in both the cases, the loss reduction achieved by KnEA algorithm is more than that achieved by the NSGA-II algorithm. Moreover, as compared to the initial configuration, the voltage stability margin of the system is improved substantially by both these algorithms and the final voltage stability margins achieved by these two algorithms are quite close to each other for both these cases. Lastly, the CPU time taken by the KnEA algorithm is less than that taken by NSGA-II algorithm for both these cases.

Thus, the performance of KnEA algorithm is better than the NSGA-II algorithm for both the cases. However, the final configuration obtained for case A and case B are different from each other. This is due to the difference in formulated problem in case A and case B (as discussed earlier, in case A, stability issue is considered as an objective function whereas in case B, it is considered as a constraint). It is to be noted that, in this work, same preference has been given to all objective functions and therefore, the final configurations have been selected based on the sum of the normalized values of all objective functions, as discussed in Section 2.3.8. As the performance of the KnEA algorithm is found to be better than that of NSGA-II algorithm, for both case A and B, the configurations obtained by KnEA algorithm as given in Table 2.3 are taken to be the final solutions.

2.5.2 Test System 2

This test system is a radial distribution system of 12.66 kV which consists of 69 buses, 5 loops and normally open switches numbered from s69 to s73 as shown in Fig 2.3. The total real and reactive power load on the system are 3.8 MW and 2.69 MVAr [72], respectively. Various parameters used in KnEA technique are as follows: the population size is 80, maximum number of generation is 20 and crossover and mutation probability are 0.9 and 0.18 respectively. The simulation results for this test system are presented in Table 2.4.

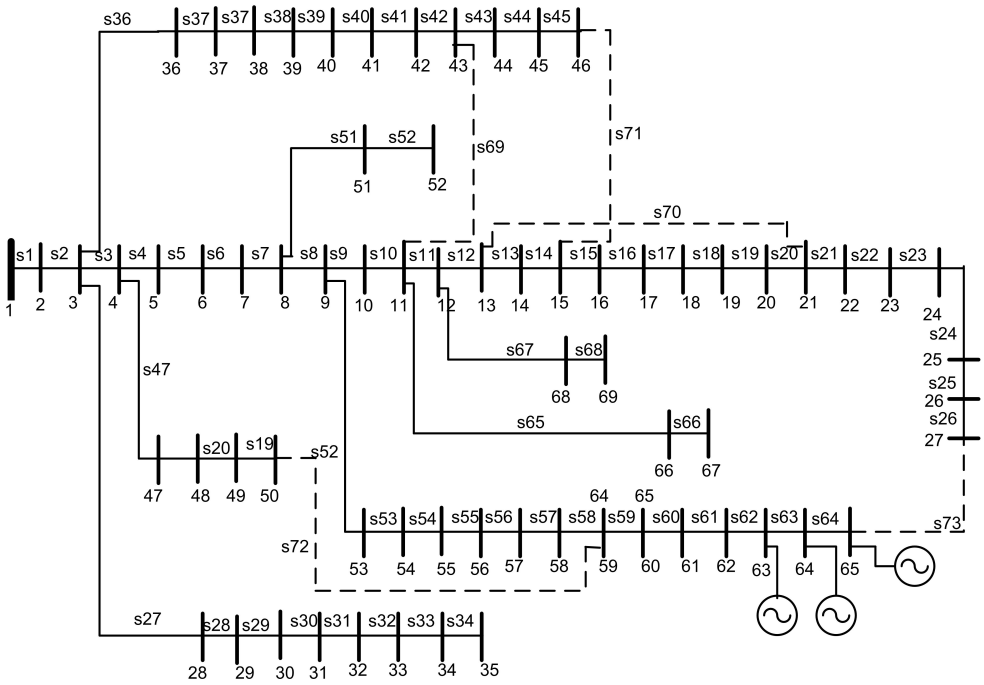

Figure 2.3: 69-bus radial distribution system.

Table 2.4: Result of 69-bus distribution system

Method	Tie switch	Power loss(kW)	Voltage stability index	Switching number	%Damping ratio**	Stability status	cpu time (s)
Case A							
Initial case	s69,s70,s71, s72,s73	75.8	0.0884	0	-0.1143	unstable	
KnEA	s11,s15,s52, s69,s71	29.1	0.0198	6	1.348	stable	33.703
NSGA-II	s10,s15,s69, s71,s72	30.33	0.0484	4	-0.679	unstable	49.586
Case B							
KnEA	s11,s15,s52, s69,s71	29.1	0.0198	6	1.342	stable	30.822
NSGA-II	s11,s13,s52, s69,s71	29.09	0.0198	6	1.331	stable	46.112

** Damping ratio of electromechanical oscillation mode is expressed in term of percentage ($\%D = 100 * D$).

From this table it is observed that for case A, the reduction in loss and improvement in voltage stability margin achieved by KnEA algorithm are more than those obtained by the NSGA-II algo-

rithm. Further, although the initial configuration is unstable, for case A, KnEA algorithm is able to find a stable configuration while NSGA-II algorithm is unable to do so. However, for case B, both these algorithms are able to find stable configurations. Thus, for ensuring stability, the stability issue should be considered as a constraint. Moreover, the results for reduction in power loss, improvement in voltage stability margin, number of switching and final damping ratio obtained by both these methods are quite comparable for case B. Further, the CPU time taken by KnEA algorithm is less than that taken by NSGA-II algorithm for both case A and B. Therefore, overall, considering both case A and case B, the performance of KnEA algorithm can be considered to be better than that of NSGA-II algorithm.

As all objective functions are given equal importance, the optimum solution is obtained by following the procedure of Section 2.3.8. Based on the smallest summation value of the normalized objective functions, the configuration given by the open switches s11, s15, s52, s69 and s71 is considered to be the best solution for Case A. On the other hand, for case B, on account of better damping ratio, the configuration obtained by KnEA algorithm can be considered to be the best solution.

2.5.3 Test System 3

This is a 119-bus distribution system, which includes 118 sectionalizing and 15 tie switches as depicted in Fig 2.4. The feeder, bus and tie line data of this system are taken from [73]. The total active and reactive power loads in this system are 22,709.7 kW and 17,041.1 kVAr, respectively. The parameters of the KnEA algorithm used for this test system are same as those used for test system 2. The results corresponding to all the objectives are shown in Table 2.5. From this table it is observed that the power loss reduction obtained by KnEA algorithm is more than that obtained by NSGA-II algorithm for both case A and case B. Also, the voltage stability margins obtained by these two algorithms are quite comparable for both case A and case B. However, for case A, the number of switching operations suggested by KnEA algorithm is quite less (as compared to that obtained by NSGA-II) while for case B, the number of switching operations obtained by both these algorithms are same. Also, both these algorithms are able to stabilise the initially unstable system for both case A and B. Lastly, the execution time required by KnEA algorithm is significantly less than that required by NSGA-II method. Therefore, for this system also, overall the performance

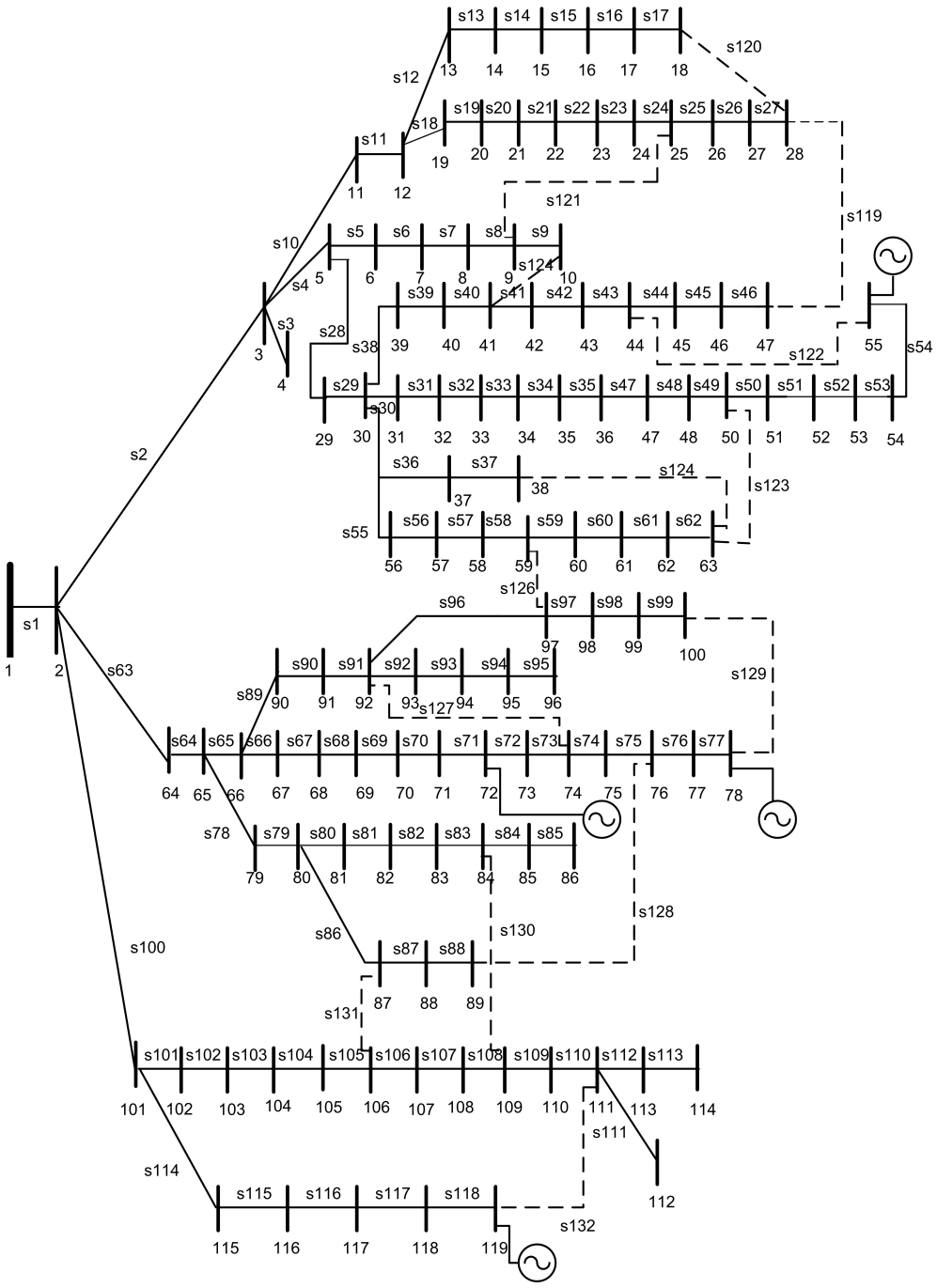

Figure 2.4: 119-bus radial distribution system.

of the KnEA algorithm can be considered to be better than that of the NSGA-II algorithm and as a result, the configurations obtained by KnEA algorithm can be taken to be the final solutions of the reconfiguration problem.

Table 2.5: Result of 119-bus distribution system

Method	Tie switch	Power loss (MW)	Voltage stability index	Switching number	%Damping ratio**	Stability status	cpu time (s)
Case A							
Initial case	s119,s120,s121,s122, s123,s124,s125,s126, s127,s128,s129,s130, s131,s132,s133	0.73951	0.3262	0	-0.9816	unstable	
KnEA	s9,s24,s61,s69,s75,s96, s110,s121,s122,s124, s125,s126,s127,s131, s132	0.440	0.15657	14	1.07	stable	98.27
NSGA-II	s9,s22,s33,s48,s58,s71, s76,s83,s87,s90,s110, s121,s124,s127,s132	0.4567	0.17845	22	0.41	stable	123.251
Case B							
KnEA	s9,s23,s42,s49,s61,s69, s77,s88,s110,s121,s122, s126,s127, s131, s132	0.4269	0.15657	18	0.4467	stable	91.89
NSGA-II	s17,s23,s34,s39,s44,s49, s71,s74,s110,s123,s126, s127,s130,s131,s132	0.4405	0.15657	18	0.9533	stable	110.830

** Damping ratio of electromechanical oscillation mode is expressed in term of percentage ($\%D = 100 * D$).

2.5.4 Further studies

Before concluding the chapter, some further studies and comments are in order.

(i) Impact of parameter T

In all the above studies, a fixed value of T has been chosen which controls the ratio of knee point to the nondominated solutions. With large values of T, less exploration in search space is obtained. On the contrary, relatively small value of T improves algorithm efficiency by preventing the solutions from getting trapped into local Pareto fronts. To investigate the effect of T on the final solution, optimum reconfiguration studies using the KnEA algorithm have been carried out on the 119 bus system for different values of T. The variation of F(s) (as defined in equation (2.50)) with respect to T is shown in Fig. 2.5. From this figure it is observed that F(s) attains a minimum value of 1.005 for $T = 0.5$. As a result, $T = 0.5$ has been used for all the systems in this work.

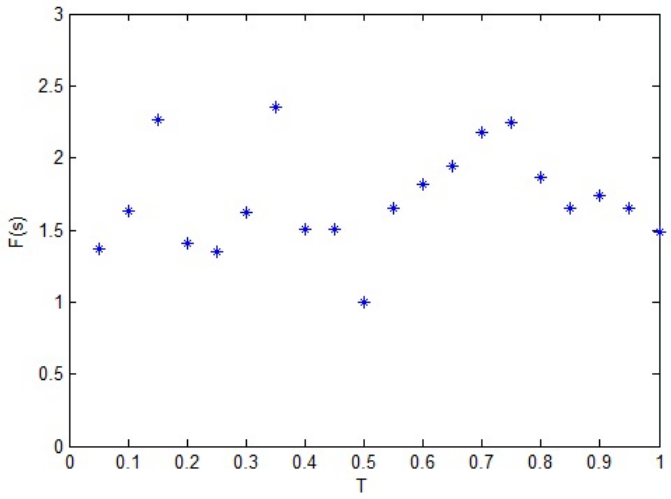

Figure 2.5: Variation of F(s) with T for test system 3.

(ii) In this chapter, the reconfiguration problem is solved as a multiobjective optimization problem (MOOP). In a true MOOP, there should be a set of objective functions, which are pareto optimal to each other. To demonstrate the MOOP nature of the reconfiguration problem studied in this chapter, the variation of objective functions (with respect to each other) for test system 3 are shown in Fig. 2.6. From this figure, it is observed that when power loss is minimized, damping ratio gets poorer (Fig. 2.6(a)). In fact, when the power loss is minimized to a large extent, the system becomes unstable. Therefore, power loss and damping ratio are pareto-optimal to each other. As observed from this figure, number of switching operations also observes pareto optimality with power loss and voltage stability index as depicted in Fig. 2.6(c) and Fig. 2.6(d), respectively.

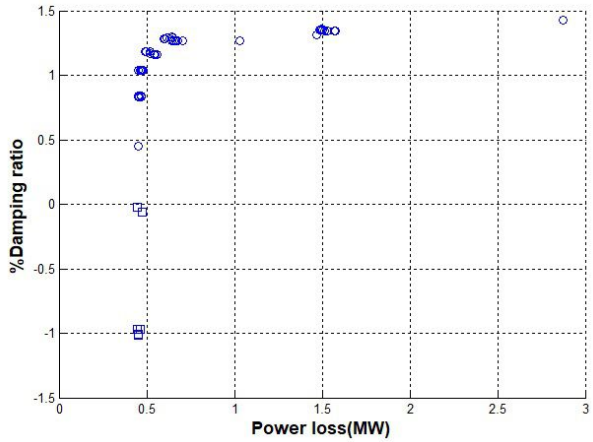

(a)

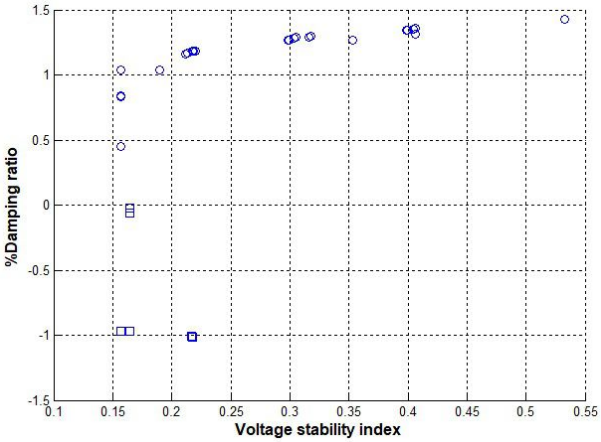

(b)

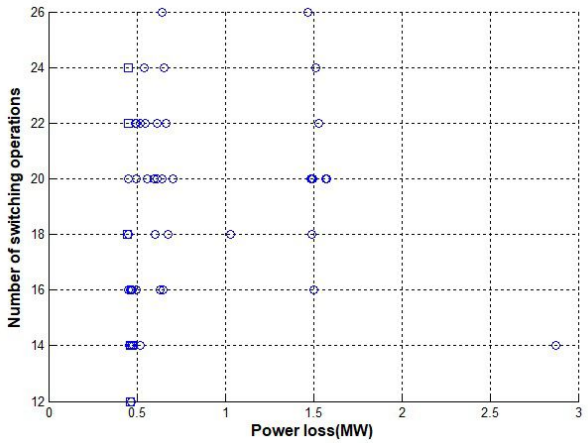

(c)

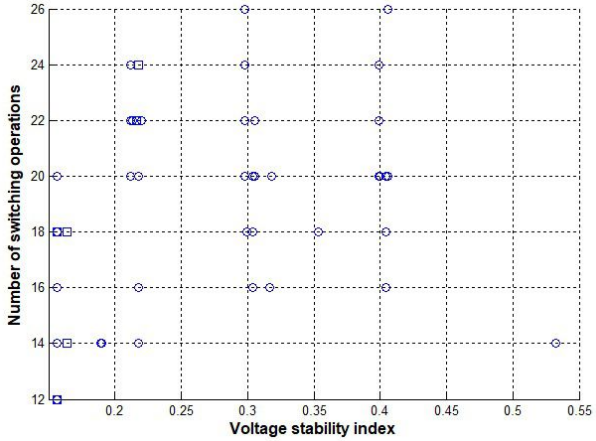

(d)

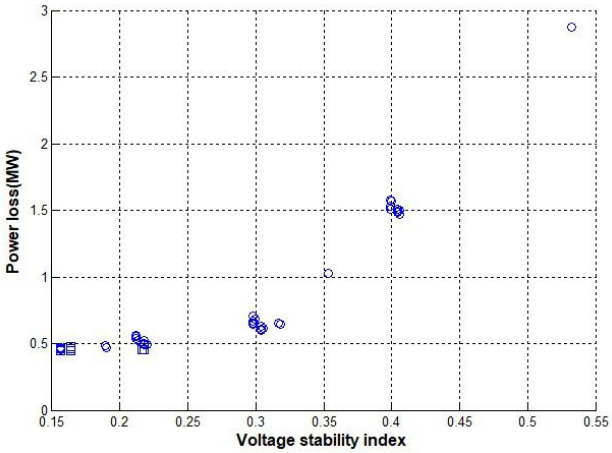

(e)

Figure 2.6: Achieved Pareto front from optimization of objective functions for test system 3 using KnEA.

On the other hand, power loss and voltage stability margin follow the same pattern (i.e. when any one of these indices improves, other index also improves). Thus, damping ratio observes pareto optimality with power loss and voltage stability margin. Therefore, the reconfiguration problem studied in this chapter is a true MOOP.

(iii) The results of Tables 2.3, 2.4 and 2.5 demonstrate the superiority of KnEA algorithm to NSGA-II for solving the feeder reconfiguration problem. For studying the statistical performance of both these methods, both these techniques have been executed 100 times. Table 2.6 illustrates the best, worst, and average solutions and standard deviation corresponding to test system 3.

Table 2.6: Comparison of two algorithms for 100 trials (test system 3)

		Best	Average	Worst	standard deviation
Power loss(MW)	KnEA	440.26	475.64	502.8	18.43
	NSGA-II	456.73	491.02	517.5	25.15
Voltage stability index	KnEA	0.15657	0.178455	0.2174	0.023226
	NSGA-II	0.178456	0.20356	0.2180	0.02555
Switching number	KnEA	14	16	22	2.350
	NSGA-II	22	24	24	3.286
Damping ratio	KnEA	-1.07	-1.0087	-0.9195	0.1537
	NSGA-II	-0.41	-0.962	-0.75	0.249

It is observed that the results obtained by the KnEA are better than those obtained by NSGA-II (in terms of lower average and lower standard deviation) which indicates the superiority of the KnEA technique over NSGA-II.

(iv) In the case studies presented in Subsections 2.5.1 to 2.5.3, power loss in the system has been minimized. However, for techno-economic reasons, instead of power loss, the cost of power purchase from the transmission grid should preferably be minimized [74]. To explore this case, another study has been carried out in which the power loss objective function f_1 is replaced with the minimization of cost of power purchased from the substation. Mathematically, this cost objective function can be evaluated as

$$\min f_1(\boldsymbol{X}) = \min(C_1 * P_G + C_2 * Q_G) \tag{2.51}$$

Where P_G and Q_G are the real and reactive power drawn by the substation respectively, C_1 (\$/kW) and C_2 (\$/kVAR) are the price coefficients of real and reactive power respectively. Further, in this study, only case B is considered as it has been already established that for ensuring stability, the stability issue should be considered as a constraint.

Therefore, in this case, the multi-objective constrained DSR problem is described by the objective functions in equations (2.5), (2.7), (2.51) and the constraints given in Subsection 2.2.2 and in equation (2.43). The results obtained for all of the three test systems are shown in Table 2.7.

Table 2.7: Result of 119-bus distribution system with minimization of power purchase cost

System	Method	Tie switch	Cost (\$)	Voltage stability index	Switching number	Cpu time (s)
	Case B					
System 1	Initial case	s33,s34,s35, s36,s37	14914.38	0.18457	0	
	KnEA	s7,s29,s34,s35,s37	14793.29,	0.0856	4	18.518
	NSGA-II	s8,s29,s33,s34,s37	14812.24	0.09263	4	25.331
	Case B					
System 2	Initial case	s69,s70,s71, s72,s73	9068.95	0.0884	0	
	KnEA	s11,s13,s52,s69, s71	8796.33	0.0198	6	31.198
	NSGA-II	s11,s16,s52,s69,s71	8808.68	0.0198	6	47.513
	Case B					
System 3	Initial case	s119,s120,s121,s122,s123,s124,s125, s126,s127,s128,s129,s130,s131,s132,s133	108617.77	0.3262	0	
	KnEA	s23,s27,s35,s39,s44,s75,s97,s110,s123, s125, s126,s127,s128, s131,s132	106656.79	0.15657	16	94.352
	NSGA-II	s17,s23,s34,s42,s48,s76,s83,s110,s120, s123, s126,s127,s128,s129,s132	106709.08	0.176692	16	119.622

The values for the coefficients C_1 and C_2 have been taken from [74]. From this table, it is observed that the reduction in power purchase cost (with respect to the base case) is more with

KnEA algorithm as compared to that obtained with NSGS-II method and voltage stability margin obtained with both these methods are quite comparable to each other. Further, in all the systems, the number of switching operations obtained by both methods are same. However, as observed earlier, KnEA algorithm requires less computational time as compared to that required by NSGA-II.

2.6 Conclusion

In this chapter, a multi-objective distribution system reconfiguration problem has been formulated and subsequently, application of KnEA algorithm has been proposed to solve the formulated problem. Based on the simulation studies carried out in three different test systems, it has been observed that a dynamically unstable distribution system can be made stable with increased small signal stability margin through reconfiguration and the stability issue should be enforced as a constraint instead of objective function in order to maintain system stability. The KnEA algorithm is superior to that of NSGA-II algorithm for solving the multi-objective network reconfiguration problem in term of the performance and accuracy. However, all this analysis is for deterministic nature of DS. Therefore, a procedure for taking into account the uncertainties of correlated loads and generations into the DSR problem is described, in the next chapter.

Chapter 3

Stability constrained optimal distribution system reconfiguration considering uncertainties in correlated loads and distributed generations

This chapter focuses on small signal stability constrained DSR methodology under uncertainties associated with the load demand and the power output of the renewable energy based distributed generation. Further, the correlation among the uncertain load demand and among the uncertain DG power output has also been considered. This formulation takes into consideration the system's probabilistic operational constraints such as maximum limit on line current, minimum and maximum limits on bus voltage magnitude, radiality of distribution system and probabilistic small signal stability constraint. A KnEA-PE approach is then utilized to solve this DSR problem.

3.1 Introduction

In the previous chapter, DSR in the presence of DGs is investigated in a deterministic environment. However, inherent intermittencies of power generation and continuous load demand variations give rise to significant level of uncertainties. In the face of these uncertainties, DS operational strategies such as DSR become more challenging. In most of the literature, only the steady-state behaviour of DGs under uncorrelated uncertainties has been taken into account during system reconfiguration. As discussed in Chapter 2, the system stability is affected with the integration of DGs in the distribution system. Therefore, small signal stability of distribution system is considered as an important probabilistic stability index for maintaining system security level while solving the DSR problem.

To address this issue, the effect of uncertainties with correlations among loads and among power outputs of DGs are considered in stability constrained DSR of DS in this chapter. In this chapter, only synchronous generator based small hydro power plants (SHPP) are considered as the DGs. Moreover, it is presumed again that the system stability is completely dependent on

the system operating condition (uncertain load injections, DG power generation and topology). The key objective of this chapter is to develop an optimum reconfiguration methodology while guaranteeing the small signal stability of the distribution system in an uncertain environment.

3.2 PROBLEM FORMULATION

3.2.1 System modelling

The objectives in the proposed formulation are minimization of expected power loss, maximization of expected voltage stability margin, and minimization of the required number of switching operations. The presented formulation employs probabilistic approach to represent the stochastic nature of the loads and power generated by DGs. The proposed formulation accounts for the system constraints by: 1) energising all load points in the system, 2) preserving the system radiality, 3) ensuring that the probability of the system to remain dynamically stable is more than some pre-defined value and 4) ensuring that the probabilities of the branch currents and bus voltages to remain within their allowable limits exceed some pre-defined values.

A brief description of various uncertain quantities is given below.

3.2.2 Uncertainty representation

In this work, two uncertain quantities are considered: (1) active and reactive power loads, (2) SHPP output power. The probabilistic models for the real as well as reactive power demand and the power generated by DG are described as follows.

1) Probabilistic Load modelling: The uncertain real and reactive power load is represented as a continuous random variable with Gaussian probability density function as [75].

$$f(l_k) = \frac{1}{\sigma_k\sqrt{(2\pi)}} e^{-\frac{(l_k-\mu_k)}{2\sigma_k^2}} \tag{3.1}$$

where l_k is real or reactive power load at the k^{th} bus, while σ_k and μ_k are the standard deviation and mean of l_k respectively.

2) Probabilistic generator modelling: In this work, the generation outputs (as percentage of rated capacity) of the SHPP are taken from [76] along with their associated discrete probability values. Table 3.1 shows the percentage output power of the SHPP and the associated probabilities used for SHPP modeling.

Table 3.1: Probabilities of SHPP power output

State no	Output power as percentage of rated capacity (%r)	% Probability
1	0.000	2
2	28.43	5.52
3	37.73	5.96
4	45.70	11.03
5	50.80	14.24
6	55.14	14.24
7	60.30	15.67
8	65.90	14.24
9	73.71	9.49
10	83.62	5.74
11	100	1.87

The DG output power P_{DG} is calculated as $P_{DG} = P_{rated} * r/100$, where P_{rated} is maximum capacity of the DG unit and r is percentage output power (of rated capacity). Thus, at every state, the DG power output and the related probabilities are determined. Subsequently, the mean, standard deviation and other moments are computed. Further, correlation among the outputs of the SHPPs has also been considered in this work.

3.2.3 Probabilistic Objective Functions

The probabilistic objective functions are described in detail below.

(1) **Minimization of expected real power loss**: With reference to Fig. 2.1, this objective function is given by,

$$\min f_1(\boldsymbol{X}) = \min E\left\{ \sum_{(k,k+1)\in B_L} \frac{R_k(P_k^2 + Q_k^2)}{|V_k|^2} \right\} \tag{3.2}$$

In equation (3.2), $E\{.\}$ stands for expectation operator.

(2) **Maximization of expected voltage stability margin**: This objective function is given by,

$$\min f_2(\boldsymbol{X}) = \min E\{(\Delta L)\} \tag{3.3}$$

A smaller value of ΔL_{k+1} (voltage stability index) indicates an improved voltage stability margin. The quantity ΔL is defined in equation (2.4)

(3) **Minimization of number of switching operation**: This objective function is given as

$$\min f_3(\boldsymbol{X}) = \min(NSW) \tag{3.4}$$

The above formulated multi-objective optimization problem is subjected to various operational and stability constraints as discussed below.

3.2.4 Limits and Constraints

(1) **Topological constraints**: During reconfiguration, system radiality should be preserved.

(2) **Probabilistic small signal stability constraint** : As described in Chapter 2, system stability is investigated by linearizing the dynamic model of the distribution system at the initial operating point. This linearized model yields the system state matrix and subsequently, the eigenvalues of this matrix are determined. From these eigenvalues, the critical eigenvalues (which are either rightmost eigenvalues or eigenvalues with least damping ratio) are identified. Now, depending on the probability density function (PDF) of the load demand and the power generated by the DGs, the critical eigenvalues will also have a certain PDF and from this PDF, the probability of stability can be determined. The detailed procedure of small signal stability analysis (SSSA) is given in Chapter 2. The following linearized dynamic model of DS at an operating point has been obtained in Chapter 2 in equation (2.38):

$$\boldsymbol{\Delta}\dot{\mathbf{x}} = \mathbf{A}_{sys}\Delta\mathbf{x} + \mathbf{E}\Delta\mathbf{u} \tag{3.5}$$

where

$\mathbf{x} = [\mathbf{x}_1^T \quad \mathbf{x}_2^T \ldots \mathbf{x}_i^T \ldots \mathbf{x}_{m_g}^T]^T, \qquad \mathbf{x}_i = [\delta_i \quad \omega_i \quad E'_{qi} \quad E_{fdi}]^T$

$\mathbf{u} = [\mathbf{u}_1^T \quad \mathbf{u}_2^T \ldots \mathbf{u}_i^T \ldots \mathbf{u}_{m_g}^T]^T, \qquad \mathbf{u_i} = [T_{Mi} \quad V_{ref_i}]^T$

From eigenvalues of $\mathbf{A}_{sys}$, the critical eigenvalue ($\lambda_c = \alpha_c + j\gamma_c$) is identified. For the system to be dynamically stable in the probabilistic sense, the probability of α_c being in the left hand side (LHS) of the complex plane should exceed some pre-specified value. Mathematically, this can be expressed as

$$P\{\alpha_c < 0\} > \beta_\alpha \tag{3.6}$$

where, α_c is real part of critical eigenvalue, $0 < \beta_\alpha < 1$ is specified probability level for ensuring the system stability and $P(x)$ denotes the probability of the random variable $'x'$.

(3) **Probabilistic operational Inequality Constraints**: The optimal configuration of the DS should guarantee that the probability of bus voltages and branch currents staying within their respective limits should exceed some pre-specified limits. Thus, these constraints are given as,

$$P_V = P\{V_k^{min} \leq V_k \leq V_k^{max}\} > \beta_V \tag{3.7}$$

$$P_I = P\{|I_{k,k+1}| \leq |I_{k,k+1}^{max}|\} > \beta_I \quad k \in B_L \tag{3.8}$$

where V_k^{min} and V_k^{max} are minimum and maximum allowable voltage magnitude of the k^{th} bus, respectively. $|I_{k,k+1}|$ is the magnitude of current flow in the branch $(k, k+1)$ and $|I_{k,k+1}^{max}|$ is the maximum allowable current flow in that branch. $0 < \beta_V < 1$ and $0 < \beta_I < 1$ are the probability levels specified according to operational requirements.

3.3 STOCHASTIC DISTRIBUTION SYSTEM RECONFIGURATION (SDSR)

A two-stage KnEA-PE technique is employed for solving the DSR problem. In the first stage, the point estimation method (PEM) [77] is implemented to evaluate the probabilistic objective function and constraints. In the second stage, a knee point driven evolutionary algorithm (KnEA) is implemented to determine the optimal control variables that would optimize the objective functions as well as satisfy all probabilistic operational and stability constraints along with topological constraint.

3.3.1 Consideration of uncertainties with PEM technique

The PEM is a well known approach for handling uncertainty which requires deterministic evaluations of few samples for calculating the moments of the output random variables and provides the results with adequate accuracy in less computational time.

3.3.1.1 Basic Point Estimate Method

In this work, the effect of uncertainty associated with SHPP power generations and load demands has been incorporated by using the three-point estimation method (3PEM) [77]. In the proposed DSR formulation, the uncertain and uncorrelated input variables can be represented as a vector $(z_1, z_2, ..., z_l, ..., z_m)$ with $m = 2L + m_g$, where L is the number of load buses with randomly varying active or reactive power demands. The 3PEM utilizes three probability concentrations to

approximate the PDF f_l (of random variable z_l) as follows.

$$z_{l,k} = \mu_{zl} + \varepsilon_{l,k}\sigma_{zl} \qquad k = 1, 2, 3 \tag{3.9}$$

where $\varepsilon_{l,k}$ is the standard location, μ_{zl} is the mean and σ_{zl} is the standard deviation of z_l. The basic steps of 3PEM are as follows [77].

1. The standard locations $\varepsilon_{l,k}$ are calculated using equation (3.10)

$$\varepsilon_{l,k} = \frac{\lambda_{l,3}}{2} + (-1)^{3-k}\sqrt{\lambda_{l,4} - \frac{3}{4}\lambda_{l,3}^2}, \quad k = 1, 2; \quad \varepsilon_{l,3} = 0, \;\; k = 3 \tag{3.10}$$

where $\lambda_{l,3}$ and $\lambda_{l,4}$ are coefficients of skewness and kurtosis of z_l respectively.

2. The three-point estimates of PDF f_l (denoted as $z_{l,1}$, $z_{l,2}$ and $z_{l,3}$ respectively) are obtained from equation (3.9). Further, the weighting factor $w_{l,k}$ corresponding to location $z_{l,k}$ is calculated as

$$w_{l,k} = \frac{(-1)^{3-k}}{\varepsilon_{l,k}(\varepsilon_{l,1} - \varepsilon_{l,2})}, \quad k = 1, 2; \quad w_{l,k} = \frac{1}{m} - \frac{1}{\lambda_{l,4} - \lambda_{l,3}^2}, \;\; k = 3 \tag{3.11}$$

Once the points and weights for all random variables are obtained, the following procedure is adopted for evaluating the probabilistic objective functions and constraints.

1. Form the input matrices $\mathbf{Z_1}$and $\mathbf{Z_2}$ as:

$$\mathbf{Z_k} = \begin{bmatrix} z_{1,k} & \mu_{z2} & \dots & \mu_{zm} \\ \mu_{z1} & z_{2,k} & \dots & \mu_{zm} \\ \vdots & \vdots & \ddots & \vdots \\ \mu_{z1} & \mu_{z2} & \dots & z_{m,k} \end{bmatrix} \tag{3.12}$$

where, k = 1, 2. Lastly, a mean value vector $\mathbf{Z_{mean}} = [\mu_{z1} \quad \mu_{z2} \quad \dots \quad \mu_{zm}]$ is formed for $k = 3$ by setting $\varepsilon_{l,3} = 0$ and $z_{l,3} = \mu_{zl}$. As a result, the total number of concentrations becomes 2m+ 1.

2. For $\mathbf{Z_{mean}}$ and each row of $\mathbf{Z_k}$, power flow and small signal stability analysis are carried out to evaluate the corresponding values of output variable s. These values are denoted as $s_{l,k}$ (corresponding to the input matrix $\mathbf{Z_k}$, k=1,2) and $s_{l,3}$ (obtained corresponding to the mean vector $\mathbf{Z_{mean}}$). It is to be noted that $l = 1, 2...m$.

3. Subsequently, the j^{th}-order moment mo_j of output s is calculated as,

$$mo_j = E(s^j) = \sum_{l=1}^{m}\sum_{k=1}^{2} w_{l,k}.(s_{l,k})^j + \sum_{l=1}^{m} w_{l,3}.(s_{l,3})^j \tag{3.13}$$

Using these moments, the expected values and cumulative distribution function (CDFs) of the output variables are obtained. The output variables include the bus voltages, branch current flows,

and eigenvalues of critical mode. The cumulative probabilities of the output variables are obtained using the Gram-Charlier expansion [78].

3.3.1.2 Consideration of correlation

The 3PEM described in Section 3.3.1.1 does not consider correlations between load demand and the power output of DGs. In this work, real and reactive loads are assumed to be normally distributed. Therefore, the correlated loads are first transformed to uncorrelated variables using Cholesky decomposition. The details of Cholesky decomposition are given in [79]. However, in this work, power generated by the DGs follows discrete distribution (non-normal distribution). Further, these power outputs are assumed to be correlated with each other (defined by a given correlation matrix). A transformation method has been implemented to handle the non-normal correlated SHPP power outputs. The details of the 3PEM with correlated input variables are given below.

Let $\mathbf{C_w}$ be the correlations matrix of the input random variables $w_1, w_2 ... w_{m_g}$

$$\mathbf{C_w} = \begin{bmatrix} 1 & \rho_{12} & ... & \rho_{1_{m_g}} \\ \rho_{21} & 1 & ... & \rho_{2_{m_g}} \\ \vdots & \vdots & \ddots & \vdots \\ \rho_{1n} & \rho_{2_{m_g}} & ... & 1 \end{bmatrix} \tag{3.14}$$

Where ρ_{ij} is the correlation coefficient between i^{th} and j^{th} random variables. In order to deal with correlated variables with non-normal probability distributions, random variables are transformed into the standard normal variables using Nataf Transformation [80]. The standard normal variables $x_1, x_2, ...x_{m_g}$ are obtained using equation (3.15)

$$x_i = \phi^{-1}[F_i(w_i)], \quad i = 1, 2...m_g \tag{3.15}$$

where F_i is the CDF of w_i and $\phi(.)$ is the CDF of standard normal distribution of x_i. Then, the modified correlation coefficient matrix $\mathbf{C_{mw}}$ of standard normally distributed random vector $\mathbf{x} = [x_1, x_2 ... x_{m_g}]^T$ is obtained from the matrix $\mathbf{C_w}$ following the procedure given in [80]. Subsequently, the correlation matrix $\mathbf{C_{mw}}$, which is equal to the covariance matrix for standard normal distribution, is decomposed using the Cholesky decomposition as

$$\mathbf{C_{mw}} = \mathbf{L}\mathbf{L}^\mathbf{T} \tag{3.16}$$

where $\mathbf{L}$ is the lower triangular matrix. The relation between the correlated standard normal random vector $\mathbf{X}$ and uncorrelated standard normal vector $\mathbf{U}$ is given by $\mathbf{U} = \mathbf{L^{-1}X}$.

In order to implement the 3PEM, with non-normal correlated random variables, following steps are followed.

1. Calculate matrix $\mathbf{L}$ from $\mathbf{C_{mw}}$ using equation (3.16).

2. The first four moments of uncorrelated standard normal distribution variables are calculated corresponding to the power output of DGs.

3. Compute the probability concentrations u_{ik} $(i = 1, 2...m_g, k = 1, 2, 3)$ and the associated weighting factors of uncorrelated normal distribution variables using equations (3.9) - (3.11). Subsequently, construct the $2m_g + 1$ uncorrelated normal distribution vector $\mathbf{U}$ according to equation (3.17) as

$$\mathbf{U} = \begin{bmatrix} \mathbf{U_1} \\ \mathbf{U_2} \\ \mathbf{U}_\mu \end{bmatrix} \tag{3.17}$$

where,

$$\mathbf{U_k} = \begin{bmatrix} u_{1,k} & \mu_{x2} & \dots & \mu_{x_{m_g}} \\ \mu_{x1} & u_{2,k} & \dots & \mu_{x_{m_g}} \\ \vdots & \vdots & \ddots & \vdots \\ \mu_{x1} & \mu_{x2} & \dots & u_{m_g,k} \end{bmatrix} \quad \textbf{and} \quad \mathbf{U}_\mu = \begin{bmatrix} \mu_{x1} & \mu_{x2} & \dots & \mu_{x_{m_g}} \end{bmatrix}$$

k=1,2.

4. The vector $\mathbf{U}$ is transformed back to the correlated normal distribution vector $\mathbf{X}$ using $\mathbf{X} = \mathbf{LU^T}$.

5. Calculate the correlated distribution variable w_i using the inverse of equation (3.15) as follows

$$w_i = F_i^{-1}[\phi(x_i)], \quad i = 1, 2...m_g \tag{3.18}$$

6. Obtain the moments of output variables using equation (3.13) with transformed correlated variables and the remaining uncorrelated variables.

3.3.2 Application of KnEA-PEM for solving the DSR problem

The procedure for application of KnEA-PEM for solving the DSR problem under uncertainties is outlined below.

1) For a given distribution test system, input the system data and specify KnEA parameters such as k, T, r_o, t_o and g_{max} (maximum number of iterations).

2) Generate initial parent population X_o of size N_p randomly that fulfills the radiality constraint and set iteration count g = 1.

3)The probabilistic output random variables (bus voltages, branch power flows and eigenvalue of critical mode) are calculated as described in Subsection 3.3.1 and subsequently objective functions given in equations (3.2), (3.3) and (3.4) are evaluated using uncertain output variables for each individual of X_0.

4) The expected value of objective functions and cumulative probabilities of steady-state bus voltages, branch current flows in equations (3.7), (3.8) are estimated based on 2m + 1 deterministic load flow results and cumulative probabilities of α_c (critical mode eigenvalue) are calculated based on the results of 2m + 1 deterministic small signal stability (SSSA).

5) The probabilistic stability constraint is evaluated from the CDF of the critical mode. If any configuration (represented by a string) is probabilistically unstable then this configuration is removed from the solution space by the addition of large penalty factor values to all the objective functions.

6) The probabilistic voltage and current constraints given in equation (3.7) and (3.8) respectively are checked for all stable N_p strings. Any violation of the operational constraints is tackled by using the penalty factors as follows:

$PT = \lambda_1[\sum_{k\in C_{VL}}(V_k - V_k^{min})^2 + \sum_{k\in C_{VU}}(V_k - V_k^{max})^2] + \lambda_2[\sum_{k\in C_{IU}}(I_{k,k+1} - I_{k,k+1}^{max})^2]$

where λ_1 and λ_2 are the penalty factors, C_{VU} and C_{VL} are the set of all buses with maximum and minimum voltage limit violation, respectively. Further, $C_{VL} \cap C_{VU} = \emptyset$, where $\emptyset$ is the null set. C_{IU} is the set of all branches with maximum current limit violation. Infeasible solutions are removed by the addition of PT having large penalty factor values.

7) Perform effective non-dominated ranking (ENS) [68] and binary tournament mating selection, crossover and mutation [81] on X_g and generate new strings as offspring population Y_g. Examine the probabilistic constraints and afterwards calculate the objective functions for strings in Y_g and

construct a combined population $R_g = X_g \cup Y_g$.

8) Decide the ranking of non dominated front using ENS [68]. Knee points are identified for combined population, as detailed in Chapter 2.

9) Select the next generation parent population X_{g+1} based on dominance comparison followed by knee point criterion, and distance from hyperplane, to form size of X_{g+1} exactly equal to N_p.

10) Increase the iteration count $g = g + 1$. Terminate the execution, if the iteration count reaches the maximum specified number of iteration, else go to step 3.

11) The outcome consists of expected value of optimal solutions (nondominated solutions). The best solution from the solution vectors N_p is selected based on normalized function [69] as explained in Section 2.3.8 of Chapter 2.

3.4 CASE STUDIES

The effectiveness of the presented methodology has been investigated on IEEE 33-bus, IEEE 69-bus and 119-bus radial distribution systems with SHPP type of DGs. For all three systems, location of DGs and their maximum capacities are assumed to be same as used for deterministic analysis in Chapter 2. All DG nodes are modeled as voltage controlled nodes. The rated terminal voltage magnitude of each DG is 1 p.u. In order to ensure the critical mode's stability, value of β_α is taken as 0.99. The values for β_V and β_I are assumed as 0.95. The performance of KnEA has been investigated by comparing the results obtained by KnEA with the results obtained by 'NSGA-II'. To compare the results obtained by KnEA and NSGA-II, for any particular distribution system, the population size, crossover and mutation probability values are kept same. Further, for all three systems, the values of KnEA parameters and penalty factors are same as given in Chapter 2. Lastly, the loads are assumed to have Gaussian probability density function with load values (real and reactive) given in [15], [72] and [73] taken as mean values. The standard deviations assumed for real and reactive power loads are 7% of the respective mean values. In this work, DSR has been carried out for the following four cases:

Case A: DSR without correlated variables.

Case B: DSR with only load correlation.

Case C: DSR with only DG correlation.

Case D: DSR with both load and DG correlation.

Further, to validate the effectiveness of probabilistic evaluation, for case D, CDFs of the probabilistic constraints (real part of critical eigenvalue α_c, bus voltage and branch current flow) before (shown with solid line) and after (shown with dashed line) reconfiguration are plotted for all three test systems. For this, the bus with minimum voltage magnitude and the line which is carrying current nearest to the prespecified limit are selected to reflect the changes of bus voltage magnitude and line current flow comprehensively.

3.4.1 Test System 1

Three SHPP type DGs are considered at buses 18, 30, and 33. The maximum capacities of the DG units considered are 100 kW, 110 kW and 1.1 MW respectively. These values correspond to 100% output power of DG in Table 3.1. These DGs are assumed to be correlated with each other with a correlation matrix $\mathbf{C_w}$ given in equation (3.19). In this system, loads at bus numbers 19, 20, 21 and 22 are also assumed to be correlated with each other with a correlation matrix $\mathbf{C_{wl}}$ given in equation (3.19).

$$\mathbf{C_w} = \begin{bmatrix} 1 & 0.3 & 0.3 \\ 0.3 & 1 & 0.3 \\ 0.3 & 0.3 & 1 \end{bmatrix} \qquad \mathbf{C_{wl}} = \begin{bmatrix} 1 & 0.8 & 0.7 & 0.5 \\ 0.8 & 1 & 0.7 & 0.6 \\ 0.7 & 0.7 & 1 & 0.5 \\ 0.5 & 0.6 & 0.5 & 1 \end{bmatrix} \tag{3.19}$$

The simulation results for this system are shown in Table 3.2 for all four cases. This table shows that incorporation of correlation results in significant changes in the final solution.

A comparison of all cases shows that the original configuration is unstable with and without correlation (as $P\{\alpha_c < 0\} < \beta_\alpha$ for all the cases). Moreover, the correlation among DGs has more influence on the probabilistic instability than the load correlation. This unstable system is subsequently made stable through reconfiguration. Compared with the initial case, the proposed DSR methodology improves the performance of the system by reducing the power loss and increasing the voltage stability margin. In this chapter, all objective functions are equally preferred and thus, as discussed in Section 2.3.8, the best solution is selected on summing the normalised values of all objective functions. It can be seen that with the consideration of correlation, the system performance changes a little (as power loss increases and the stability margin reduces marginally compared to case A). Further, correlation among DGs has more pronounced effect on the final

Table 3.2: Result of 33-bus distribution system

	Case A	Case B	Case C	Case D
Initial case				
Power loss(kW)	98.457	99.228	98.915	99.411
Voltage stability index	0.21872	0.21914	0.22050	0.21912
Switching number	0	0	0	0
$P\{\alpha_c < 0\}$	0.952	0.952	0.9360	0.9340
Stability status	unstable	unstable	unstable	unstable
Reconfigured system				
Open switch	s9,s16,s33,s34,s37	s9,s16,s33,s34,s37	s11,s29,s33,s34,s37	s11,s29,s33,s34,s37
Power loss(kW)	73.614	74.314	78.740	79.2824
Voltage stability index	0.135013	0.135488	0.164343	0.160524
Switching number	4	4	4	4
$P\{\alpha_c < 0\}$	0.999	0.998	0.998	0.997
Stability status	stable	stable	stable	stable

configuration than the correlation among loads (as results of case C and case D are quite similar to each other while the results of case B and case C are comparatively different). Therefore, the final topological structures of DS for case C and D are different from those obtained for case A and B. To show the changes occurred in probabilistic constraints due to reconfiguration, CDFs of different constraints before (solid line) and after (dashed line) reconfiguration for case D are depicted in Fig 3.1. In Fig 3.1, CDF of α_c, voltage magnitude of bus 18 and current flow in line 3-4, are shown. At the initial operating point before reconfiguration, the probabilistic stability and current carrying limit constraints are not satisfied with the acceptable confidence level as shown in Fig. 3.1. As depicted in Fig. 3.1(a), the critical mode eigenvalue has a probability of 0.9340 to remain in the left hand side of the complex plane which indicates that the system could become unstable with a possibility of 6.6%. After DS reconfiguration, as shown in Fig. 3.1(a), the probability at point B is 0.998 which indicates that the probability of the system being stable is very high. On the other hand, the probability at point C in Fig. 3.1(b) is 0.005 and therefore, the probability of voltage magnitude of bus 18 being in the range of [0.90, 1.05] is 0.995 ($1 - 0.005 = 0.995$). This indicates that the probabilistic voltage constraint is maintained with the satisfactory confidence level. Before

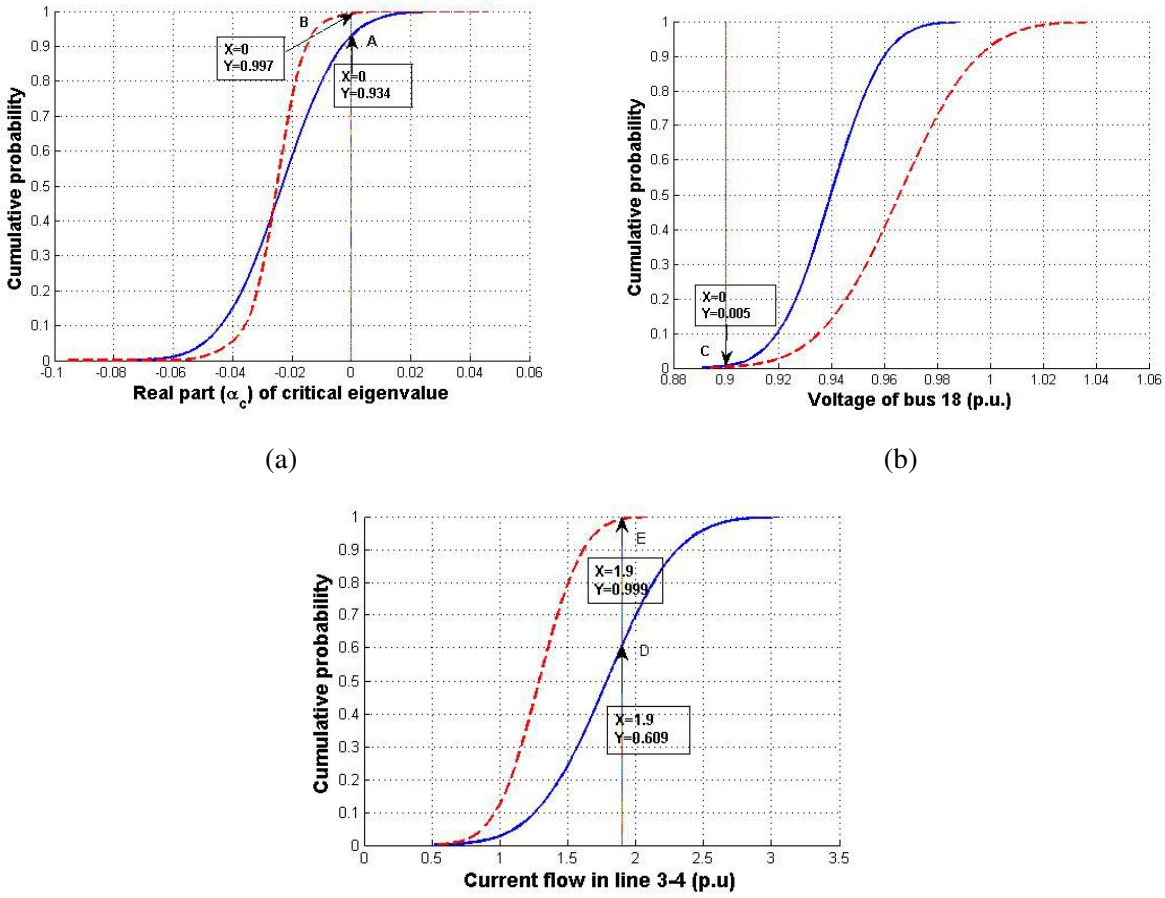

Figure 3.1: CDFs of the probabilistic constraints before (solid line) and after (dashed line) reconfiguration for 33-bus system.

reconfiguration, the branch current constraint for line 3-4 is also violated as shown in Fig. 3.1(c) as the probability at point D is 0.609 indicating that the probability of over-loading for line 3-4 is $1 - 0.609 = 0.391$. After reconfiguration, the probability of current flow in line 3-4 to become more than the current carrying limit is only 0.001 (as shown in Fig. 3.1(c)). Thus, the optimized configuration is probabilistically stable and all other probabilistic constraints are also satisfied as shown in Fig. 3.1. Hence, while considering uncertainties, the proposed method guarantees that all probabilistic constraints are satisfied during reconfiguration.

3.4.2 Test System 2

Three SHPP type DGs connected to buses 63, 64 and 65 are considered to have maximum active power capacity of 0.550, 0.750 and 1.2 MW respectively. These values correspond to 100% output power of DGs in Table 3.1. For test system 2, the values of the parameters of KnEA algorithm are same as that of test system 1. The same correlation matrix $\mathbf{C_w}$ given in equation (3.19), has been used for the power output of SHPP. In this system, loads at bus number 26, 27, 28 and 29 are also assumed to be correlated with each other with a correlation matrix $\mathbf{C_{wl}}$ given in equation (3.19). For a further evaluation of the proposed algorithm, results of the above mentioned four cases are shown in Table 3.3.

Table 3.3: Result of 69-bus distribution system

	Case A	Case B	Case C	Case D
Initial case				
Power loss(kW)	86.335	90.256	67.406	67.312
Voltage stability index	0.16671	0.18367	0.162047	0.157062
Switching number	0	0	0	0
$P\{\alpha_c < 0\}$	0.9537	0.9542	0.856	0.8480
Stability status	unstable	unstable	unstable	unstable
Reconfigured system				
Open switch	s9,s16,s24,s58,s71	s9,s16,s24,s58,s71	s12,s18,s58,s69,s71	s12,s18,s58,s69,s71
Power loss(kW)	34.0288	32.651	42.141	42.574
Voltage stability index	0.09462	0.094718	0.083939	0.084716
Switching number	8	8	6	6
$P\{\alpha_c < 0\}$	0.991	0.991	0.995	0.996
Stability status	stable	stable	stable	stable

For initial case, the probability of the critical eigenvalue remaining in the left half-plane is 0.8480. Hence the system could become unstable with possibility of 15.2%, when the stochastic variation of load and SHPP generation is considered with correlation. This can be made stable

through reconfiguration with the acceptable security level as shown in Fig. 3.2(a) and Table 3.3. Similarly, Fig. 3.2(c) shows that before reconfiguration, the current carrying limit in line 5-6 is not satisfied with the acceptable confidence limit but after reconfiguration, the desired confidence level is obtained for this constraint.

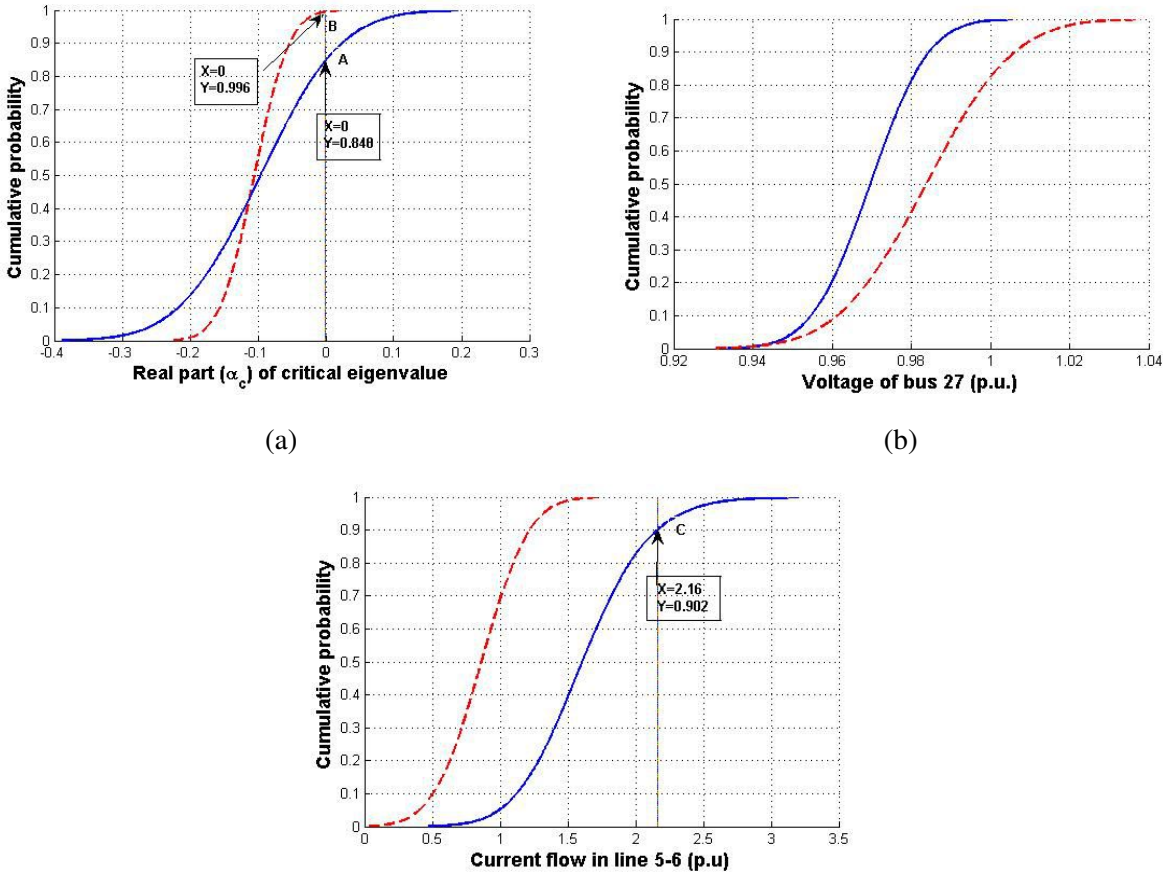

Figure 3.2: CDFs of the probabilistic constraints before (solid line) and after (dashed line) reconfiguration for 69-bus system.

3.4.3 Test System 3

Four SHPP type DGs connected to buses 55, 72, 78, and 119 are considered to have maximum active power capacity of 2.5, 2, 1.5 and 1 MW respectively. These values correspond to 100% output power of DG in Table 3.1. Various parameters used in KnEA technique are as follows: the population size is 40, maximum number of iteration is 20 and mutation and crossover probability

are 0.18 and 0.9, respectively. The correlation matrix $\mathbf{C_w}$ assumed for these four SHPPs is given in equation (3.20).

$$\mathbf{C_w} = \begin{bmatrix} 1 & 0.1 & 0.1 & 0.1 \\ 0.1 & 1 & 0.1 & 0.1 \\ 0.1 & 0.1 & 1 & 0.1 \\ 0.1 & 0.1 & 0.1 & 1 \end{bmatrix} \qquad \mathbf{C_{wl}} = \begin{bmatrix} 1 & 0.5 & 0.3 & 0.25 & 0.2 \\ 0.5 & 1 & 0.3 & 0.3 & 0.3 \\ 0.3 & 0.3 & 1 & 0.55 & 0.6 \\ 0.25 & 0.3 & 0.55 & 1 & 0.2 \\ 0.2 & 0.3 & 0.6 & 0.2 & 1 \end{bmatrix} \tag{3.20}$$

Further, the loads at buses 92, 93, 94, 95 and 96 are assumed to be correlated with each other with a correlation matrix $\mathbf{C_{wl}}$ given in equation (3.20). The simulation results corresponding to all the objective functions with stability degree are shown in Table 3.4 for all four cases.

Table 3.4: Result of 119-bus distribution system

	Case A	Case B	Case C	Case D
Initial case				
Power loss(kW)	779.029	779.344	781.189	781.432
Voltage stability index	0.327453	0.327537	0.327496	0.327059
Switching number	0	0	0	0
$P\{\alpha_e < 0\}$	0.7247	0.725	0.712	0.712
Stability status	unstable	unstable	unstable	unstable
Reconfigured system				
Open switch	s23,s27,s35,s39,s44, s75,s77,s110,s123, s125,s126,s127,s128, s131,s132	s23,s27,s35,s39,s44, s75,s77,s110,s123, s125,s126,s127,s128, s131,s132	s23,s27,s35,s39,s44, s75,s97,s110,s123, s125,s126,s127,s128, s131,s132	s23,s27,s35,s39,s44,s75, s97,s110,s123,s125,s126, s127,s128,s131,s132
Power loss(kW)	536.379	536.882	527.150	527.757
Voltage stability index	0.19307	0.193209	0.202187	0.196650
Switching number	16	16	16	16
$P\{\alpha_e < 0\}$	0.9980	0.9980	0.9980	0.9980
Stability status	stable	stable	stable	stable

From this table, it is observed that initially, the system (before reconfiguration) is unstable. However, after reconfiguration, the system becomes stable although, with the consideration of

correlation, the stability of the system reduces marginally. Further, for this system also, the results corresponding to case C and case D are quite similar. On the other hand, there are some appreciable differences between the results of case B and case C. Thus, for this system also, it can be concluded that the correlation among DGs has more pronounced effect on the final configuration of DS than the correlation among the loads. Fig. 3.3 depicts the CDFs of the operating constraints and stability constraints before and after reconfiguration. For initial case, all the probabilistic constraints are not satisfied with the acceptable confidence level. For example, it can be observed from Fig. 3.3(a) that before reconfiguration, the system is unstable with a probability of 0.712 and after reconfiguration, the system becomes stable with a high probability of 0.998.

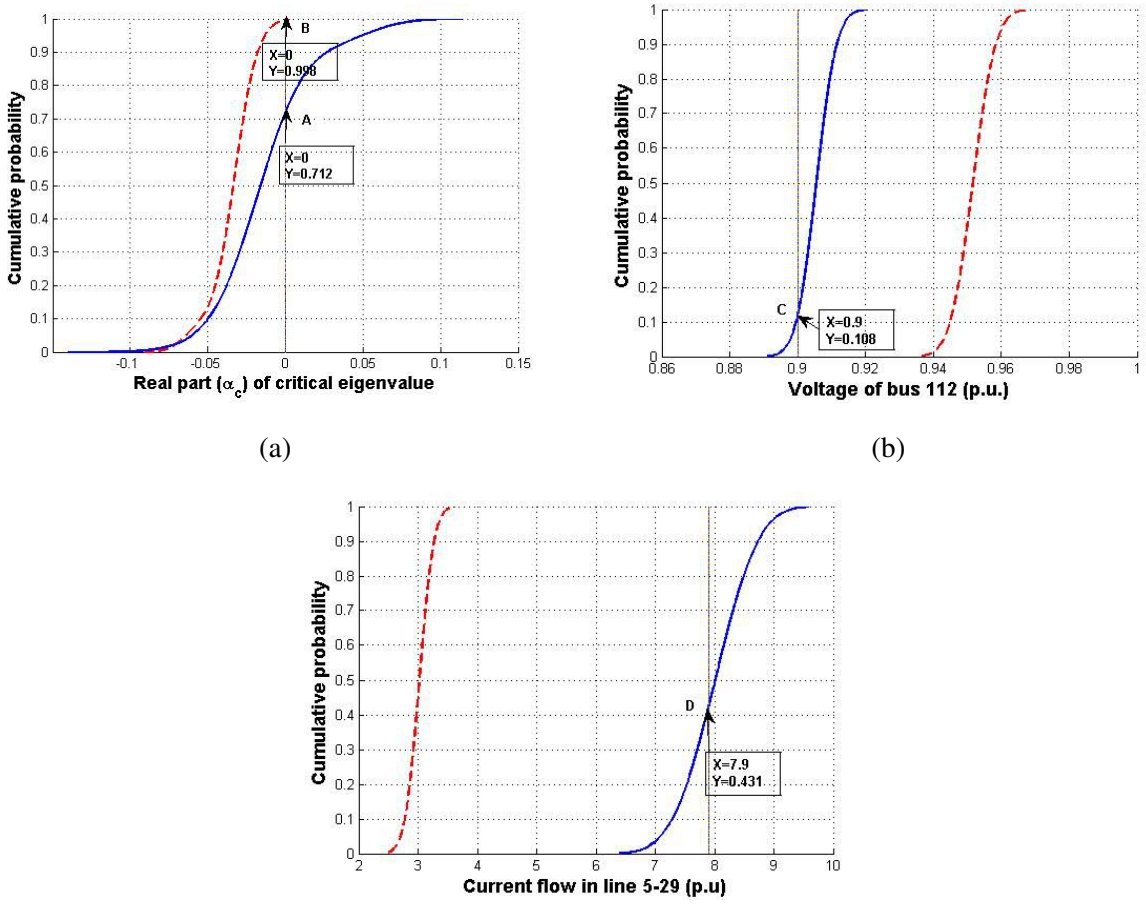

Figure 3.3: CDFs of the probabilistic constraints before (solid line) and after (dashed line) reconfiguration for 119-bus system.

Similarly, Fig. 3.3(b) shows that before reconfiguration, the probability of voltage magnitude of bus 112 being in range [0.9, 1.05] is $1 - 0.108 = 0.892$. This indicates that the probabilistic voltage constraint is not satisfied with the desired confidence level of 0.95. After reconfiguration, the desired confidence level is attained for this constraint. Moreover, as shown in Fig. 3.3(c), before reconfiguration, the probability of overloading at point D is 0.431 which indicates that the current carrying limit is not satisfied with the acceptable confidence limit. After reconfiguration, the probability of current flow in line $5 - 29$ to remain below the current carrying limit is 1. Thus, it is again observed from Fig. 3.3 that the presented DSR formulation satisfy all the probabilistic constraints with acceptable confidence level.

For this test system, Fig. 3.4 demonstrates the MOOP nature of the DSR problem. As observed from this figure, number of switching operations observes pareto optimality with power loss and voltage stability margin as depicted in Fig. 3.4(a) and Fig. 3.4(b), respectively.

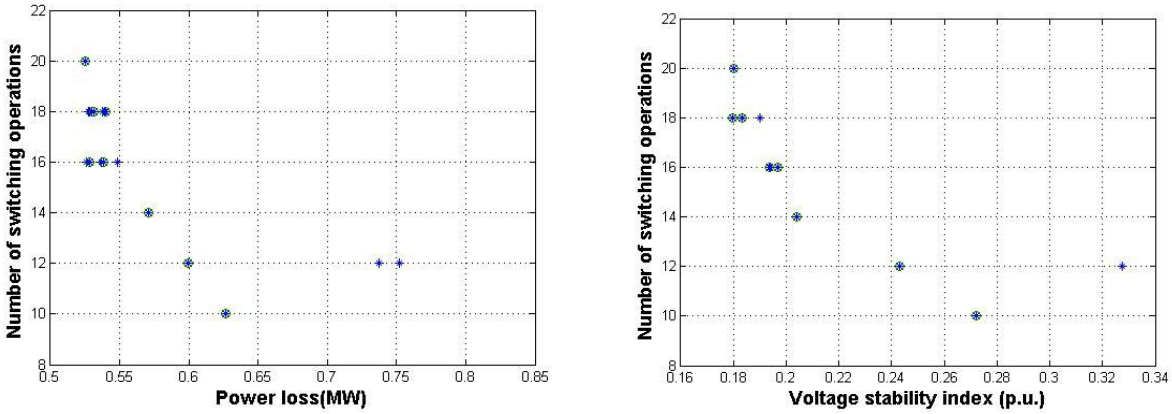

(a) (b)

Figure 3.4: Obtained Pareto front for test system 3 using KnEA

To investigate the comparative performance of KnEA and NSGA-II, the results obtained by both the approaches are shown in Table 3.5 for the three test systems considered. This table shows that the results obtained by these two methods are quite comparable for 33-bus and 69-bus systems. For 119-bus system, the expected power loss and the number of switching operations obtained with KnEA are smaller than those obtained by NSGA-II. Therefore, it can be concluded that the performance of the KnEA is better than that of NSGA-II.

Table 3.5: Comparison of two algorithms for case D

Status	Open switches	Expected Power loss(kW)	Expected Voltage stability index	Switching number	$P\{\alpha_c < 0\}$	Stability status
33-bus system						
KnEA	s11,s29,s33,s34, s37	79.282	0.160524	4	0.998	stable
NSGA-II	s9,s29,s33,s34, s37	79.231	0.178108	4	0.998	stable
69-bus system						
KnEA	s12,s18,s58,s69,s71	42.574	0.084716	6	0.996	stable
NSGA-II	s12,s20,s56,s69,s71	42.81	0.08649	6	0.996	stable
119-bus system						
KnEA	s23,s27,s35,s39,s44,s75,s97,s110, s123,s125,s126,s127,s128,s131,s132	527.757	0.196650	16	0.998	stable
NSGA-II	s23,s27,s35,s39,s44,s69,s74,s98,s110, s123,s125,s126,s127,s131,s132	529.235	0.1795541	18	0.998	stable

From the results of these three test systems, it is observed that the correlation among the DGs has more pronounced effect on the final result than the correlation among the loads. This is due to the fact that in this work, stability issues have been considered for the DSR problem. In this work, only passive loads have been considered and therefore, the stability of the system is entirely determined by the dynamics of the DGs. As stability is an integral part of the proposed DSR formulation, dynamics of the DGs play a major role in the final solution. As a result, the correlation among the DGs plays more prominent role in the final solution than the correlation among the passive loads. Further, in all the above studies, a fixed correlation matrix and constant power loads only have been considered. To investigate the performance of proposed algorithm for different levels of correlation, following additional studies have also been carried out.

3.4.4 FURTHER STUDIES

To investigate the effect of different levels of correlation among the DGs and the loads, analysis has been carried out on test system 3 considering different correlation matrices. The results are given in Table 3.6 and 3.7. In Table 3.6, only the correlation among loads is considered while in Table 3.7, only the correlation among the DGs is considered. For Table 3.6, the considered correlation matrix $\mathbf{C_{wl}}$, and for Table 3.7, the considered correlation matrix $\mathbf{C_w}$ are given in equation (3.21). In these two tables, the quantity 'r1' denotes the correlation coefficient. In this study, three different

values of 'r1' namely 0.3, 0.5 and 0.8 have been considered.

$$\mathbf{C_{wl}} = \begin{bmatrix} 1 & r1 & r1 & r1 & r1 \\ r1 & 1 & r1 & r1 & r1 \\ r1 & r1 & 1 & r1 & r1 \\ r1 & r1 & r1 & 1 & r1 \\ r1 & r1 & r1 & r1 & 1 \end{bmatrix} \qquad \mathbf{C_w} = \begin{bmatrix} 1 & r1 & r1 & r1 \\ r1 & 1 & r1 & r1 \\ r1 & r1 & 1 & r1 \\ r1 & r1 & r1 & 1 \end{bmatrix} \tag{3.21}$$

From Table 3.6, it is observed that the correlation only among the loads has a marginal effect on the final results of reconfiguration. In fact, Table 3.6 shows that when the correlation among the loads is considered, the level of correlation does not have any effect on the final configuration of the system and the number of switching operations.

Table 3.6: Reconfiguration of test system 3, considering different levels of correlation among loads

	r1=0.3	r1=0.5	r1=0.8
Initial case			
Power loss(kW)	779.950	780.156	778.760
Voltage stability index	0.32768	0.32736	0.32753
Switching number	0	0	0
$P\{\alpha_c < 0\}$	0.7239	0.72814	0.72622
Stability status	unstable	unstable	unstable
Reconfigured system			
Open switch	s23,s27,s35,s39,s44,s75, s77,s110,s123,s125,s126, s127,s128,s131,s132	s23,s27,s35,s39,s44,s75, s77,s110,s123,s125,s126, s127,s128,s131,s132	s23,s27,s35,s39,s44,s75, s77,s110,s123,s125,s126, s127,s128,s131,s132
Power loss(kW)	536.792	537.431	537.174
Voltage stability index	0.192824	0.193212	0.193143
Switching number	16	16	16
$P\{\alpha_c < 0\}$	0.99003	0.99001	0.99006
Stability status	stable	stable	stable

Also, with variation in correlation level, power loss of the system, voltage stability index and

small signal stability index change very marginally. On the other hand, Table 3.7 shows that the correlation among the DGs has much more pronounced effect on the final result of reconfiguration. With the variation of correlation level among the DGs, the final configuration of the system and the number of switching in the system change quite significantly, although the changes in power loss, voltage stability index and small signal stability index are much less pronounced.

Table 3.7: Reconfiguration of test system 3, considering different levels of correlation among DGs

	r1=0.3	r1=0.5	r1=0.8
Initial case			
Power loss(kW)	782.339	779.47766	788.5543
Voltage stability index	0.327508	0.327300	0.3274103
Switching number	0	0	0
$P\{\alpha_c < 0\}$	0.689	0.737	0.625
Stability status	unstable	unstable	unstable
Reconfigured system			
Open switch	s23,s27,s35,s39,s44,s75,s97, s110,s123,s125,s126,s127,s128, s131,s132	s23,s39,s74,s98,s110,s121,s122, s123,s124,s125,s126,s127,s128, s131,s132	s23,s39,s43,s75,s97,s110,s121, s122,s123,s124,s125,s126,s127, s128,s131,s132
Power loss(kW)	527.150	546.667	538.438
Voltage stability index	0.1894325	0.17953	0.197933
Switching number	16	10	12
$P\{\alpha_c < 0\}$	0.9950	0.9990	0.9910
Stability status	stable	stable	stable

3.5 CONCLUSION

In this chapter, a probabilistic small signal stability constrained multi-objective distribution system reconfiguration problem has been formulated. Subsequently, application of KnEA-PE approach has been proposed to solve the formulated problem with an acceptable confidence level. The developed procedure has been tested on IEEE-33, 69 and 119 bus systems and the results show that stability of dynamically unstable DS is achieved through reconfiguration with a desired confidence

level. The correlation between the SHPP-DGs and between loads has been taken into consideration and it has been found out that correlation among the uncertain load demand and among the uncertain DG power output have an influence on the final configuration of the system. Moreover, correlation among DGs has more pronounced effect on the final configuration than the correlation among the loads.

The impact of network reconfiguration on small signal stability margin of the distribution system is analyzed in the next chapter in the presence of photovoltaic based distributed generation (PV-DGs) and small hydro power plant based DG (SHPP-DGs).

Chapter 4

Stochastic Distribution system reconfiguration considering stability, correlated PV and SHPP DGs

This chapter explores applications of KnEA-PE approach in the small-signal stability constrained DSR in the presence of uncertain and correlated solar photovoltaic generation, generation from SHPP based DGs and load demands. Further, the impact of PV penetration on the small signal stability constrained DSR is assessed. It is also shown that the stochastic variation of PV-DG can cause system instability. With increasing level of PV-DG penetration, the probability of the system becoming unstable increases. Therefore, to deal with such unstable status, distribution system is reconfigured to achieve stable topology.

4.1 Introduction

In the last chapter, integration of only SHPP-DGs are considered during reconfiguration. However, recently, focus on green energy technologies has significantly increased the deployment of renewable energy source based DGs in the DS. These renewable energy based DGs (RES-DGs) are characterised by high level of intermittent and uncertain power generation. Large scale incorporation of these renewable energy based DGs, such as photovoltaic DGs (PV-DGs), small hydro power plant (SHPP) based DGs etc. makes the operating condition of the distribution system stochastic rather than deterministic.

In the literature it is shown that integration of PV-DGs does not have only positive [59] but also adverse [58]- [60] effect on system stability. When PV-DGs are introduced in the system, the system inertia reduces which, in turn, will have detrimental impact of system stability [60]. Further, the intermittent generation from PV-DGs also alters the network flows significantly [59]-[58], thereby again affecting the system stability. Therefore, in this work, probabilistic DSR is implemented to consider uncertainties associated with RES-DGs and loads. In this chapter, along with PV-DGs, SHPP-DGs have also been considered. Further, the effect of different mean values

of irradiance on the optimal final reconfiguration and probability of stability is assessed.

4.2 Problem formulation

In this case, the multi-objective constrained DSR problem is described by the objective functions in equations (3.2), (3.3), (3.4) and the voltage, current and radility constraints given in Subsection 3.2.4 of Chapter 3.

4.2.1 Uncertainty representation of PV-DGs

As PV power output is dependent on solar irradiation, for probabilistic modelling of PV power output, probability density function (PDF) of solar irradiation is required. In this work, the solar radiation PDF is assumed to follow beta distribution function [61] as given by

$$f(S,\alpha,\beta) = \frac{\Gamma(\alpha+\beta)}{\Gamma(\alpha)\Gamma(\beta)} S^{(\alpha-1)}(1-S)^{(\beta-1)} \quad 0 \leq S \leq 1, \alpha > 0 \quad and \quad \beta > 0 \tag{4.1}$$

where S is the solar irradiance (W/m^2), α and β are the shape parameters of the distribution, and Γ is the Gamma function. To calculate the parameters of the beta distribution function, the mean and standard deviation [61] of the random variable are utilized as follows:

$$\beta = (1-\mu) * (\frac{\mu * (1-\mu)}{\sigma^2} - 1) \tag{4.2}$$

$$\alpha = \frac{\mu * \beta}{1-\mu} \tag{4.3}$$

Where μ and σ are mean and standard deviation of beta distribution, respectively. The power delivered by j^{th} PV-DG is calculated as follows:

The PV array is represented by an equivalent circuit shown in Fig. 4.1 [52] and described by the following current – voltage equation [52]:

$$I_{pvj} = N_{pj}\Big\{I_{phj} - I_{0j}\Big\{\exp\Big(\frac{qV_{pvj}}{nN_{sj}kT}\Big)\Big\}\Big\} \quad 1 \leq j \leq m_{pv} \tag{4.4}$$

where V_{pvj} and I_{pvj} are the voltage and current of the array, respectively, I_{phj} is the photocurrent of one string of the array, I_{0j} is the reverse saturation current of the diode, q is the coulomb constant $(1.602 \times 10^{-19}C)$, k is Boltzmanns constant $(1.38 \times 10^{-23}J/K)$, T denotes the cell temperature and 'm_{pv}' is the number of PV-DGs. In the above circuit, I_{phj} is given by

$$I_{phj} = \frac{S}{S_{ref}}(I_{phref} + \rho(T - T_{ref})) \tag{4.5}$$

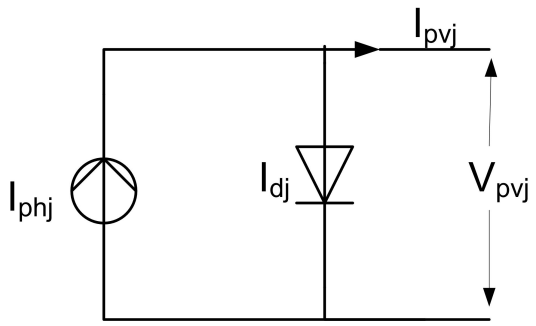

Figure 4.1: Equivalent circuit of a PV module .

where I_{phref} is the reference photocurrent current; ρ is the temperature coefficient; T_{ref} and T are the reference and actual temperature, respectively; and S_{ref} and S are the the reference solar irradiance and the actual solar irradiance, respectively.

The current I_{pvj} causes PV power (P_{PVj}) to flow. The power delivered by the PV-DG [52] can be determined using equation (4.6) as a function of S for a given temperature:

$$P_{pvj} = f(V_{pvj}, T, S) = N_{pj}\Big\{V_{pvj}I_{phj} - V_{pvj}I_{0j}\Big\{\exp\left(\frac{qV_{pvj}}{nN_{sj}kT}\right)\Big\}\Big\} \tag{4.6}$$

The output power of PV-DG is dependent on the solar irradiance and ambient temperature of the site as well as the characteristics of the module. Now, the optimum power occurs at the maximum point of P-V curve, where the slope of tangent line is equal to zero. By differentiating equation (4.6) with respect to voltage V_{pvj} and making it equal to zero, the value of voltage (V_{pvmaxj}) corresponding to maximum power is obtained. This value of voltage is substituted into equation (4.6) in order to obtain the optimum PV-DG power output.

Further, representation for uncertainties considered for SHPP output power as well as active and reactive power loads are same as described in Chapter 3.

4.2.2 Mathematical model of a photovoltaic DGs with SHPP

Let 'm_g', and 'm_{pv}' are the number of SHPP-DGs and PV-DGs connected to the distribution system, respectively. Let, $\mathbf{E} = \{e(1), e(2)...e(i)...e(m_g)\}$ and $\mathbf{E}g_{pv} = \{ep(1), ep(2)...ep(j)...ep(m_{pv})\}$ are the set of SHPP-DG and PV-DG buses, respectively, where $e(i)$ indicates the bus number at which i^{th} SHPP-DG is located. Similiarly $ep(j)$ denotes the bus number at which j^{th} PV-DG is located. Further, $2 \leq e(i), ep(j) \leq N$, and $e(i), ep(j) \neq s$, for $i = 1, 2...m_g$, and $j = 1, 2...m_{pv}$, where s is the substation bus.

Detailed mathematical model of SHPP-DGs has been presented in Chapter 2.

4.2.2.1 Mathematical model of a PV-DG

In this work, the PV array, DC/DC boost converter, maximum power point tracking control and DC/AC converter are included to form a two-stage PV-DG model [58]. From equation (4.6), it can be observed that the PV output power is affected by the irradiance and cell temperature. Thus the change in irradiance will result in the fluctuation in PV generation which will subsequently influence system stability. Therefore, depending on uncertainties of power generated by the PV-DGs, SHPP-DGs and load demands, the PDF of the critical eigenvalues is determined and subsequently, the probability of system stability can be evaluated.

Model of the DC/DC converter:

The schematic diagram of the two-stage converter system used to integrate PV-DG to the distribution system is shown below in Fig. 4.2.

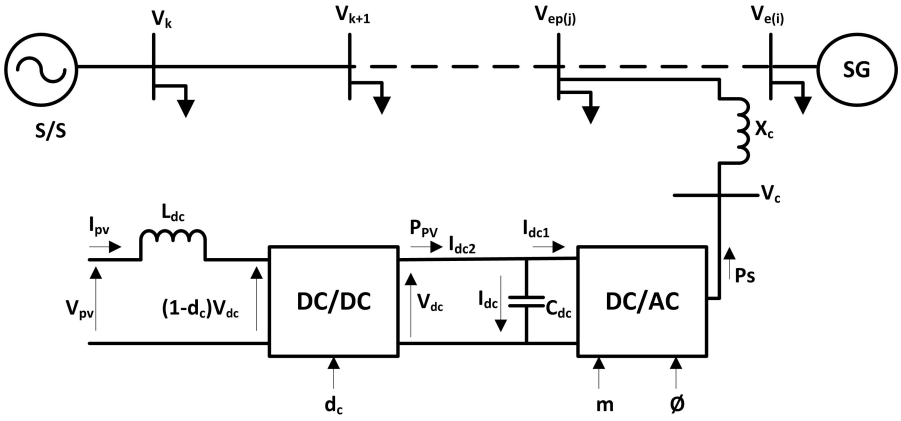

Figure 4.2: Single line diagram of a distribution system with a PV generating station.

The DC/DC converter is mainly employed for the maximum power point tracking (MPPT) control to extract maximum possible power by controlling the duty ratio d_{cj} of the DC/DC converter. The duty ratio of a converter [58] is given by

$$d_{cj} = 1 - (V_{ep(j)}/V_{dcj}) \tag{4.7}$$

where $V_{ep(j)}$ is the voltage of the $ep(j)$ bus where PV-DG is installed and V_{dcj} is the dc link voltage.

In this work, the function of the MPPT is described by the following expression [58].

$$d_{cj} = \left(K_{ppj} + \frac{K_{pij}}{s}\right)(P_{pvj} - P_{pvmax,j}) \tag{4.8}$$

In equation 4.8, K_{ppj} and K_{pij} are proportional and integral control gains of the MPPT controller, respectively.

The model of the DC/DC converter [58] is described by

$$\dot{I}_{pvj} = \frac{1}{L_{dcj}}[V_{pvj} - (1 - d_{cj})V_{dcj}] \tag{4.9}$$

Now, under steady state, $P_{pvj} = I_{pvj}V_{pvj} = I_{dc2j}V_{dcj} = (1 - d_cj)V_{dcj}I_{pvj}$ and therefore $I_{dc2j} = (1 - d_{cj})I_{pvj}$. From equations (4.8) and (4.9), it can be seen that the MPPT control system controls the output current from the PV-DG. Further, the maximum power, P_{pvmaxj}, can be calculated from equation (4.6).

Model of DC/AC converter

The DC/AC converter employs pulse width modulation (PWM) technique to regulate the exchange of active and reactive power between the PV-DGs and the rest of the distribution system. This can be achieved by controlling the modulation ratio m_j and phase ϕ_j of the PWM control signal through the following [58] equations:

$$m_j = \left(K_{acpj} + \frac{K_{acj}}{s}\right)(V_{ep(j)} - V_{ref,j}) \tag{4.10}$$

$$\phi_j = \left(K_{dcpj} + \frac{K_{dcj}}{s}\right)(V_{dcj} - V_{dcrefj}) \tag{4.11}$$

Where K_{acpj} and K_{dcpj} are proportional gains and K_{acij} and K_{dcij} are integral control gains, respectively.

Each PV-DG model is expressed in its own reference frame which needs to be transformed into the system reference frame. The voltage at the terminal of the DC/AC converter, V_{cj}, can be expressed in the network coordinate as

$$\bar{V}_{cj} = v_{cdj} + iv_{cqj} = m_j V_{dcj}\angle\psi_j = m_j V_{dcj}(cos\psi_j + isin\psi_j); \qquad i = \sqrt{-1} \tag{4.12}$$

where $\psi_j = \theta_{ep(j)} + \phi_j$, $\theta_{ep(j)}$ is angle of the voltage of bus $ep(j)$, where PV-DG is installed as shown in Fig. 4.2. The DC and AC sides are connected by the following power balance relationship

$$V_{dcj}I_{dc1j} = i_{pdj}v_{cdj} + i_{pqj}v_{cqj} \tag{4.13}$$

where subscript d and q denotes the d-axis and q-axis component of the corresponding variable, respectively. i_{pdj} and i_{pqj} are the output currents of the DC/AC converter and v_{cdj} and v_{cqj} are the output voltages of j^{th} PV-DG. By substituting values of v_{cdj} and v_{cqj} from equation (4.12) to equation (4.13), we get

$$V_{dcj}I_{dc1j} = i_{pdj}v_{cdj} + i_{pqj}v_{cqj} = i_{pdj}m_jV_{dcj}cos\psi_j + i_{pqj}m_jV_{dcj}sin\psi_j \tag{4.14}$$

Hence,

$$I_{dc1j} = i_{pdj}m_jcos\psi_j + i_{pqj}m_jsin\psi_j \tag{4.15}$$

The active power supply from the PV-DG is $P_{pvj} = I_{pvj}V_{pvj} = I_{dc2j}V_{dcj}$ and $V_{dcj} = V_{pvj}/(1-d_{cj})$. The model of the DC/AC converter is described by

$$\dot{V}_{dcj} = \frac{1}{C_{dcj}}[I_{dc2j} - I_{dc1j}] \tag{4.16}$$

where $I_{dc1j} = i_{pdj}m_jcos\psi_j + i_{pqj}m_jsin\psi_j$ and $I_{dc2j} = (1-d_{cj})I_{pvj}$. Thus, in mathematical terms, a PV-DG is represented by five differential equations as follows:

$$\frac{dx_{pv1j}}{dt} = k_{pvi}(P_{pvj} - P_{pvmaxj}) \tag{4.17}$$

$$\frac{dx_{pv2j}}{dt} = k_{aci}(V_{eprefj} - V_{ep(j)}) \tag{4.18}$$

$$\frac{dx_{pv3j}}{dt} = k_{dci}(V_{dcrefj} - V_{dcj}) \tag{4.19}$$

$$\frac{dV_{dcj}}{dt} = \frac{1}{C_{dcj}}[(1-d_{cj})I_{pvj} - I_{dc2j}] \tag{4.20}$$

$$\frac{dI_{pvj}}{dt} = \frac{1}{L_{dcj}}[V_{pvj} - (1-d_{cj})V_{dcj}] \tag{4.21}$$

$$d_{cj} = x_{pv1j} + k_{pvpj}(P_{pvmaxj} - P_{pvj}) \tag{4.22}$$

$$m_j = x_{pv2j} + k_{acpj}(V_{eprefj} - V_{ep(j)}) \tag{4.23}$$

$$\phi_j = x_{pv3j} + k_{dcpj}(V_{dcrefj} - V_{dcj}) \tag{4.24}$$

To study the impact of the PV-DG, these differential equations are linearized as follows

$$\frac{d\Delta x_{pv1j}}{dt} = k_{pvi}(-I_{dc1j}\Delta V_{dcj} - V_{dcj}\Delta I_{dc1j}) \tag{4.25}$$

$$\frac{d\Delta x_{pv2j}}{dt} = k_{aci}(-\Delta V_{ep(j)}) \tag{4.26}$$

$$\frac{d\Delta x_{pv3j}}{dt} = k_{dci}(-\Delta V_{dcj}) \tag{4.27}$$

$$\frac{d\Delta V_{dcj}}{dt} = \frac{1}{C_{dcj}}[(1-d_{cj})\Delta I_{pv} - I_{pv}\Delta d_{cj} - \Delta I_{dc2j}] \tag{4.28}$$

$$\frac{d\Delta I_{pvj}}{dt} = \frac{1}{L_{dcj}}[N\Delta I_{pvj} - (1-d_{cj})\Delta V_{dcj} + V_{dcj}\Delta d_{cj} + V_{dcj}\Delta d_{cj}] \tag{4.29}$$

$$\Delta d_{cj} = \Delta x_{pv1j} + k_{pvpj}(\Delta P_{pvmaxj} - I_{dc1j}\Delta V_{dcj} - V_{dcj}\Delta I_{dc1j}) \tag{4.30}$$

$$\Delta m_j = k_{acij}\Delta x_{pv2j} + k_{acpj}(\Delta V_{eprefj} - \Delta V_{ep(j)}) \tag{4.31}$$

$$\Delta \phi_j = k_{dcij}\Delta x_{pv3j} + k_{dcpj}(\Delta V_{dcrefj} - \Delta V_{dcj}) \tag{4.32}$$

where, state variables x_{pv1j}, x_{pv2j} and x_{pv3j} are related to the DC/DC and AC/DC converter controllers. Collecting equations (2.25)-(2.26), and (4.25)-(4.32) for all PV-DGs and SHPP-DGs together and writing them in matrix form, one obtains

$$\Delta \dot{\mathbf{x}} = \mathbf{A}\Delta\mathbf{x} + \mathbf{B}_G\Delta\mathbf{I}_g + \mathbf{B}_p\Delta\mathbf{I}_p + \mathbf{B}_1\Delta\mathbf{Z}_G + \mathbf{B}_{1p}\Delta\mathbf{Z}_{Gp} + \mathbf{E}\Delta\mathbf{u} \tag{4.33}$$

The algebraic equations corresponding to j^{th} PV-DG ($1 \leq j \leq m_{pv}$) can be written as

$$V_{cj}\cos\psi_j - V_{ep(j)}\cos\theta_{ep(j)} + X_{cj}I_{pqj} = 0 \tag{4.34}$$

$$V_{cj}\sin\psi_j - V_{ep(j)}\sin\theta_{ep(j)} - X_{cj}I_{pdj} = 0 \tag{4.35}$$

Where X_{cj} denotes interfacing reactance between the j^{th} PV-DG and rest of the system. I_{pdj} and I_{pqj} are d and q-axis current flowing to system from j^{th} PV-DG. By the linearization of algebraic equations, we get

$$\begin{aligned}(m_j\Delta V_{dcj} + V_{dcj}\Delta m_j)\cos(\theta_{ep(j)} + \phi_j) - m_jV_{dcj}sin(\theta_{ep(j)} + \phi_j)\Delta\phi_j - m_jV_{dcj}\\ \sin(\theta_{ep(j)} + \phi_j)\Delta\theta_{ep(j)} + V_{ep(j)}\sin\theta_{ep(j)}\Delta\theta_{ep(j)} - \cos\theta_{ep(j)}\Delta V_{ep(j)} + X_{cj}\Delta I_{pqj} = 0\end{aligned} \tag{4.36}$$

$$\begin{aligned}(m_j\Delta V_{dcj} + V_{dcj}\Delta m_j)\sin(\theta_{ep(j)} + \phi_j) + m_jV_{dcj}cos(\theta_{ep(j)} + \phi_j)\Delta\phi_j + m_jV_{dcj}\\ \cos(\theta_{ep(j)} + \phi_j)\Delta\theta_{ep(j)} - V_{ep(j)}\cos\theta_{ep(j)}\Delta\theta_{ep(j)} - \sin\theta_{ep(j)}\Delta V_{ep(j)} - X_{cj}\Delta I_{pdj} = 0\end{aligned} \tag{4.37}$$

Rewriting equations (4.36) and (4.37), in matrix form, we obtain

$$\mathbf{0} = \mathbf{A}_{1p}\Delta\mathbf{x} + \mathbf{B}_{2p}\Delta\mathbf{I}_p + \mathbf{B}_{3p}\Delta\mathbf{Z}_{Gp} \tag{4.38}$$

Network equations

The network equations for distribution system are described by the power balance equations as

$$\sum_{k=1}^{N} V_{e(i)} V_k Y_{e(i)k} \cos(\theta_{e(i)} - \theta_k - \alpha_{e(i)k}) - PL_{e(i)} - I_{di} V_{e(i)} \sin(\delta_i - \theta_{e(i)}) - I_{qi} V_{e(i)} \cos(\delta_i - \theta_{e(i)}) = 0 \tag{4.39}$$

$$\sum_{k=1}^{N} V_{e(i)} V_k Y_{e(i)k} \sin(\theta_{e(i)} - \theta_k - \alpha_{e(i)k}) - QL_{e(i)} - I_{di} V_{e(i)} \cos(\delta_i - \theta_{e(i)}) + I_{qi} V_{e(i)} \sin(\delta_i - \theta_{e(i)}) = 0 \tag{4.40}$$

$$1 \leq i \leq m_g$$

$$\sum_{k=1}^{N} V_{ep(j)} V_k Y_{ep(j)k} \cos(\theta_{ep(j)} - \theta_k - \alpha_{ep(j)k}) - PL_{ep(j)} + I_{pdj} V_{ep(j)} \cos(\theta_{ep(j)}) + I_{pqj} V_{ep(j)} \sin(\theta_{ep(j)}) = 0 \tag{4.41}$$

$$\sum_{k=1}^{N} V_{ep(j)} V_k Y_{ep(j)k} \sin(\theta_{ep(j)} - \theta_k - \alpha_{ep(j)k}) - QL_{ep(j)} + I_{pdj} V_{ep(j)} \sin(\theta_{ep(j)}) - I_{pqj} V_{ep(j)} \cos(\theta_{ep(j)}) = 0 \tag{4.42}$$

$$1 \leq j \leq m_{pv}$$

$$\sum_{k=1}^{N} V_l V_k Y_{lk} \cos(\theta_l - \theta_k - \alpha_{lk}) - PL_l = 0 \tag{4.43}$$

$$\sum_{k=1}^{N} V_l V_k Y_{lk} \sin(\theta_l - \theta_k - \alpha_{lk}) - QL_l = 0 \tag{4.44}$$

$$2 \leq l \leq N; 1 \notin \mathbf{E}; l \notin \mathbf{E} g_{pv}$$

$$\sum_{k=1}^{N} V_s V_k Y_{sk} \cos(\theta_s - \theta_k - \alpha_{sk}) = P_s \tag{4.45}$$

$$\sum_{k=1}^{N} V_s V_k Y_{sk} \sin(\theta_s - \theta_k - \alpha_{sk}) = Q_s \tag{4.46}$$

Linearizing the network equations (4.39)- (4.42),(4.45) and (4.46), following expressions are ob-

tained

$$\sum_{\substack{k=1\\k\neq e(i)}}^{N} V_k Y_{e(i)k}\cos(\theta_{e(i)}-\theta_k-\alpha_{e(i)k})\Delta V_{e(i)}+I_{qi}\cos(\delta_i-\theta_{e(i)})\Delta V_{e(i)}+I_{di}\sin(\delta_i-\theta_{e(i)})\Delta V_{e(i)}+$$

$$\sum_{k=1}^{N} V_{e(i)}Y_{e(i)k}\cos(\theta_{e(i)}-\theta_k-\alpha_{e(i)k})\Delta V_k+\sum_{k=1}^{N} V_{e(i)}V_k Y_{e(i)k}\sin(\theta_{e(i)}-\theta_k-\alpha_{e(i)k})\Delta\theta_k-$$

$$\sum_{\substack{k=1\\k\neq e(i)}}^{N} V_{e(i)}V_k Y_{e(i)k}\sin(\theta_{e(i)}-\theta_k-\alpha_{e(i)k})\Delta\theta_{e(i)}-I_{di}V_{e(i)}\cos(\delta_i-\theta_{e(i)})\Delta\theta_{e(i)}+I_{qi}V_{e(i)}\sin(\delta_i-\theta_{e(i)})\Delta\theta_{e(i)}$$

$$-\Delta PL_{e(i)}-\Delta I_{di}V_{e(i)}\sin(\delta_i-\theta_{e(i)})+I_{di}V_{e(i)}\cos(\delta_i-\theta_{e(i)})\Delta\delta_i+\Delta I_{qi}V_{e(i)}\cos(\delta_i-\theta_{e(i)})+$$

$$I_{qi}V_{e(i)}\sin(\delta_i-\theta_{e(i)})\Delta\delta_i=0 \quad (4.47)$$

$$\sum_{\substack{k=1\\k\neq e(i)}}^{N} V_k Y_{e(i)k}\sin(\theta_{e(i)}-\theta_k-\alpha_{e(i)k})\Delta V_{e(i)}-I_{qi}\sin(\delta_i-\theta_{e(i)})\Delta V_{e(i)}+I_{di}\cos(\delta_i-\theta_{e(i)})\Delta V_{e(i)}+$$

$$\sum_{k=1}^{N} V_{e(i)}V_k Y_{e(i)k}\sin(\theta_{e(i)}-\theta_k-\alpha_{e(i)k})\Delta V_k-\sum_{k=1}^{N} V_{e(i)}V_k Y_{e(i)k}\cos(\theta_{e(i)}-\theta_k-\alpha_{e(i)k})\Delta\theta_k-$$

$$\sum_{\substack{k=1\\k\neq e(i)}}^{N} V_{e(i)}V_k Y_{e(i)k}\cos(\theta_{e(i)}-\theta_k-\alpha_{e(i)k})\Delta\theta_{e(i)}+I_{di}V_{e(i)}\sin(\delta_i-\theta_{e(i)})\Delta\theta_{g(i)}+I_{qi}V_{e(i)}\cos(\delta_i-\theta_{e(i)})\Delta\theta_{e(i)}$$

$$-\Delta QL_{e(i)}+\Delta I_{di}V_{e(i)}\cos(\delta_i-\theta_{e(i)})-I_{di}V_{e(i)}\sin(\delta_i-\theta_{e(i)})\Delta\delta_i-V_{g(i)}\sin(\delta_i-\theta_{e(i)})\Delta I_{qi}+$$

$$I_{qi}V_{e(i)}\cos(\delta_i-\theta_{e(i)})\Delta\delta_i=0 \quad (4.48)$$

$$(\sum_{\substack{k=1\\k\neq ep(j)}}^{N} V_k Y_{ep(j)k}\cos(\theta_{ep(j)}-\theta_k-\alpha_{ep(j)k})+I_{pqj}\sin(\theta_{ep(j)})+I_{pdj}\cos(\theta_{ep(j)}))\Delta V_{ep(j)}-\Delta PL_{ep(j)}+$$

$$V_{ep(j)}(-\sum_{\substack{k=1\\k\neq ep(j)}}^{N} V_k Y_{ep(j)k}\sin(\theta_{ep(j)}-\theta_k-\alpha_{ep(j)k})+I_{pqj}\cos(\theta_{ep(j)})-I_{pdj}\sin(\theta_{ep(j)}))\Delta\theta_{ep(j)}+$$

$$V_{ep(j)}\cos(\theta_{ep(j)})\Delta I_{pdj}+V_{ep(j)}\sin(\theta_{ep(j)})\Delta I_{pqj}+(\sum_{k=1}^{N} V_{ep(j)}Y_{ep(j)k}\cos(\theta_{ep(j)}-\theta_k-\alpha_{ep(j)k}))\Delta V_k+$$

$$(\sum_{k=1}^{N} V_k V_{ep(j)}Y_{ep(j)k}\sin(\theta_{ep(j)}-\theta_k-\alpha_{ep(j)k}))\Delta\theta_k=0 \quad (4.49)$$

$$(\sum_{\substack{k=1\\k\neq ep(j)}}^{N} V_k Y_{ep(j)k}\sin(\theta_{ep(j)}-\theta_k-\alpha_{ep(j)k})+I_{pdj}\sin(\theta_{ep(j)})-I_{pqj}\cos(\theta_{ep(j)}))\Delta V_{ep(j)}-\Delta QL_{ep(j)}+$$

$$V_{ep(j)}(-\sum_{\substack{k=1\\k\neq ep(j)}}^{N} V_k Y_{ep(j)k}\cos(\theta_{ep(j)}-\theta_k-\alpha_{ep(j)k})+I_{pdj}\cos(\theta_{ep(j)})+I_{pdj}\sin(\theta_{ep(j)}))\Delta\theta_{ep(j)}+$$

$$V_{ep(j)}\sin(\theta_{ep(j)})\Delta I_{pdj}-V_{ep(j)}\cos(\theta_{ep(j)})\Delta I_{pqj}+(\sum_{k=1}^{N} V_{ep(j)}Y_{ep(j)k}\sin(\theta_{ep(j)}-\theta_k-\alpha_{ep(j)k}))\Delta V_k-$$

$$(\sum_{k=1}^{N} V_k V_{ep(j)}Y_{ep(j)k}\cos(\theta_{ep(j)}-\theta_k-\alpha_{ep(j)k}))\Delta\theta_k=0 \quad (4.50)$$

where PL_l and QL_l are real and reactive power demand at bus l, respectively, α_{jk} and Y_{jk} is angle and magnitude of the $(j,k)^{th}$ element of the bus admittance matrix respectively. Further, V_k and θ_k are the voltage magnitude and angle of the k^{th} bus respectively.

$$\Delta P_s=\sum_{k=1}^{N} V_s Y_{sk}\cos(\theta_s-\theta_k-\alpha_{sk})\Delta V_k+\sum_{k=1}^{N} V_s V_k Y_{sk}\sin(\theta_s-\theta_k-\alpha_{sk})\Delta\theta_k+\Delta V_{e(i)}$$
$$\sum_{\substack{k=1\\k\neq e(i)}}^{N} V_k Y_{se(i)}\cos(\theta_s-\theta_e(i)-\alpha_{sk})+\sum_{\substack{k=1\\k\neq e(i)}}^{N} V_{e(i)}V_k Y_{se(i)}\sin(\theta_s-\theta_e(i)-\alpha_{sk})\Delta\theta_{e(i)}+\Delta V_{ep(j)}$$
$$\sum_{\substack{k=1\\k\neq ep(j)}}^{N} V_k Y_{sep(j)}\cos(\theta_s-\theta_{ep(j)}-\alpha_{sk})+\sum_{\substack{k=1\\k\neq ep(j)}}^{N} V_{ep(j)}V_k Y_{sep(j)}\sin(\theta_s-\theta_{ep(j)}-\alpha_{sk})\Delta\theta_{ep(j)} \quad (4.51)$$

$$\Delta Q_s=\sum_{k=1}^{N} V_s Y_{sk}\sin(\theta_s-\theta_k-\alpha_{sk})\Delta V_k-\sum_{k=1}^{N} V_s V_k Y_{sk}\cos(\theta_s-\theta_k-\alpha_{sk})\Delta\theta_k+\Delta V_{e(i)}$$
$$\sum_{\substack{k=1\\k\neq e(i)}}^{N} V_k Y_{se(i)}\sin(\theta_s-\theta_e(i)-\alpha_{sk})-\sum_{\substack{k=1\\k\neq e(i)}}^{N} V_{e(i)}V_k Y_{se(i)}\sin(\theta_s-\theta_e(i)-\alpha_{sk})\Delta\theta_{e(i)}+$$
$$\Delta V_{ep(j)}\sum_{\substack{k=1\\k\neq ep(j)}}^{N} V_k Y_{sep(j)}\sin(\theta_s-\theta_{ep(j)}-\alpha_{sk})-\sum_{\substack{k=1\\k\neq ep(j)}}^{N} V_{ep(j)}V_k Y_{sep(j)}\sin(\theta_s-\theta_{ep(j)}-\alpha_{sk})\Delta\theta_{ep(j)} \quad (4.52)$$

Further, the linearized algebraic power flow equations (4.47)- (4.48) for all SHPP-DGs can be

written in matrix form as,

$$\mathbf{0} = \mathbf{C}_1\Delta\mathbf{x} + \mathbf{C}_2\Delta\mathbf{I}_g + \mathbf{C}_3\Delta\mathbf{Z}_G + \mathbf{C}_4\Delta\mathbf{Z}_l + \mathbf{C}_5\Delta\mathbf{Z}_{Gp} \tag{4.53}$$

Collecting equations (4.49)- (4.50) for all PV-DGs together and writing them in matrix form gives,

$$\mathbf{0} = \mathbf{C}_{1p}\Delta\mathbf{x} + \mathbf{C}_{2p}\Delta\mathbf{I}_p + \mathbf{C}_{3p}\Delta\mathbf{Z}_{Gp} + \mathbf{C}_{4p}\Delta\mathbf{Z}_l + \mathbf{C}_{5p}\Delta\mathbf{Z}_G \tag{4.54}$$

Rewriting equations (4.51) and (4.52), in matrix form, we obtain,

$$\mathbf{0} = \mathbf{D}_3\Delta\mathbf{Z}_G + \mathbf{D}_{3p}\Delta\mathbf{Z}_{Gp} + \mathbf{D}_4\Delta\mathbf{Z}_l + \mathbf{D}_5\Delta\mathbf{S} \tag{4.55}$$

Similarly, the lineraized real and reactive power balance equations (2.34)- (2.35) at all the buses other than the DG buses can be written in matrix form as

$$\mathbf{0} = \mathbf{D}_1\Delta\mathbf{Z}_G + \mathbf{D}_{1p}\Delta\mathbf{Z}_{Gp} + \mathbf{D}_2\Delta\mathbf{Z}_l \tag{4.56}$$

Equations (2.27), (4.33), (4.38),(4.53) (4.54), (4.55) and (4.56) are utilized to obtain the following linearized equations:

$$\begin{aligned}
\Delta\dot{\mathbf{x}} &= \mathbf{A}\Delta\mathbf{x} + \mathbf{B}_G\Delta\mathbf{I}_g + \mathbf{B}_p\Delta\mathbf{I}_p + \mathbf{B}_1\Delta\mathbf{Z}_G + \mathbf{B}_{1p}\Delta\mathbf{Z}_{Gp} + \mathbf{E}\Delta\mathbf{u} && (4.57)\\
\mathbf{0} &= \mathbf{A}_1\Delta\mathbf{x} + \mathbf{B}_2\Delta\mathbf{I}_g + \mathbf{B}_3\Delta\mathbf{Z}_G && (4.58)\\
\mathbf{0} &= \mathbf{C}_1\Delta\mathbf{x} + \mathbf{C}_2\Delta\mathbf{I}_g + \mathbf{C}_3\Delta\mathbf{Z}_G + \mathbf{C}_4\Delta\mathbf{Z}_l + \mathbf{C}_5\Delta\mathbf{Z}_{Gp} && (4.59)\\
\mathbf{0} &= \mathbf{D}_1\Delta\mathbf{Z}_G + \mathbf{D}_{1p}\Delta\mathbf{Z}_{Gp} + \mathbf{D}_2\Delta\mathbf{Z}_l && (4.60)\\
\mathbf{0} &= \mathbf{D}_3\Delta\mathbf{Z}_G + \mathbf{D}_{3p}\Delta\mathbf{Z}_{Gp} + \mathbf{D}_4\Delta\mathbf{Z}_l + \mathbf{D}_5\Delta\mathbf{S} && (4.61)\\
\mathbf{0} &= \mathbf{A}_{1p}\Delta\mathbf{x} + \mathbf{B}_{2p}\Delta\mathbf{I}_p + \mathbf{B}_{3p}\Delta\mathbf{Z}_{Gp} && (4.62)\\
\mathbf{0} &= \mathbf{C}_{1p}\Delta\mathbf{x} + \mathbf{C}_{2p}\Delta\mathbf{I}_p + \mathbf{C}_{3p}\Delta\mathbf{Z}_{Gp} + \mathbf{C}_{4p}\Delta\mathbf{Z}_l + \mathbf{C}_{5p}\Delta\mathbf{Z}_G && (4.63)
\end{aligned}$$

where

$\mathbf{x} = [\mathbf{x}_G^T \quad \mathbf{x}_P^T]^T$

$\mathbf{x}_G = [\mathbf{x}_1^T \quad \mathbf{x}_2^T \ldots \mathbf{x}_i^T \ldots \mathbf{x}_{m_g}^T]^T, \qquad \mathbf{x}_i = [\delta_i \quad \omega_i \quad E'_{qi} \quad E_{fdi}]^T$

$\mathbf{x}_P = [\mathbf{x}_1^T \quad \mathbf{x}_2^T \ldots \mathbf{x}_j^T \ldots \mathbf{x}_{m_{pv}}^T]^T, \qquad \mathbf{x}_i = [V_{dcj} \quad I_{pvj} \quad x_{pv1j} \quad x_{pv2j} \quad x_{pv3j}]^T$

$\mathbf{I}_g = [\mathbf{I}_{g1}^T \quad \mathbf{I}_{g2}^T \ldots \mathbf{I}_{gi}^T \ldots \mathbf{I}_{gm_g}^T]^T, \qquad \mathbf{I}_{gi} = [I_{di} \quad I_{qi}]^T$

$\mathbf{I}_p = [\mathbf{I}_{p1}^T \quad \mathbf{I}_{p2}^T \ldots \mathbf{I}_{pj}^T \ldots \mathbf{I}_{pm_{pv}}^T]^T, \qquad \mathbf{I}_{pj} = [I_{dpj} \quad I_{qpj}]^T$

$\mathbf{u} = [\mathbf{u}_G^T \quad \mathbf{u}_P^T]^T$

$\mathbf{u}_G = [\mathbf{u}_1^T \quad \mathbf{u}_2^T \ldots \mathbf{u}_i^T \ldots \mathbf{u}_{m_g}^T]^T, \qquad \mathbf{u_i} = [T_{Mi} \quad V_{ref_i}]^T$

$\mathbf{u}_p = [\mathbf{u}_1^T \quad \mathbf{u}_2^T \ldots \mathbf{u}_j^T \ldots \mathbf{u}_{m_{pv}}^T]^T, \qquad \mathbf{u_j} = [m_j \quad \phi_j]^T$

$\mathbf{Z}_G = [V_{e(1)} \quad V_{e(2)} \ldots V_{e(m_g)} \;\; \theta_{e(1)} \quad \theta_{e(2)} \ldots \theta_{e(m_g)}]^T$

$\mathbf{Z}_{Gp} = [V_{ep(1)} \quad V_{ep(2)} \ldots V_{ep(m_{pv})} \;\; \theta_{ep(1)} \quad \theta_{ep(2)} \ldots \theta_{ep(m_{pv})}]^T$

$\mathbf{Z}_l = [V_2 \quad V_3 \ldots V_e \ldots V_N \quad \theta_2 \quad \theta_3 \ldots \theta_e \ldots \theta_N]^T \qquad 2 \leq e \leq N; e \notin \mathbf{E}; e \notin \mathbf{E}g_{pv}$

$\mathbf{S} = [P_s \quad Q_s]^T = [P_1 \quad Q_1]^T$

$1 \leq i \leq m_g, 1 \leq j \leq m_{pv}$

where $\mathbf{x}$ is a vector of state variables and $\mathbf{u}$ is vector of input variables. Equations (4.58)-(4.63) can be written in the following form: ‘

$$\begin{bmatrix} \mathbf{B_2} & 0 & \mathbf{B_3} & \mathbf{0} & \mathbf{0} & \mathbf{0} \\ \mathbf{C_2} & 0 & \mathbf{C_3} & \mathbf{C_5} & \mathbf{C_4} & \mathbf{0} \\ \mathbf{0} & \mathbf{0} & \mathbf{D_1} & \mathbf{D_{1p}} & \mathbf{D_2} & \mathbf{0} \\ \mathbf{0} & \mathbf{0} & \mathbf{D_3} & \mathbf{D_{3p}} & \mathbf{D_4} & \mathbf{D_5} \\ \mathbf{0} & \mathbf{B_{2p}} & \mathbf{0} & \mathbf{B_{3p}} & \mathbf{0} & \mathbf{0} \\ \mathbf{0} & \mathbf{C_{2p}} & \mathbf{C_{5p}} & \mathbf{C_{3p}} & \mathbf{C_{4p}} & \mathbf{0} \end{bmatrix} \begin{bmatrix} \mathbf{\Delta I}_g \\ \mathbf{\Delta I}_p \\ \mathbf{\Delta Z}_G \\ \mathbf{\Delta Z}_{Gp} \\ \mathbf{\Delta Z}_l \\ \mathbf{\Delta S} \end{bmatrix} = \begin{bmatrix} -\mathbf{A_1} \\ -\mathbf{C_1} \\ \mathbf{0} \\ \mathbf{0} \\ -\mathbf{A_{1p}} \\ -\mathbf{C_{1p}} \end{bmatrix} \Big[\mathbf{\Delta x}\Big] \tag{4.64}$$

By extracting rows corresponding to $\mathbf{\Delta I}_g$, $\mathbf{\Delta I}_p$, $\mathbf{\Delta Z}_{Gp}$ and $\mathbf{\Delta Z}_G$ from equation (4.64) and substituting it into equation (4.57), we get,

$$\mathbf{\Delta \dot{x}} = \mathbf{A}_{sys}\Delta\mathbf{x} + \mathbf{E}\Delta\mathbf{u} \tag{4.65}$$

Mathematically, probabilistic small signal stability constraint can be expressed as in equation (3.6).

4.3 CASE STUDIES

The effectiveness of the presented methodology has been investigated on all three radial distribution systems considered in previous chapters, with PV-DGs and SHPP type of DGs. The KnEA parameters adopted for all test distribution systems, locations and maximum capacities of SHPP-DGs, modelling of load uncertainties and SHPP generations are same as used in the previous chapter. In this work, the solar irradiation is assumed to follow beta probability distribution function with mean and standard deviation as 721 W/m^2 and 200 W/m^2, [52] respectively. Utilizing the solar irradiation level in equation (4.6), the reference maximum power point P_{pvmaxj} is determined, at which the PV-DGs operate, for all three systems. For 33 bus system, one PV-DG is assumed to be connected at bus 8 with $N_s = 600$ and $N_p = 50$. For 69 bus system, two PV-DGs are assumed

to be connected at buses 17 and 55, each with $N_s = 600$ and $N_p = 50$. For 119-bus system, two PV-DGs are assumed to be connected at buses 36 and 108, each with $N_s = 1200$ and $N_p = 200$. All DG nodes are modeled as voltage controlled nodes. The rated terminal voltage magnitude of each DG is 1 p.u. All the parameters of the PV-DGs system are given in the Appendix B. It is to be noted that the correlation between power output of DGs and loads is also considered in this work. For 33-bus and 69-bus systems, the powers generated by the SHPP-DGs are assumed to be correlated with each other with a correlation matrix $\mathbf{C_w}$ given in equation (3.19) of Chapter 3. For 119-bus system, the powers generated by the SHPP-DGs are assumed to be correlated with each other with a correlation matrix $\mathbf{C_w}$ given in equation (3.20) of Chapter 3. The correlation matrix $\mathbf{C_{pv}}$ of the solar radiation for 69-bus and 119-bus systems is given in equation (4.66) [82]:

$$\mathbf{C_{pv}} = \begin{bmatrix} 1 & 0.5 \\ 0.5 & 1 \end{bmatrix} \tag{4.66}$$

Further, correlation among the loads of selected buses has been considered as specified in Chapter 3. Two cases are included in this study: case 1) non-correlated load and non-correlated DG power outputs and case 2) correlated load and correlated DG power outputs, along with initial cases. The results corresponding to both cases, are shown in Table 4.1, Table 4.2, and Table 4.3 for all three systems, respectively. These results also include the state variables associated with unstable critical eigenvalues, participation factors [65] and the corresponding probability of stability. Participation factors more than 0.2 are listed in these tables. For 33-bus system, in the initial configurations of both the cases, the electromechanical modes contribute to the system instability. These modes are associated with the states of SHPP-DG3. Similarly, from Table 4.2 and 4.3, it is observed that, in the initial configurations of 69-bus (for case 1) and 119-bus system (for both the cases) DC/DC converter control modes contribute to the instability of the system. For 69 bus system, these unstable modes are associated with the states of PV-DG2, whereas for 119 bus system, the states of PV-DG1 contribute to the system instability. For 69 bus system, for case 2, these unstable modes are associated with the states of SHPP-DG3. Further, the results of Table 4.1, 4.2 and 4.3 indicate that all these unstable modes are made stable through reconfiguration.

Table 4.1: Result of 33-bus distribution system

	Open switch	Power loss	Voltage stability index	Switching number	Modes	participating generator	Dominant states	participation factor	$P\{\alpha_c < 0\}$	status
case 1										
Initial network		89.95	0.20868	0	λ_3	SHPP-DG3	δ_3	1,	0.87406	unstable
					λ_6		ω_3	0.999		
Reconfigured network	s7,s9,s15, s34,s37	66.437	0.130551	6	λ_3	SHPP-DG3	δ_3	1,	1	stable
					λ_6		ω_3	0.999		
case 2										
Initial network		90.73	0.2090	0	λ_3,	SHPP-DG3	δ_3	1,	0.8668	unstable
					λ_6		ω_3	0.999		
Reconfigured network	s8,s15,s33, s34, s37	68.99	0.128586	4	λ_3,	SHPP-DG3	δ_3	1,	1	stable
					λ_6		ω_3	0.999		

Table 4.2: Result of 69-bus distribution system

	Open switch	Power loss	Voltage stability index	Switching number	Modes	participating generator	Dominant states	participation factor	$P\{\alpha_c < 0\}$	status
case 1										
Initial network		77.48	0.097745	0	λ_{16},	PV-DG2	I_{pv2},	1.00,	0.789	unstable
					λ_{18},		x_{pv12},	0.929,		
					λ_{22},		x_{pv32},	0.514,		
					λ_{20}		x_{pv22}	0.336		
Reconfigured network	s11,s14,s20, s58,s69	38.627	0.084641	8	λ_{16},	PV-DG2	I_{pv2},	1.0	1	stable
					λ_{18},		x_{pv12},	0.9656		
					λ_{22},		x_{pv32},	0.5817		
					λ_{20}		x_{pv22}	0.4095		
case 2										
Initial network		58.820	0.09035	0	λ_3,	SHPP-DG3	δ_3	1.00	0.6616	unstable
					λ_6		ω_3	0.9999		
Reconfigured network	s5,s10,s12, s24,s70	31.947	0.062054	8	λ_3,	SHPP-DG3	δ_3	1.00	1	stable
					λ_6		ω_3	0.9999		

Table 4.3: Result of 119-bus distribution system

	Open switch	Power loss	Voltage stability index	Switching number	Modes	participating generator	Dominant states	participation factor	$P\{\alpha_c < 0\}$	status
case 1										
Initial network		706.55	0.30183	0	λ_{19}, λ_{21}, λ_{25}	PV-DG1	I_{pv1}, x_{pv11}, x_{pv31}	1.00, 0.829 0.369	0.6031	unstable
Reconfigured network	s23,s35,s44,s75, s77,s110,s120, s121,s123,s125, s126,s127,s128, s131, s132	510.013	0.193388	12	λ_{19}, λ_{21}, λ_{25}	PV-DG1	I_{pv1}, x_{pv11}, x_{pv31}	1.00 0.866 0.3187	1	stable
case 2										
Initial network		708.350	0.30186	0	λ_{19}, λ_{21}, λ_{25}	PV-DG1	I_{pv1}, x_{pv11}, x_{pv31}	1.0 0.8645 0.2573	0.591756	unstable
Reconfigured network	s8,s9,s25,s35, s55,s69,s74,s98, s110,s124,s125, s126,s127,s131, s132	548.676	0.187924	18	λ_{19}, λ_{21}, λ_{25}	PV-DG1	I_{pv1}, x_{pv11}, x_{pv31}	1.0 0.9149 0.317	1	stable

Further, the results of these studies show that the stability margins obtained for case 1 (non-correlated load and DG) are more than the stability margins for case 2 (correlated load and DG). Thus, correlation among the uncertain quantities deteriorates the system stability.

Also, the effect of different mean values of irradiance on the optimal final reconfiguration and probability of stability is assessed. For this purpose, three different PDFs of solar irradiance (shown in Table 4.4) are considered with different mean values and same standard deviation, for all three systems. Fig 4.3 shows the plots of the three PDFs.

Table 4.4: Different distribution of irradiance

	Low	Medium	High
Mean	140	721	980
Deviation	50	50	50

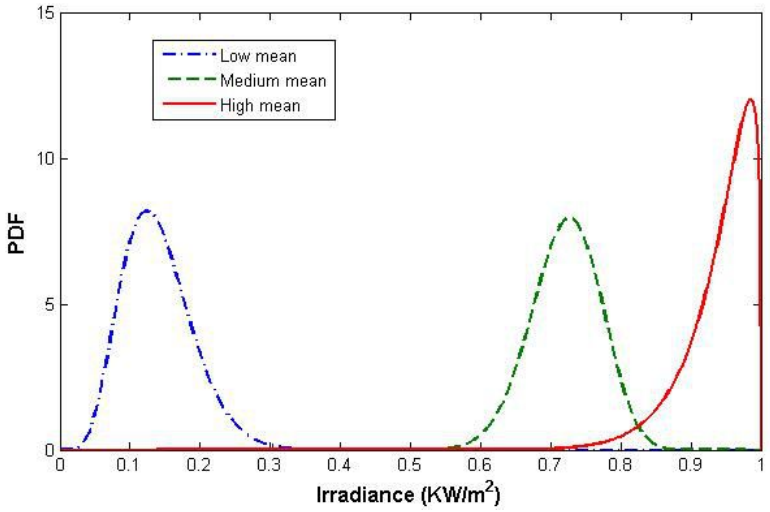

Figure 4.3: PDFs of solar irradiance.

Moreover, two scenarios are considered to examine the impacts of DGs more closely, with all these three PDFs. These are: scenario 1) when only PV-DGs are present in the system and, scenario 2) when both PV-DGs and SHPP-DGs are present in the system. Results corresponding to the above three PDFs of solar irradiance are shown in Tables 4.5, 4.6, and 4.7, for all three systems, respectively with both the above mentioned scenerios. For these studies, both correlated loads and correlated DG power output have been considered (as in case 2 described above). The conditional probabilities of critical mode eigenvalue, number of violations in operational constraint (bus voltage constraint, branch current constraint) and state variables of different DGs associated with critical eigenvalues are listed in Tables 4.5, 4.6, and 4.7. For all three test systems, it is observed that the stability margin of the systems decreases with the increase in the solar irradiance level. Therefore, in the daytime or summer season, when irradiance is high, risk of instability is more and thus, periods with high irradiance require more attention. This risk of instability can be reduced to a large extent by reconfiguring the system appropriately. Moreover, the results clearly demonstrate the positive effect of reconfiguration on the system performance indices (power loss, voltage stability index and number of switching operations). Moreover, it is also seen that, as irradiance increases, deterioration in probabilistic stability margin occurs for all three test systems and the percentage improvement made in power loss reduction and voltage stability index is reduced. Further, due to the dynamic interaction between SHPP-DGs and PV-DGs, presence of both these

Table 4.5: Result of 33-bus distribution system with different PDFs of solar irradiance

	Low mean	Medium mean	High mean
Initial case with PV-DG only (scenario 1)			
Power loss(kW)	212.27	201.16	196.48
Voltage stability index	0.303537	0.2951	0.29151
Switching number	0	0	0
$P\{\alpha_c < 0\}$	1.00	0.9844	0.41970
Critical state and generator	I_{pv1},x_{pv11},x_{pv21},x_{pv31}, and PV-DG1	I_{pv1},x_{pv11},x_{pv21},x_{pv31}, and PV-DG1	I_{pv1},x_{pv11},x_{pv21},x_{pv31}, and PV-DG1
Number of violations in bus voltage constraint	0	0	0
Number of violations in line flow constraint	3	3	3
Stability status	stable	unstable	unstable
Reconfigured system			
Open switch	s9,s16,s28,s33,s34	s10,s25,s32,s33,s34	s9,s16,s28,s33,s34
Power loss(kW)	162.211	159.115	155.051
Voltage stability index	0.258005	0.232463	0.255676
Switching number	6	6	6
$P\{\alpha_c < 0\}$	1	1	1
Critical state and generator	I_{pv1},x_{pv11},x_{pv21},x_{pv31} and PV-DG1	I_{pv1},x_{pv11},x_{pv21},x_{pv31} and PV-DG1	I_{pv1},x_{pv11},x_{pv21},x_{pv31} and PV-DG1
Number of violations in bus voltage constraint	0	0	0
Number of violations in line flow constraint	0	0	0
Stability status	stable	stable	stable
Initial case with PV-DGs and SHPP-DGs (scenario 2)			
Power loss(kW)	97.86	90.74	87.552
Voltage stability index	0.21754	0.20909	0.20500
Switching number	0	0	0
$P\{\alpha_c < 0\}$	0.89332	0.88734	0.36293
Critical states and generator	δ_3, ω_3 and SHPP-DG3	δ_3, ω_3 and SHPP-DG3	I_{pv1},x_{pv11},x_{pv21},x_{pv31}, and PV-DG1
Number of violations in bus voltage constraint	0	0	0
Number of violations in line flow constraint	0	0	0
Stability status	unstable	unstable	unstable
Reconfigured system			
Open switch	s9,s15,s33,s34,s37	s9,s16,s33,s34,s37	s8, s15,s33,s34,s37
Power loss(kW)	73.056	69.145	67.199
Voltage stability index	0.11936	0.134602	0.128296
Switching number	4	4	4
$P\{\alpha_c < 0\}$	0.999	1	1
Critical state and generator	δ_3, ω_3 and SHPP-DG3	δ_3, ω_3 and SHPP-DG3	I_{pv1},x_{pv11},x_{pv21},x_{pv31}, and PV-DG1
Number of violations in bus voltage constraint	0	0	0
Number of violations in line flow constraint	0	0	0
Stability status	stable	stable	stable

Table 4.6: Result of 69-bus distribution system with different PDFs of solar irradiance

	Low mean	Medium mean	High mean
Initial case with PV-DG only (scenario 1)			
Power loss(kW)	233.60	219.176	212.738
Voltage stability index	0.31586	0.30915	0.30579
Switching number	0	0	0
$P\{\alpha_c < 0\}$	1	1	0.96384
Critical state and generator	I_{pv2},x_{pv12},x_{pv22},x_{pv32} and PV-DG2	I_{pv2},x_{pv12},x_{pv22},x_{pv32} and PV-DG2	I_{pv2},x_{pv12},x_{pv22},x_{pv32} and PV-DG2
Number of violations in bus voltage constraint	0	0	0
Number of violations in line flow constraint	0	0	0
Stability status	stable	stable	unstable
Reconfigured system			
Open switch	s4,s18,s56,s71,s73	s4,s18,s54,s61,s71	s4,s18,s54,s61,s71
Power loss(kW)	146.159	122.02	117.13
Voltage stability index	0.263775	0.20421	0.20093
Switching number	6	8	8
$P\{\alpha_c < 0\}$	0.999	0.998	0.998
Critical state and generator	I_{pv2},x_{pv12},x_{pv22},x_{pv32} and PV-DG2	I_{pv2},x_{pv12},x_{pv22},x_{pv32} and PV-DG2	I_{pv2},x_{pv12},x_{pv22},x_{pv32} and PV-DG2
Number of violations in bus voltage constraint	0	0	0
Number of violations in line flow constraint	0	0	0
Stability status	stable	stable	stable
Initial case with PV-DGs and SHPP-DGs (scenario 2)			
Power loss(kW)	66.081	58.699	55.912
Voltage stability index	0.111482	0.09068	0.08067
Switching number	0	0	0
$P\{\alpha_c < 0\}$	0.660273	0.660552	0.06754
Critical state and generator	δ_3, ω_3 and SHPP-DG3	δ_3, ω_3 and SHPP-DG3	I_{pv2},x_{pv12},x_{pv22},x_{pv32} and PV-DG2
Number of violations in bus voltage constraint	0	0	0
Number of violations in line flow constraint	0	0	0
Stability status	unstable	unstable	unstable
Reconfigured system			
Open switch	s5,s10,s12,s24,s70	s5,s12,s26,s52,s70	s4,s20,s26,s52,s71
Power loss(kW)	37.290	43.783	48.912
Voltage stability index	0.071061	0.078327	0.056026
Switching number	8	8	8
$P\{\alpha_c < 0\}$	0.999	0.99	0.998
Critical state and generator	δ_3, ω_3 and SHPP-DG3	δ_3, ω_3 and SHPP-DG3,	I_{pv2},x_{pv12},x_{pv22},x_{pv32} and PV-DG2
Number of violations in bus voltage constraint	0	0	0
Number of violations in line flow constraint	0	0	0
Stability status	stable	stable	stable

Table 4.7: Result of 119-bus distribution system with different PDFs of solar irradiance

	Low mean	Medium mean	High mean
Initial case with PV-DG only (scenario 1)			
Power loss(kW)	1301.853	1224.687	1190.498
Voltage stability index	0.430060	0.43047	0.429952
Switching number	0	0	0
$P\{\alpha_c < 0\}$	1	1	0.74922
Critical state and generator	I_{pv1}, x_{pv11}, x_{pv31} and PV-DG1	I_{pv1}, x_{pv11}, x_{pv31} and PV-DG1	I_{pv1}, x_{pv11}, x_{pv31} and PV-DG1
Number of violations in bus voltage constraint	8	8	8
Number of violations in line flow constraint	1	1	0
Stability status	stable	stable	unstable
Reconfigured system			
Open switch	s23,s27,s35,s40,s43,s51,s59,s74,s83, s99,s110,s126,s127,s128,s132	s23,s35,s40,s74,s83,s99,s110,s121, s123,s124,s125,s126,s127,s128,s132	s9,s24,s27,s35,s43,s51,s74,s83,s99, s110,s123,s126,s127,s128,s132
Power loss(kW)	965.70	907.15	866.394
Voltage stability index	0.252112	0.249540	0.24956
Switching number	14	14	20
$P\{\alpha_c < 0\}$	0.999	0.998	0.990
Critical state and generator	I_{pv1}, x_{pv11}, x_{pv31} and PV-DG1	I_{pv1}, x_{pv11}, x_{pv31} and PV-DG1	I_{pv1}, x_{pv11}, x_{pv31} and PV-DG1
Number of violations in bus voltage constraint	0	0	0
Number of violations in line flow constraint	0	0	0
Stability status	stable	stable	stable
Initial case with PV-DGs and SHPP-DGs (scenario 2)			
Power loss(kW)	768.923	707.640	681.951
Voltage stability index	0.323250	0.30183	0.291331
Switching number	0	0	0
$P\{\alpha_c < 0\}$	0.89606	0.77680	0.01902
Critical state and generator	δ_2, ω_2 and SHPP-DG2	I_{pv1}, x_{pv11}, x_{pv31} and PV-DG1	I_{pv1}, x_{pv11}, x_{pv31} and PV-DG1
Number of violations in bus voltage constraint	0	0	0
Number of violations in line flow constraint	1	0	0
Stability status	unstable	unstable	unstable
Reconfigured system			
Open switch	s39,s44,s69,s74,s98,s110,s119,s121, s122,s123,s125,s126,s127,s131,s132	s9,s23,s35,s44,s75,s97,s110,s121, s123,s125,s126,s127, s128,s131,s132	s9,s23,s42,s49,s69,s77,s88,s110,s121, s122,s123,s126,s127,s131,s132
Power loss(kW)	550.121	500.682	539.012
Voltage stability index	0.179412	0.196633	0.204875
Switching number	12	14	16
$P\{\alpha_c < 0\}$	0.999	0.998	0.995
Critical state and generator	δ_2, ω_2 and SHPP-DG3	I_{pv1}, x_{pv11}, x_{pv31} and PV-DG1	I_{pv1}, x_{pv11}, x_{pv31} and PV-DG1
Number of violations in bus voltage constraint	0	0	0
Number of violations in line flow constraint	0	0	0
Stability status	stable	stable	stable

types of DGs in the system affects the system stability, operational constraints and final configuration of the system quite significantly. In fact, stability of the system is more negatively affected in the presence of both PV-DGs and SHPP-DGs as compared to the presence of PV-DGs only. Lastly, Table 4.7 shows that for larger system, with increasing solar irradiation level, the number of switch operations increases to achieve a stable configuration.

4.4 Conclusion

In this chapter, a multiobjective DSR problem in the presence of PV-DG and SHPP-DG has been formulated and subsequently, KnEA-PE method has been applied to solve the formulated problem. Detailed investigations have been carried out on three different test systems with different PDFs of solar irradiance. From the obtained results on the three systems, it can be concluded that both PV-DGs and SHPP-DGs can contribute to the system instability depending on the system operating conditions. At higher level of solar irradiance level, the impact of PV-DGs on the system instability is quite significant.

To enhance the system reliability, wind power generations are integrated in DS along with other DGs. Therefore, appropriate combination of solar, wind and small hydro based DGs can enhance the efficiency and reliability of the system. Toward this goal, the uncertainty and correlation of system input variables such as the load and SHPP, wind, and solar power generation are taken into account in DSR scheme, in the next chapter.

Chapter 5

Stability constrained probabilistic DSR in presence of correlated loads and hybrid Wind Photovoltaic SHPP DGs

This chapter studies the impact of doubly fed induction generators (DFIG) with SHPP-DGs and PV-DGs on the stability of a distribution system with different topologies during reconfiguration. The effects of different levels of wind penetration on DSR are also taken into account. Altered power flow patterns as a result of the varying wind speed may lead to increased number of unstable critical modes of the system. To identify the critical modes of the system and the effect of the high wind penetration on these modes and in turn on system configuration, simulation studies have been carried out on IEEE 33-bus, 69-bus and 119-bus radial distribution systems.

5.1 Introduction

Increasing power generation from renewable energy sources (RES), such as wind, PV-DGs and SHPP-DGs would help in reducing carbon emissions, and hence, minimizes the effect of global warming. Among various RES, wind power generation (WPG) has become a viable alternative source of energy and as a result, penetration of WPG has increased significantly around the world due to its high efficiency and relatively small rating of power converters [83]. However, large integration of the wind generators to the system may bring unexpected threat to the stability of distribution system. Accordingly, the principal objective of this chapter is to investigate the impact of DFIGs on system small-signal stability when the distribution system is reconfigured for improving operational performance and mitigating violation of operational constraint. In the literature, dynamic stability of a grid-connected DFIG has been investigated only with fixed topology of the grid. Therefore stability issues of DS with RESs during reconfiguration requires further study, which is the focus of this chapter.

5.2 Mathematical model of DFIGs, PV-DGs with SHPP type DGs

5.2.1 Probabilistic DFIG modelling

The power generated by DFIG is dependent on the wind speed, which is intermittent. Hence, wind speed can be modeled as a random variable. In this work, wind speed is assumed to follow a Weibull probability distribution [84].

$$f(v) = \frac{K_w}{C_w} * (\frac{v}{C_w})^{K_w-1} exp(-\frac{v}{C_w})^{K_w} \tag{5.1}$$

where v is wind speed (m/s), K_w and C_w are shape and scale parameter of weibull distribution, respectively. These Weibull parameters are expressed using the following equations [85]:

$$K_w = (\sigma_w/\mu_w)^{-1.086} \tag{5.2}$$

$$C_w = (\mu_w/\Gamma(1+1/K_w)) \tag{5.3}$$

where $\Gamma(.)$ is the gamma function, μ_w and σ_w are the mean and standard deviation of wind speed, respectively. For modelling the uncertainty of DFIG power output, the wind speed samples are generated by 3PE method. The generated wind speed samples are transformed to wind turbine output power through wind speed-power curve using equation (5.4) [86].

$$\begin{aligned} P_{wtg} &= 0, \qquad if \quad v \le V_i \quad or \quad V_o \le v \\ P_{wtg} &= P_r \frac{v - V_i}{V_r - V_i}, \qquad if \quad V_i \le v \le V_r \\ P_{wtg} &= P_r, \qquad if \quad V_r \le v \le V_o \end{aligned} \tag{5.4}$$

Where, P_r is capacity of installed DFIG, v, V_i, V_o and V_r are wind speed, cut-in speed, cut-out speed and rated wind speed, respectively.

5.2.2 Mathematical model of DFIG with PV-DGs and SHPP

Let 'm_g', 'm_{pv}' and 'm_{wg}' are the number of SHPP-DGs, PV-DGs and DFIGs connected to the distribution system, respectively. Let, $\mathbf{E} = \{e(1), e(2)...e(i)...e(m_g)\}$, $\mathbf{E}g_{pv} = \{ep(1), ep(2)...ep(j)...ep(m_{pv})\}$ and $\mathbf{E}g_{wg} = \{ew(1), ew(2)...ew(h)...ew(m_{wg})\}$ are the set of SHPP-DGs, PV-DGs and DFIGs buses, respectively, where $ew(h)$ denotes the bus number at which h^{th} DFIG is installed. Further, $2 \le e(i), ep(j), ew(h) \le N$, and $e(i), ep(j), ew(h) \ne s$, for $i = 1, 2...m_g$,, $j = 1, 2...m_{pv}$ and $h = 1, 2...m_{wg}$, where s is the substation bus. Detailed mathematical model of PV-DGs and

SHPP-DGs have been presented in Chapter 4 and Chapter 2, respectively. The details of the DFIG mathematical model is given below.

5.2.2.1 Mathematical model of a DFIGs

The dynamic equations describing DFIG are derived using the basic flux linkage, torque and voltage equations which are transformed into a two-axis synchronously rotating frame (dq axis) applying the standard transformations. The stator and rotor equations of the DFIG in terms of their flux linkages are the following [87]

$$\frac{1}{w_s}\frac{d\psi_{qsh}}{dt} = V_{qsh} + R_{sh}I_{qsh} - \psi_{dsh} \tag{5.5}$$

$$\frac{1}{w_s}\frac{d\psi_{dsh}}{dt} = V_{dsh} + R_{sh}I_{dsh} + \psi_{qsh} \tag{5.6}$$

$$\frac{1}{w_s}\frac{d\psi_{qrh}}{dt} = V_{qrh} - R_{rh}I_{qrh} - \frac{(w_s - w_{rh})}{w_s}\psi_{drh} \tag{5.7}$$

$$\frac{1}{w_s}\frac{d\psi_{drh}}{dt} = V_{drh} - R_{rh}I_{drh} + \frac{(w_s - w_{rh})}{w_s}\psi_{qrh} \tag{5.8}$$

$$\psi_{qsh} = -X_{sh}I_{qsh} + X_{mh}I_{qrh} \tag{5.9}$$

$$\psi_{dsh} = -X_{sh}I_{dsh} + X_{mh}I_{drh} \tag{5.10}$$

$$\psi_{qrh} = X_{rh}I_{qrh} - X_{mh}I_{drh} \tag{5.11}$$

$$\psi_{drh} = X_{rh}I_{drh} - X_{mh}I_{qrh} \tag{5.12}$$

where I, V, R, X, ψ, w denote current, voltage, resistance, reactance, flux linkage and angular speed respectively, and the subscripts 'sh' and 'rh' denote stator and rotor quantities of h^{th} DFIG respectively. Similarly, the subscripts 'q' and 'd' denote q-axis and d-axis quantities respectively, X_{mh} is mutual reactance between the stator and the rotor and w_s is synchronous speed.

In dynamics simulation studies, it has been observed that stator dynamics are faster than rotor dynamics [88], [89], [87]. Therefore, in this work, third order model has been utilized for DFIG representation. This can be achieved by removing stator flux derivatives from equations (5.5) and (5.6). Expression for I_{qrh} and I_{drh} obtained from equations (5.11) and (5.12) are as follows:

$$I_{qrh} = \frac{\psi_{qrh}}{X_{rh}} + \frac{X_{mh}}{X_{rh}} I_{qsh} \quad I_{drh} = \frac{\psi_{drh}}{X_{rh}} + \frac{X_{mh}}{X_{rh}} I_{dsh} \tag{5.13}$$

Multiply equations (5.7) and (5.8) by X_{mh}/R_{rh} and replace I_{qrh} and I_{drh} to obtain

$$\frac{X_{rh}}{w_{sh}R_{rh}} \frac{d\psi_{drh}\frac{X_{mh}}{X_{rh}}}{dt} = \frac{X_{mh}}{R_{rh}} V_{drh} - \frac{X_{mh}}{X_{rh}} \psi_{drh} - \frac{X_{mh}^2}{X_{rh}} I_{dsh} + \frac{w_{sh} - w_{rh}}{w_{sh}} \frac{X_{rh}}{R_{rh}} \Big(\frac{X_{mh}}{X_{rh}} \psi_{qrh} \Big) \tag{5.14}$$

$$\frac{X_{rh}}{w_{sh}R_{rh}} \frac{d\psi_{qrh}\frac{X_{mh}}{X_{rh}}}{dt} = \frac{X_{mh}}{R_{rh}} V_{qrh} - \frac{X_{mh}}{X_{rh}} \psi_{qrh} - \frac{X_{mh}^2}{X_{rh}} I_{qsh} + \frac{w_{sh} - w_{rh}}{w_{sh}} \frac{X_{rh}}{R_{rh}} \Big(\frac{X_{mh}}{X_{rh}} \psi_{drh} \Big) \tag{5.15}$$

Replace $X_{mh}\psi_{drh}/X_{rh}$, $-X_{mh}\psi_{qrh}/X_{rh}$, $X_{rh}/w_{sh}R_{rh}$ by e_{dh}, e_{qh} and T_{oh}, respectively, where e_{dh} and e_{qh} are defined as the equivalent d and q-axis transient rotor voltages, respectively, and T_{oh} is transient open-circuit time constant of h^{th} DFIG and w_{sh} is synchronous speed. After these substitutions, the reduced third order model of the DFIG becomes [87]:

$$\frac{de_{dh}}{dt} = -\frac{1}{T_{oh}} e_{dh} + (X_{sh} - X'_h) i_{qsh} + s_h w_{sh} e_{qh} - w_{sh} \frac{X_{mh}}{X_{rh}} V_{qrh} \tag{5.16}$$

$$\frac{de_{qh}}{dt} = -\frac{1}{T_{oh}} e_{qh} - (X_{sh} - X'_h) i_{dsh} - s_h w_{sh} e_{dh} + w_{sh} \frac{X_{mh}}{X_{rh}} V_{drh} \tag{5.17}$$

$$\frac{dw_{rh}}{dt} = \frac{1}{2H_h} (T_{mh} - T_{eh}) \tag{5.18}$$

Where $X'_h = w_{sh}(X_{sh} - X_{mh}^2/X_{rh})$, T_{mh} and T_{eh} are the mechanical and generator torque respectively. The electromagnetic torque T_{eh} and mechanical torque T_{mh} are given by,

$$T_{eh} = e_{qsh} i_{qsh} + e_{dsh} i_{dsh} \tag{5.19}$$

$$T_{mh} = \frac{0.5\rho\pi r^2 w_{sh} C_p(\lambda, \theta_p) v_{wh}^3}{w_{rh}} \tag{5.20}$$

where ρ is the air density, r is rotor radius, $C_p(\lambda, \theta_p)$ is the power coefficient which can be approximated as [88]

$$C_p(\lambda, \theta_p) = c_1 (\frac{c_2}{\lambda_i} - c_3\theta_p - c_4) exp(\frac{-c_5}{\lambda_i}) \tag{5.21}$$

where

$$\lambda_i = (\frac{1}{\lambda + c_6\theta_p} - \frac{c_7}{\theta_p^3 + 1})^{-1}$$

In the above equations, $c_1 - c_7$ are constant coefficients, λ_h is tip speed ratio ($\lambda_h = r_h w_{rh}/v_{wh}$) and θ_p is pitch angle of DFIG. For a wind turbine with a fixed pitch angle, power curves (which are function of the wind speed and the electrical rotor speed) are depicted in Fig. 5.1 [87].

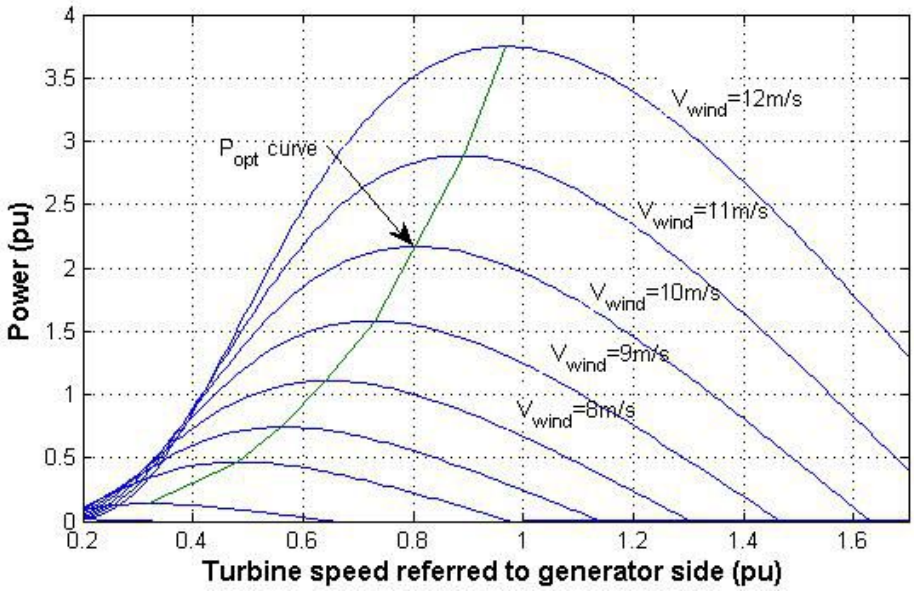

Figure 5.1: wind turbine characteristics

In this work, it is assumed that the q-axis leads the d-axis by 90 in the direction of rotation. The rotating frame (dq-axes) can be aligned with any synchronously rotating variable such as the terminal voltage or stator flux [90]. In this work, the DFIG model is composed of a single-mass model, active and reactive power controllers (as shown in Fig. 5.2). A decoupled control scheme for the active power and reactive power of DFIG has been presented in [91]. In this work, the d-axis flux is oriented along the stator flux axis [87], [92]. Therefore, $\psi_s = \psi_{dsh}$ and $\psi_{qsh} = 0$. In addition, stator resistance R_{sh} is considered very low (neglected) and therefore, equations (5.5) and (5.6) can be utilized to get $V_{qsh} = \psi_{dsh} = V_{ew(h)}$, $V_{dsh} = \psi_{qsh} = 0$, where $V_{ew(h)}$ is the voltage magnitude of the bus $ew(h)$ corresponding to h^{th} DFIG. Consider the flux equations (5.9) and (5.10) to obtain,

$$I_{qsh} = \frac{X_{mh}}{X_{sh}} I_{qrh}, \quad I_{dsh} = \frac{X_{mh}}{X_{sh}} I_{drh} - \frac{V_{ew(h)}}{X_{sh}} \tag{5.22}$$

Then, the complex power leaving the DFIG's stator is

$$P_{sh} + iQ_{sh} = (V_{dsh} I_{dsh} + V_{qsh} I_{qsh}) + i(V_{qsh} I_{dsh} - V_{dsh} I_{qsh}) \tag{5.23}$$

$$P_{sh} + iQ_{sh} = V_{ew(h)}(\frac{X_{mh}}{X_{sh}} I_{qrh}) + iV_{ew(h)}(\frac{X_{mh}}{X_{sh}} I_{drh} - \frac{V_{ew(h)}}{X_{sh}}) \tag{5.24}$$

Equation (5.24) implies that the active and reactive power control can be performed independently

varying I_{qrh} and I_{drh}, respectively. The purpose of the active power controller is to maximize the power extracted from the wind. This maximum power is obtained by P_{opt} curve (shown in Fig. 5.1) which is plotted by joining maximum power points corresponding to each wind speed curve. The obtained power from the P_{opt} curve can be used as power reference for active power controller. This reference is expressed as $P_{opt} = P_{refh} = K_{opt} w_{rh}^3$ (p.u.), where k_{opt} [93] is the optimal gain and calculated by

$$k_{opt} = \frac{0.5\rho\pi r^5 C_{pmax}}{(\lambda_{opt} G_n)^3} \tag{5.25}$$

where G_n is gearbox transformation ratio of a wind turbine generator. As the power coefficient C_p is a nonlinear function of λ and θ_p, so there is an optimal tip-speed ratio λ_{opt} to achieve the optimal power coefficient C_{pmax} for a constant pitch angle. The aim of the reactive power controller is to maintain a prespecified reactive power.

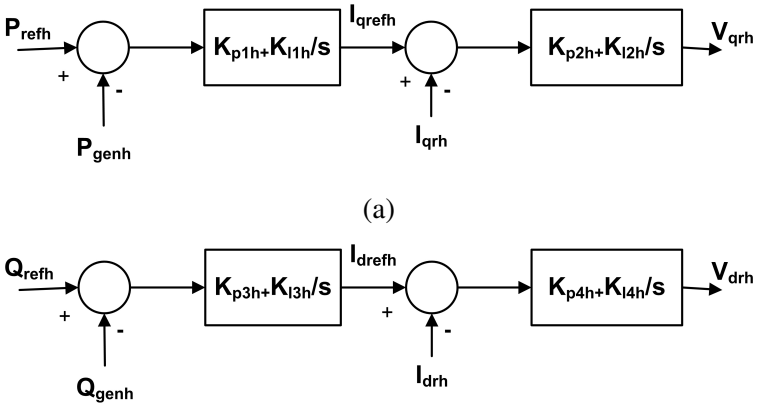

Figure 5.2: (a) Real-power controller (b) reactive power controller

The set of differential and algebraic equations of the power controllers can be written as [94]

$$\frac{dx_{1h}}{dt} = k_{I1h}(P_{refh} - P_{genh}) \tag{5.26}$$

$$\frac{dx_{2h}}{dt} = k_{I2h}[k_{p1h}(P_{refh} - P_{genh}) + x_{1h} - I_{qrh}] \tag{5.27}$$

$$V_{qrh} = k_{p2h}[k_{p1h}(P_{refh} - P_{genh}) + x_{1h} - I_{qrh}] + x_{2h} \tag{5.28}$$

$$\frac{dx_{3h}}{dt} = k_{I3h}(Q_{refh} - Q_{genh}) \tag{5.29}$$

$$\frac{dx_{4h}}{dt} = k_{l4h}[k_{p3h}(Q_{refh} - Q_{genh}) + x_{3h} - I_{drh}] \tag{5.30}$$

$$V_{drh} = k_{p4h}[k_{p3h}(Q_{refh} - Q_{genh}) + x_{3h} - I_{drh}] + x_{4h} \tag{5.31}$$

In the above equations, the state variables x_{1h},x_{2h}, x_{3h} and x_{4h} are related to active and reactive power controllers. P_{refh} and Q_{refh} are real and reactive power reference, whereas P_{genh} and Q_{genh} are generated real and reactive power, respectively. k_{p1h}, k_{p2h} and k_{l1h}, k_{l2h} are the proportional and integral control gains of the active power controller, respectively. k_{p3h}, k_{p4h} and k_{l3h}, K_{l4h} are the proportional and integral control gains of the reactive power controller, respectively. In order to achieve unity power factor, Q_{ref} is set as 0. Further, it is well known that there are four modes of operation for wind turbine control [84] as expressed in equation (5.4). In the first region, the wind speed is lower than the cut-in speed and the wind turbine is unable to produce power; in the second region, MPPT control is adopted to extract the maximum wind power at different wind speeds by maintaining the optimal tip-speed ratio λ_{opt}; in the third region, the wind speed is higher than the rated wind speed and hence the pitch control is adopted to maintain constant power; in the fourth region, the wind speed is higher than the cut-off speed and hence wind turbine is shut down to avoid damage. In this analysis, the wind speed, and therefore the active power output, is assumed to be within its limits and operating in second region to extract the maximum power from the wind. Consequently, the pitch angle controller is not included in the presented DFIG model.

Stator voltage equations corresponding to h^{th} DG ($1 \leq i \leq m_{wg}$) can be written as [87]

$$V_{dsh} = -R_{sh}i_{dsh} + X'_h i_{qsh} + e_{dh} \tag{5.32}$$

$$V_{qsh} = -R_{sh}i_{qsh} - X'_h i_{dsh} + e_{qh} \tag{5.33}$$

Network equations

The network equations for distribution system are described by the power balance equations as

$$\begin{aligned}\sum_{k=1}^{N} V_{e(i)}V_k Y_{e(i)k}\cos(\theta_{e(i)} - \theta_k - \alpha_{e(i)k}) - PL_{e(i)} - I_{di}V_{e(i)}\sin(\delta_i - \theta_{e(i)}) \\ -I_{qi}V_{e(i)}\cos(\delta_i - \theta_{e(i)}) = 0\end{aligned} \tag{5.34}$$

$$\sum_{k=1}^{N} V_{e(i)}V_kY_{e(i)k}\sin(\theta_{e(i)}-\theta_k-\alpha_{e(i)k})-QL_{e(i)}-I_{di}V_{e(i)}\cos(\delta_i-\theta_{e(i)}) \\ +I_{qi}V_{e(i)}\sin(\delta_i-\theta_{e(i)})=0 \\ 1\le i\le m_g \tag{5.35}$$

$$\sum_{k=1}^{N} V_{ep(j)}V_kY_{ep(j)k}\cos(\theta_{ep(j)}-\theta_k-\alpha_{ep(j)k})-PL_{ep(j)}+I_{pdj}V_{ep(j)}\cos(\theta_{ep(j)}) \\ +I_{pqj}V_{ep(j)}\sin(\theta_{ep(j)})=0 \tag{5.36}$$

$$\sum_{k=1}^{N} V_{ep(j)}V_kY_{ep(j)k}\sin(\theta_{ep(j)}-\theta_k-\alpha_{ep(j)k})-QL_{ep(j)}+I_{pdj}V_{ep(j)}\sin(\theta_{ep(j)}) \\ -I_{pqj}V_{ep(j)}\cos(\theta_{ep(j)})=0 \\ 1\le j\le m_{pv} \tag{5.37}$$

$$\sum_{k=1}^{N} V_{ew(h)}V_kY_{ew(h)k}\cos(\theta_{ew(h)}-\theta_k-\alpha_{ew(h)k})-PL_{ew(h)}-I_{qsh}V_{ew(h)}-I_{qrh}V_{qrh}- \\ I_{drh}V_{drh}=0 \tag{5.38}$$

$$\sum_{k=1}^{N} V_{ew(h)}V_kY_{ew(h)k}\sin(\theta_{ew(h)}-\theta_k-\alpha_{ew(h)k})-QL_{ew(h)}+I_{dsh}V_{ew(h)}=0 \\ 1\le i\le m_{wg} \tag{5.39}$$

$$\sum_{k=1}^{N} V_sV_kY_{sk}\cos(\theta_s-\theta_k-\alpha_{sk})=P_s \tag{5.40}$$

$$\sum_{k=1}^{N} V_sV_kY_{sk}\sin(\theta_s-\theta_k-\alpha_{sk})=Q_s \tag{5.41}$$

$$\sum_{k=1}^{N} V_lV_kY_{lk}\cos(\theta_l-\theta_k-\alpha_{lk})-PL_l=0 \tag{5.42}$$

$$\sum_{k=1}^{N} V_lV_kY_{lk}\sin(\theta_l-\theta_k-\alpha_{lk})-QL_l=0 \\ 2\le l\le N \tag{5.43}$$

Probabilistic SSSA has been performed in the presence of DFIG with SHPP-DGs and PV-DGs

in distribution system. Basically, the steps of this analysis can be summarized as follows: (a) calculate an equilibrium point; (b) linearize the set of equations around the equilibrium point; (c) obtain the system state matrix (A_{sys}) as described in the previous chapters; and (d) calculate the eigenvalues.

By linearizing the differential equations (5.16)-(5.18) and (5.26)-(5.31), following expressions are obtained:

$$\frac{d\Delta e_{dh}}{dt} = -\frac{1}{T_{oh}}\Delta e_{dh} + (X_{sh} - X'_h)\Delta i_{qsh} + s_h w_{sh}\Delta e_{qh} + w_{sh} e_{qh}\Delta s_h - w_{sh}\frac{X_{mh}}{X_{rh}}\Delta V_{qrh} \quad (5.44)$$

$$\frac{d\Delta e_{qh}}{dt} = -\frac{1}{T_{oh}}\Delta e_{qh} - (X_{sh} - X'_h)\Delta i_{dsh} - s_h w_{sh}\Delta e_{dh} - w_{sh} e_{dh}\Delta s_h + w_{sh}\frac{X_{mh}}{X_{rh}}\Delta V_{drh} \quad (5.45)$$

$$\frac{d\Delta w_{rh}}{dt} = \frac{1}{2H_h}(\Delta T_{mh} - \Delta T_{eh}) \quad (5.46)$$

$$\frac{d\Delta x_{1h}}{dt} = k_{l1h}(\Delta P_{refh} - \Delta P_{genh}) \quad (5.47)$$

$$\frac{d\Delta x_{2h}}{dt} = k_{l2h}[k_{p1h}(\Delta P_{refh} - \Delta P_{genh}) + \Delta x_{1h} - \Delta I_{qrh}] \quad (5.48)$$

$$\frac{d\Delta x_{3h}}{dt} = k_{l3h}(\Delta Q_{refh} - \Delta Q_{genh}) \quad (5.49)$$

$$\frac{d\Delta x_{4h}}{dt} = k_{l4h}[k_{p3h}(\Delta Q_{refh} - \Delta Q_{genh}) + \Delta x_{3h} - \Delta I_{drh}] \quad (5.50)$$

$$\Delta V_{qrh} = k_{p2h}[k_{p1h}(\Delta P_{refh} - \Delta P_{genh}) + \Delta x_{1h} - \Delta I_{qrh}] + \Delta x_{2h} \quad (5.51)$$

$$\Delta V_{drh} = k_{p4h}[k_{p3h}(\Delta Q_{refh} - \Delta Q_{genh}) + \Delta x_{3h} - \Delta I_{drh}] + \Delta x_{4h} \quad (5.52)$$

Equations (2.20)-(2.23), (4.25)-(4.32) and (5.44)-(5.52), for all DGs can be written in the following form:

$$\Delta\dot{\mathbf{x}} = \mathbf{A}\Delta\mathbf{x} + \mathbf{B}_G\Delta\mathbf{I}_g + \mathbf{B}_p\Delta\mathbf{I}_p + \mathbf{B}_w\Delta\mathbf{I}_w + \mathbf{B}_1\Delta\mathbf{Z}_G + \mathbf{B}_{1p}\Delta\mathbf{Z}_{Gp} + B_{1w}\Delta\mathbf{Z}_{Gw} + \mathbf{E}\Delta\mathbf{u} \quad (5.53)$$

By the linearization of algebric equations (5.32) and (5.33), we get,

$$-\Delta V_{dsh} - R_{sh}\Delta i_{dsh} + X'_h\Delta i_{qsh} + \Delta e_{dh} = 0 \quad (5.54)$$

$$-\Delta V_{qsh} - R_{sh}\Delta i_{qsh} - X'_h\Delta i_{dsh} + \Delta e_{qh} = 0 \quad (5.55)$$

Rewriting equations (5.54)-(5.55), for all DFIGs together, in matrix form gives

$$\mathbf{0} = \mathbf{A}_{1w}\Delta\mathbf{x} + \mathbf{B}_{2w}\Delta\mathbf{I}_w + \mathbf{B}_{3w}\Delta\mathbf{Z}_{Gw} \quad (5.56)$$

Linearizing the network equations (5.34) and (5.41), following expressions are obtained

$$\sum_{\substack{k=1\\k\neq e(i)}}^{N} V_k Y_{e(i)k}\cos(\theta_{e(i)}-\theta_k-\alpha_{e(i)k})\Delta V_{e(i)}+I_{qi}\cos(\delta_i-\theta_{e(i)})\Delta V_{e(i)}+I_{di}\sin(\delta_i-\theta_{e(i)})\Delta V_{e(i)}+$$

$$\sum_{k=1}^{N} V_{e(i)}Y_{e(i)k}\cos(\theta_{e(i)}-\theta_k-\alpha_{e(i)k})\Delta V_k+\sum_{k=1}^{N} V_{e(i)}V_k Y_{e(i)k}\sin(\theta_{e(i)}-\theta_k-\alpha_{e(i)k})\Delta\theta_k-$$

$$\sum_{\substack{k=1\\k\neq e(i)}}^{N} V_{e(i)}V_k Y_{e(i)k}\sin(\theta_{e(i)}-\theta_k-\alpha_{e(i)k})\Delta\theta_{e(i)}-I_{di}V_{e(i)}\cos(\delta_i-\theta_{e(i)})\Delta\theta_{e(i)}+I_{qi}V_{e(i)}\sin(\delta_i-\theta_{e(i)})\Delta\theta_{e(i)}$$

$$-\Delta PL_{e(i)}-\Delta I_{di}V_{e(i)}\sin(\delta_i-\theta_{e(i)})+I_{di}V_{e(i)}\cos(\delta_i-\theta_{e(i)})\Delta\delta_i+\Delta I_{qi}V_{e(i)}\cos(\delta_i-\theta_{e(i)})+$$

$$I_{qi}V_{e(i)}\sin(\delta_i-\theta_{e(i)})\Delta\delta_i=0 \quad (5.57)$$

$$\sum_{\substack{k=1\\k\neq e(i)}}^{N} V_k Y_{e(i)k}\sin(\theta_{e(i)}-\theta_k-\alpha_{e(i)k})\Delta V_{e(i)}-I_{qi}\sin(\delta_i-\theta_{e(i)})\Delta V_{e(i)}+I_{di}\cos(\delta_i-\theta_{e(i)})\Delta V_{e(i)}+$$

$$\sum_{k=1}^{N} V_{e(i)}V_k Y_{e(i)k}\sin(\theta_{e(i)}-\theta_k-\alpha_{e(i)k})\Delta V_k-\sum_{k=1}^{N} V_{e(i)}V_k Y_{e(i)k}\cos(\theta_{e(i)}-\theta_k-\alpha_{e(i)k})\Delta\theta_k-$$

$$\sum_{\substack{k=1\\k\neq e(i)}}^{N} V_{e(i)}V_k Y_{e(i)k}\cos(\theta_{e(i)}-\theta_k-\alpha_{e(i)k})\Delta\theta_{e(i)}+I_{di}V_{e(i)}\sin(\delta_i-\theta_{e(i)})\Delta\theta_{g(i)}+I_{qi}V_{e(i)}\cos(\delta_i-\theta_{e(i)})\Delta\theta_{e(i)}$$

$$-\Delta QL_{e(i)}+\Delta I_{di}V_{e(i)}\cos(\delta_i-\theta_{e(i)})-I_{di}V_{e(i)}\sin(\delta_i-\theta_{e(i)})\Delta\delta_i-V_{g(i)}\sin(\delta_i-\theta_{e(i)})\Delta I_{qi}+$$

$$I_{qi}V_{e(i)}\cos(\delta_i-\theta_{e(i)})\Delta\delta_i=0 \quad (5.58)$$

$$(\sum_{\substack{k=1\\k\neq ep(j)}}^{N} V_k Y_{ep(j)k}\cos(\theta_{ep(j)}-\theta_k-\alpha_{ep(j)k})+I_{pqj}\sin(\theta_{ep(j)})+I_{pdj}\cos(\theta_{ep(j)}))\Delta V_{ep(j)}-\Delta PL_{ep(j)}+$$

$$V_{ep(j)}(-\sum_{\substack{k=1\\k\neq ep(j)}}^{N} V_k Y_{ep(j)k}\sin(\theta_{ep(j)}-\theta_k-\alpha_{ep(j)k})+I_{pqj}\cos(\theta_{ep(j)})-I_{pdj}\sin(\theta_{ep(j)}))\Delta\theta_{ep(j)}+$$

$$V_{ep(j)}\cos(\theta_{ep(j)})\Delta I_{pdj}+V_{ep(j)}\sin(\theta_{ep(j)})\Delta I_{pqj}+(\sum_{k=1}^{N} V_{ep(j)}Y_{ep(j)k}\cos(\theta_{ep(j)}-\theta_k-\alpha_{ep(j)k}))\Delta V_k+$$

$$(\sum_{k=1}^{N} V_k V_{ep(j)}Y_{ep(j)k}\sin(\theta_{ep(j)}-\theta_k-\alpha_{ep(j)k}))\Delta\theta_k=0 \quad (5.59)$$

$$(\sum_{\substack{k=1\\k\neq ep(j)}}^{N} V_k Y_{ep(j)k}\sin(\theta_{ep(j)}-\theta_k-\alpha_{ep(j)k})+I_{pdj}\sin(\theta_{ep(j)})-I_{pqj}\cos(\theta_{ep(j)}))\Delta V_{ep(j)}-\Delta QL_{ep(j)}+$$

$$V_{ep(j)}(-\sum_{\substack{k=1\\k\neq ep(j)}}^{N} V_k Y_{ep(j)k}\cos(\theta_{ep(j)}-\theta_k-\alpha_{ep(j)k})+I_{pdj}\cos(\theta_{ep(j)})+I_{pdj}\sin(\theta_{ep(j)}))\Delta\theta_{ep(j)}+$$

$$V_{ep(j)}\sin(\theta_{ep(j)})\Delta I_{pdj}-V_{ep(j)}\cos(\theta_{ep(j)})\Delta I_{pqj}+(\sum_{k=1}^{N} V_{ep(j)}Y_{ep(j)k}\sin(\theta_{ep(j)}-\theta_k-\alpha_{ep(j)k}))\Delta V_k-$$

$$(\sum_{k=1}^{N} V_k V_{ep(j)}Y_{ep(j)k}\cos(\theta_{ep(j)}-\theta_k-\alpha_{ep(j)k}))\Delta\theta_k=0 \quad (5.60)$$

$$(\sum_{\substack{k=1\\k\neq ew(h)}}^{N} V_k Y_{ew(h)k}\cos(\theta_{ew(h)}-\theta_k-\alpha_{ew(h)k})-I_{qsh})\Delta V_{ew(h)}-I_{qrh}\Delta V_{ew(h)}-\Delta PL_{ew(h)}-I_{qrh}\Delta V_{qrh}-$$

$$I_{drh}\Delta V_{drh}+V_{ew(h)}\Delta I_{qsh}+V_{ew(h)}(-\sum_{\substack{k=1\\k\neq ew(h)}}^{N} V_k Y_{ew(h)k}\sin(\theta_{ew(h)}-\theta_k-\alpha_{ew(h)k}))\Delta\theta_{ew(h)}+$$

$$+(\sum_{k=1}^{N} V_{ew(h)}Y_{ew(h)k}\cos(\theta_{ew(h)}-\theta_k-\alpha_{ew(h)k}))\Delta V_k+$$

$$(\sum_{k=1}^{N} V_k V_{ew(h)}Y_{ew(h)k}\sin(\theta_{ew(h)}-\theta_k-\alpha_{ew(h)k}))\Delta\theta_k=0 \quad (5.61)$$

$$(\sum_{\substack{k=1\\k\neq ew(h)}}^{N} V_k Y_{ew(h)k}\sin(\theta_{ew(h)}-\theta_k-\alpha_{ew(h)k})+I_{dsh})\Delta V_{ew(h)}+V_{ew(h)}\Delta I_{dsh}-\Delta QL_{ew(h)}+$$

$$V_{ew(h)}(-\sum_{\substack{k=1\\k\neq ew(h)}}^{N} V_k Y_{ew(h)k}\cos(\theta_{ew(h)}-\theta_k-\alpha_{ew(h)k}))\Delta\theta_{ew(h)}+$$

$$+(\sum_{k=1}^{N} V_{ew(h)}Y_{ew(h)k}\sin(\theta_{ep(j)}-\theta_k-\alpha_{ew(h)k}))\Delta V_k-$$

$$(\sum_{k=1}^{N} V_k V_{ew(h)}Y_{ew(h)k}\cos(\theta_{ew(h)}-\theta_k-\alpha_{ew(h)k}))\Delta\theta_k=0 \quad (5.62)$$

where $V_{ew(h)}$ and $\theta_{ew(h)}$ are the voltage magnitude and angle of the bus $ew(h)$ corresponding to h^{th}

DFIG respectively.

$$\Delta P_s = \sum_{k=1}^{N} V_s Y_{sk} \cos(\theta_s - \theta_k - \alpha_{sk}) \Delta V_k + \sum_{k=1}^{N} V_s V_k Y_{sk} \sin(\theta_s - \theta_k - \alpha_{sk}) \Delta\theta_k + \Delta V_{e(i)}$$
$$\sum_{\substack{k=1 \\ k \neq e(i)}}^{N} V_k Y_{se(i)} \cos(\theta_s - \theta_e(i) - \alpha_{sk}) + \sum_{\substack{k=1 \\ k \neq e(i)}}^{N} V_{e(i)} V_k Y_{se(i)} \sin(\theta_s - \theta_e(i) - \alpha_{sk}) \Delta\theta_{e(i)} + \Delta V_{ep(j)}$$
$$\sum_{\substack{k=1 \\ k \neq ep(j)}}^{N} V_k Y_{sep(j)} \cos(\theta_s - \theta_{ep(j)} - \alpha_{sk}) + \sum_{\substack{k=1 \\ k \neq ep(j)}}^{N} V_{ep(j)} V_k Y_{sep(j)} \sin(\theta_s - \theta_{ep(j)} - \alpha_{sk}) \Delta\theta_{ep(j)} \tag{5.63}$$

$$\Delta Q_s = \sum_{k=1}^{N} V_s Y_{sk} \sin(\theta_s - \theta_k - \alpha_{sk}) \Delta V_k - \sum_{k=1}^{N} V_s V_k Y_{sk} \cos(\theta_s - \theta_k - \alpha_{sk}) \Delta\theta_k + \Delta V_{e(i)}$$
$$\sum_{\substack{k=1 \\ k \neq e(i)}}^{N} V_k Y_{se(i)} \sin(\theta_s - \theta_e(i) - \alpha_{sk}) - \sum_{\substack{k=1 \\ k \neq e(i)}}^{N} V_{e(i)} V_k Y_{se(i)} \sin(\theta_s - \theta_e(i) - \alpha_{sk}) \Delta\theta_{e(i)} +$$
$$\Delta V_{ep(j)} \sum_{\substack{k=1 \\ k \neq ep(j)}}^{N} V_k Y_{sep(j)} \sin(\theta_s - \theta_{ep(j)} - \alpha_{sk}) - \sum_{\substack{k=1 \\ k \neq ep(j)}}^{N} V_{ep(j)} V_k Y_{sep(j)} \sin(\theta_s - \theta_{ep(j)} - \alpha_{sk}) \Delta\theta_{ep(j)} \tag{5.64}$$

Rewriting linearized power flow equations (5.57) and (5.58), in matrix form, gives

$$\mathbf{0} = \mathbf{C}_1 \Delta\mathbf{x} + \mathbf{C}_2 \Delta\mathbf{I}_g + \mathbf{C}_3 \Delta\mathbf{Z}_G + \mathbf{C}_4 \Delta\mathbf{Z}_l + \mathbf{C}_5 \Delta\mathbf{Z}_{Gp} + \mathbf{C}_6 \Delta\mathbf{Z}_{Gw} \tag{5.65}$$

In matrix form, equations (5.59) and (5.60), can be written as

$$\mathbf{0} = \mathbf{C}_{1p} \Delta\mathbf{x} + \mathbf{C}_{2p} \Delta\mathbf{I}_p + \mathbf{C}_{3p} \Delta\mathbf{Z}_{Gp} + \mathbf{C}_{4p} \Delta\mathbf{Z}_l + \mathbf{C}_{5p} \Delta\mathbf{Z}_G + \mathbf{C}_{6p} \Delta\mathbf{Z}_{Gw} \tag{5.66}$$

Similarly, In matrix form, equations (5.61) and (5.62), can be written as

$$\mathbf{0} = \mathbf{C}_{1w} \Delta\mathbf{x} + \mathbf{C}_{2w} \Delta\mathbf{I}_w + \mathbf{C}_{3w} \Delta\mathbf{Z}_{Gw} + \mathbf{C}_{4w} \Delta\mathbf{Z}_l + \mathbf{C}_{5w} \Delta\mathbf{Z}_G + \mathbf{C}_{6w} \Delta\mathbf{Z}_{Gp} \tag{5.67}$$

Rewriting equations (5.63) and (5.64), in matrix form, we obtain

$$\mathbf{0} = \mathbf{D}_3 \Delta\mathbf{Z}_G + \mathbf{D}_{3p} \Delta\mathbf{Z}_{Gp} + \mathbf{D}_{3w} \Delta\mathbf{Z}_{Gw} + \mathbf{D}_4 \Delta\mathbf{Z}_l + \mathbf{D}_5 \Delta\mathbf{S} \tag{5.68}$$

The lineraized real and reactive power balance equations (2.34)- (2.35) at all the buses other than the DG buses can be written in matrix form as

$$\mathbf{0} = \mathbf{D}_1 \Delta\mathbf{Z}_G + \mathbf{D}_{1p} \Delta\mathbf{Z}_{Gp} + \mathbf{D}_{1w} \Delta\mathbf{Z}_{Gw} + \mathbf{D}_2 \Delta\mathbf{Z}_l \tag{5.69}$$

Equation (2.27), (4.38), (5.56), (5.65), (5.66), (5.67), (5.68) and (5.69) can be written in the following form:

$$\begin{bmatrix} \mathbf{B_2} & 0 & 0 & \mathbf{B_3} & \mathbf{0} & \mathbf{0} & \mathbf{0} & \mathbf{0} \\ \mathbf{C_2} & 0 & 0 & \mathbf{C_3} & \mathbf{C_5} & \mathbf{C_6} & \mathbf{C_4} & \mathbf{0} \\ \mathbf{0} & \mathbf{0} & \mathbf{0} & \mathbf{D_1} & \mathbf{D_{1p}} & \mathbf{D_{1w}} & \mathbf{D_2} & \mathbf{0} \\ \mathbf{0} & \mathbf{0} & \mathbf{0} & \mathbf{D_3} & \mathbf{D_{3p}} & \mathbf{D_{3w}} & \mathbf{D_4} & \mathbf{D_5} \\ \mathbf{0} & \mathbf{B_{2p}} & \mathbf{0} & \mathbf{0} & \mathbf{B_{3p}} & \mathbf{0} & \mathbf{0} & \mathbf{0} \\ \mathbf{0} & \mathbf{C_{2p}} & \mathbf{0} & \mathbf{C_{5p}} & \mathbf{C_{3p}} & \mathbf{C_{6p}} & \mathbf{C_{4p}} & \mathbf{0} \\ \mathbf{0} & \mathbf{0} & \mathbf{B_{2w}} & \mathbf{0} & \mathbf{0} & \mathbf{B_{3w}} & \mathbf{0} & \mathbf{0} \\ \mathbf{0} & \mathbf{0} & \mathbf{C_{2w}} & \mathbf{C_{5w}} & \mathbf{C_{6w}} & \mathbf{C_{3w}} & \mathbf{C_{4w}} & \end{bmatrix} \begin{bmatrix} \mathbf{\Delta I}_g \\ \mathbf{\Delta I}_p \\ \mathbf{\Delta I}_w \\ \mathbf{\Delta Z}_G \\ \mathbf{\Delta Z}_{Gp} \\ \mathbf{\Delta Z}_{Gw} \\ \mathbf{\Delta Z}_l \\ \mathbf{\Delta S} \end{bmatrix} = \begin{bmatrix} -\mathbf{A_1} \\ -\mathbf{C_1} \\ \mathbf{0} \\ \mathbf{0} \\ -\mathbf{A_{1p}} \\ -\mathbf{C_{1p}} \\ -\mathbf{A_{1w}} \\ -\mathbf{C_{1w}} \end{bmatrix} \Big[\mathbf{\Delta X}\Big] \tag{5.70}$$

The vectors of state variables, $\mathbf{x}$ and algebraic variables, $\mathbf{Y_s}$, for this system are the following:

$\mathbf{x} = [\mathbf{x_G^T} \quad \mathbf{x_P^T} \quad \mathbf{x_W^T}]^\mathbf{T}$

$\mathbf{x_G} = [\mathbf{x_1^T} \quad \mathbf{x_2^T} \ldots \mathbf{x_i^T} \ldots \mathbf{x_{m_g}^T}]^\mathbf{T}, \qquad \mathbf{x}_i = [\delta_i \quad \omega_i \quad E'_{qi} \quad E_{fdi}]^T$

$\mathbf{x_P} = [\mathbf{x_1^T} \quad \mathbf{x_2^T} \ldots \mathbf{x_j^T} \ldots \mathbf{x_{m_{pv}}^T}]^\mathbf{T}, \qquad \mathbf{x}_j = [V_{dcj} \quad I_{pvj} \quad x_{pv1j} \quad x_{pv2j} \quad x_{pv3j}]^T$

$\mathbf{x_W} = [\mathbf{x_1^T} \quad \mathbf{x_2^T} \ldots \mathbf{x_h^T} \ldots \mathbf{x_{m_{wg}}^T}]^\mathbf{T}, \qquad \mathbf{x}_h = [e_{dh} \quad e_{qh} \quad w_{rh} \quad x_{1h} \quad x_{2h} \quad x_{3h} \quad x_{4h}]^T$

$\mathbf{Y}_s = [\mathbf{I}_g^T \quad \mathbf{I}_p^T \quad \mathbf{I}_w^T \quad \mathbf{Z}_G^T \quad \mathbf{Z}_{Gp}^T \quad \mathbf{Z}_{Gw}^T \quad \mathbf{Z}_l^T]^T$

$\mathbf{I}_g = [\mathbf{I}_{g1}^T \quad \mathbf{I}_{g2}^T \ldots \mathbf{I}_{gi}^T \ldots \mathbf{I}_{gm_g}^T]^T, \qquad \mathbf{I}_{gi} = [I_{di} \quad I_{qi}]^T$

$\mathbf{I}_p = [\mathbf{I}_{p1}^T \quad \mathbf{I}_{p2}^T \ldots \mathbf{I}_{pj}^T \ldots \mathbf{I}_{pm_{pv}}^T]^T, \qquad \mathbf{I}_{pj} = [I_{dpj} \quad I_{qpj}]^T$

$\mathbf{I}_w = [\mathbf{I}_{w1}^T \quad \mathbf{I}_{w2}^T \ldots \mathbf{I}_{wh}^T \ldots \mathbf{I}_{wm_{wg}}^T]^T, \qquad \mathbf{I}_{wh} = [I_{dsh} \quad I_{qsh}]^T$

$\mathbf{Z}_G = [V_{e(1)} \quad V_{e(2)} \ldots V_{e(m_p)} \quad \theta_{e(1)} \quad \theta_{e(2)} \ldots \theta_{e(m_{pv})}]^T$

$\mathbf{Z}_{Gp} = [V_{ep(1)} \quad V_{ep(2)} \ldots V_{ep(m_{pv})} \quad \theta_{ep(1)} \quad \theta_{ep(2)} \ldots \theta_{ep(m_{pv})}]^T$

$\mathbf{Z}_{Gw} = [V_{w(1)} \quad V_{w(2)} \ldots V_{w(m_{wg})} \quad \theta_{w(1)} \quad \theta_{w(2)} \ldots \theta_{w(m_{wg})}]^T$

$\mathbf{Z}_l = [V_2 \quad V_3 \ldots V_e \ldots V_N \quad \theta_2 \quad \theta_3 \ldots \theta_e \ldots \theta_N]^T \qquad 2 \leq e \leq N; p \notin \mathbf{E}_g; e \notin \mathbf{E}g_{pv}; e \notin \mathbf{E}g_{wg}$

$\mathbf{S} = [P_s \quad Q_s]^T = [P_1 \quad Q_1]^T$

$1 \leq i \leq m_g, 1 \leq j \leq m_{pv}, 1 \leq h \leq m_{wg}$

By extracting rows corresponding to $\mathbf{\Delta I}_g$, $\mathbf{\Delta I}_p$, $\mathbf{\Delta I}_w$, $\mathbf{\Delta Z}_{Gp}$, $\mathbf{\Delta Z}_{Gw}$and $\mathbf{\Delta Z}_G$ from equation (5.70) and substituting it into equation (5.53), we get

$$\mathbf{\Delta \dot{x}} = \mathbf{A}_{sys}\Delta\mathbf{x} + \mathbf{E}\Delta\mathbf{u} \tag{5.71}$$

Mathematically, probabilistic small signal stability constraint can be expressed as in equation (3.6). Stability of system is judged by the conditional probability of real part of the critical mode eigenvalue.

5.3 Case studies

In this work, Weibull distribution is used to model the probabilistic wind speed with the scale parameter of 9.0 m/s and the shape parameter of 3 m/s. The output active powers of DFIGs are obtained according to equation (5.4), where the wind speed distribution parameters are taken as, V_i = 3 m/s, V_o= 25 m/s and V_r = 12 m/s, [75] respectively. Further, to examine the effect of addition of DFIG, one DFIG is assumed to be located as bus 24 in 33 bus system and at bus 27 for 69 bus system with an installed capacity of 250 kW [95]. For 119 bus system, two DFIGs are assumed to be connected at buses 28 and 47, each with installed capacity of 660 kW [96]. The parameters for DFIGs are given in Appendix B. The speeds of theses wind turbines are assumed to be correlated to each other by a correlation coefficient 0.3. In this work, all DFIGs are considered to generate power at unity power factor. It is to be noted that the correlation between power output of DGs and between loads are also considered in this work. As in Chapter 3, same correlation matrices for loads and DGs have been considered for all three systems. Details related to sizing and location of SHPP-DGs and PV-DGs are same as given in Chapter 3 and 4.

In this work, the effect of DFIGs and impact of dynamic interactions among DFIGs, PV-DGs and SHPP-DGs on DSR, are considered under two scenarios. These are:

1) when only DFIGs are present in the system,

2) when DFIGs, PV-DGs and SHPP-DGs are present in the system.

The results obtained are shown in Table 5.1 for both scenarios. The difference between the optimal topologies obtained under both scenarios are noticeable because of the interaction among all DGs. It is seen that addition of DFIG in the presence of PV-DGs and SHPP-DGs can generate more infeasible solutions as a result of violation of system stability and other operational constraints.

Table 5.1: Result of DSR for all three systems

	33 bus system	69 bus system	119 bus system
Initial case with DFIG only (scenario 1)			
Power loss(kW)	209.118	227.57	1288.66
Voltage stability index	0.303469	0.314214	0.4308
Switching number	0	0	0
$P\{\alpha_c < 0\}$	0.92620	0.98331	0.77341
Participating DGs and associated states	DFIG1 and e_{d1}, e_{q1}	DFIG1 and e_{d1}, e_{q1}	DFIG2 and e_{d2}, e_{q2}
Number of violations in bus voltage constraint	0	0	8
Number of violations in line flow constraint	0	0	0
Stability status	unstable	unstable	unstable
Reconfigured system			
Open switch	s7,s9,s34,s36,s37	s9,s16,s62,s71,s72	s23,s35,s44,s74,s98,s110,s120,s121,s123, s125,s126,s127,s128,s131,s132
Power loss(kW)	152.177	154.514	948.225
Voltage stability index	0.238817	0.239466	0.261242
Switching number	4	6	12
$P\{\alpha_c < 0\}$	1	1	1
Number of violations in bus voltage constraint	0	0	0
Number of violations in line flow constraint	0	0	0
Stability status	stable	stable	stable
Initial case with DFIG, PV-DGs and SHPP-DGs (scenario 2)			
Power loss(kW)	81.152	55.062	680.088
Voltage stability index	0.19132	0.065478	0.3020
Switching number	0	0	0
$P\{\alpha_c < 0\}$	0.471330	0.32370	0.3912
Participating DGs and associated states	SHPP-DG3 and δ, ω	DFIG1 and e_{d1}, e_{q1}	DFIG2 and e_{d2}, e_{q2}
Number of violations in bus voltage constraint	0	0	0
Number of violations in line flow constraint	0	0	0
Stability status	unstable	unstable	unstable
Reconfigured system			
Open switch	s11,s29,s33,s34,s37	s13,s52,s69,s71,s73	s9,s23,s42,s49,s61,s75,s97,s110,s121,s122, s126, s127,s128,s131,s132
Power loss(kW)	69.340	43.606	499.389
Voltage stability index	0.159168	0.05692	0.195823
Switching number	4	4	16
$P\{\alpha_c < 0\}$	0.999	1	1
Number of violations in bus voltage constraint	0	0	0
Number of violations in line flow constraint	0	0	0
Stability status	stable	stable	stable

The reconfiguration of the DS improves the operating conditions by maximizing system power loss reduction and voltage stability margin which in turn improves the stability of the system.

5.3.1 Probabilistic analysis for different levels of wind penetration

Since the wind mean speed may vary from time to time, levels of wind penetration are variable, and therefore the operating condition of the distribution system may change, which can bring variations in probabilistic stability margin and affect the system reconfiguration process. Hence probabilistic analysis is carried out for all the three distribution systems with different levels of wind generation. For this purpose, two different wind Weibull distributions W1 and W2 are assumed. The parameters and mean value of each Weibull distribution are given in Table 5.2.

Table 5.2: Parameter and means of two wind speed weibull distribution

	K_w	C_w	mean
W1 (case 1)	3.8981	7.73	7
W2 (case 2)	6.9996	12.82	12

Table 5.3 shows the variation in the oscillatory modes (unstable modes) along with the participating states and participating DGs with different wind power penetrations for initial configuration of the system. It is observed from Table 5.3 that in 33 bus system for case 1, critical unstable mode is associated with PV-DG1, whereas for case 2, critical unstable mode is associated with electrical and control mode of DFIG1. For case 1, second unstable mode is mechanical mode corresponding to SHPP-DG3. Similarly, third unstable mode is associated with DFIG1, which contributes to instability with probability of 0.9715. On the other hand, in case 2, stability margins associated with SHPP-DG3 and PV-DG1 improve marginally compared to the stability margin obtained in case 1 whereas stability probability of DFIG1 decreases considerably to 0.4100. Similarly, for 69 bus system, state variables participating in the first unstable mode are rotor electrical and power controller variables of DFIG1 with probabilistic stability margin of 0.3112. Similarly, δ_3 and ω_3 are the states associated with SHPP-DG3 with a small signal stability (SSS) probability of 0.6608 and the third unstable mode is associated with DC/DC control mode of PV-DG2 with a SSS probability

Table 5.3: Selected unstable eigenvalues of all three system (initial case)

System	eigenvalue	participating generator	Dominant state with their participation factor	$P\{\alpha_c < 0\}$
	Case 1			
33 bus system				
	0.000154 ± 0.3597i	PV-DG1	I_{pv2}=1.00 x_{pv12}= 0.860, x_{pv31}= 0.579, x_{pv21}=0.298	0.47131
	-0.03151 ± 28.08i	SHPP-DG3	δ_3=1.000, ω_3=0.999	0.86292
	-0.251 ± + 481.80i	DFIG1	e_{d1}=1.0, e_{q1}=0.980, x_{4h}= 0.4690, x_{2h}=0.296	0.9715
69 bus system				
	0.4631 ± 335.67i	DFIG1	e_{d1}=1.0, e_{q1}= 0.997 , x_{4h}= 0.449, x_{2h}=0.241	0.3112
	-0.186 ±15.55i	SHPP-DG3	δ_3=1.000, ω_3 = 0.999	0.6608
	-0.0080 ± 0.2739i	PV-DG2	I_{pv2}=1.000, x_{pv12}= 0.931, x_{pv31}= 0.492, x_{pv21}=0.324	0.7486
119 bus system				
	0.1298 ± 360.23i	DFIG2	e_{q2}= 1.00, e_{d2}= 0.989, x_{4h}= 0.5434 x_{2h}=0.3128	0.3742
	-0.00318 ± 0.3835i	PV-DG1	I_{pv1}=1.00, x_{pv11}=0.835 x_{pv31}= 0.347	0.5408
	-0.06011 ± 31.69i	SHPP-DG2	δ_2= 1.00, ω_2=0.999	0.9688
	Case 2			
33 bus system				
	0.00076 ± 0.3596i	DFIG1	e_{d1}=1.0, e_{q1}=0.9783, x_{4h}= 0.51814, x_{2h}=0.350	0.4100
	-0.0622 ± 452.669i	PV-DG1	I_{pv2}=1.00 x_{pv12}= 0.860, x_{pv31}= 0.579, x_{pv21}=0.298	0.4754
	-0.0324 ± 28.06i	SHPP-DG3	δ_3=1.000, ω_3=0.999	0.87757
69 bus system				
	1.3342 ± 304.87i	DFIG1	e_{d1}=1.00, e_{q1}=0.9955, x_{4h}= 0.523, x_{2h}=0.269	0.00625
	-0.1897 ±15.56i	SHPP-DG3	δ_3=1.000, ω_3= 0.999	0.661087
	-0.0085 ± 0.273i	PV-DG2	I_{pv2}=1.00 x_{pv12}= 0.930, x_{pv31}= 0.499, x_{pv21}= 0.324	0.7620
119 bus system				
	0.4641 ± 348.84i	DFIG2	e_{q2}= 1.00, e_{d2}=0.9842, x_{4h}= 0.6282, x_{2h}=0.3826	0.0170
	-0.06350 ± 0.3835i	PV-DG1	I_{pv1}=1.00, x_{pv11}=0.9062 x_{pv31}=0.3182	0.54427
	-0.0033 ± 32.24i	SHPP-DG2	δ_2= 1.00, ω_2=0.999	0.96879

of 0.7481. In particular, the first unstable mode is critical mode because of its lowest stability probability. On the other hand, for case 2, probability of the critical mode is reduced to 0.00625 and the stability probabilities for other two unstable modes become 0.6610 and 0.7620, respectively with high wind power penetration. For 119 bus system, in case 1, the first unstable response mode is associated with DFIG2 which is identified to be the critical mode with the smallest SSS probability of 0.3742 and for other two unstable response modes, PV-DG1 and SHPP-DG2 contribute. However, for case 2, the stability probability associated with DFIG1 decreases notably. It has been

noticed that stability margin of unstable modes associated with SHPP-DGs and PV-DGs are not much affected by wind penetration level. However, marginal improvement in unstable modes associated with PV-DGs and SHPP-DGs are achieved at higher wind power penetration level. Further, Table 5.4 shows the DSR result corresponding to different Weibull distribution parameters of wind given in Table 5.2. After reconfiguration, the system stability can be ensured.

Table 5.4: Result of DSR for different wind penetration conditions

	Open switch	Power loss	Voltage stability index	Switching number	$P\{\alpha_c < 0\}$	status
33 bus system						
Case 1						
Initial network		87.013	0.207530	0	0.4713	unstable
Reconfigured network	s11,s29,s33,s34,s37	69.988	0.15948	4	1	stable
Case 2						
Initial network		83.101	0.20560	0	0.4100	unstable
Reconfigured network	s11,s29,s33,s34,s37	66.583	0.159127	4	1	stable
69 bus system						
Case 1						
Initial network		55.213	0.06922	0	0.3112	unstable
Reconfigured network	s18,s56,s69,s71,s73	42.772	0.049163	4	1	stable
Case 2						
Initial network		53.142	0.048987	0	0.00625	unstable
Reconfigured network	s13,s52,s69,s71,s73	41.326	0.045061	4	1	stable
119 bus system						
Case 1						
Initial network		684.63	0.302046	0	0.37422	unstable
Reconfigured network	s9,s23,s44,s49,s74,s98,s110,s121, s122,s123,s126,s127,s128,s131,s132	540.439	0.238587	14	0.996	stable
Case 2						
Initial network		667.89	0.3020	0	0.01707	unstable
Reconfigured network	s9,s23,s42,s49,s61,s75,s97,s110, s121,s122,s126,s127,s128,s131,s132	490.017	0.195374	16	1	stable

5.4 Conclusion

In this chapter, a detailed study on three different test systems is conducted to analyze the effects of reconfiguration on small signal stability margin of distribution system in presence of DFIGs, PV-DGs and SHPP-DGs. This formulation considers stability risk with the increasing level of wind penetration in the reconfiguration problem and optimal configuration is selected based on improved performance indices with acceptable stability margin. It is observed that DSR improves the voltage stability margin and reduces the power loss with minimum number of switching operations in the network.

So far in this work, only constant power loads are considered. Hence, in next chapter, ZIP load models are considered during DSR and appropriate switching sequence is determined to achieve the configured system.

Chapter 6

Optimal switching sequence path for DSR considering voltage dependent loads

This chapter highlights the importance of considering voltage dependent loads in DSR problem. Further, KnEA-PE algorithm is implemented for determining the appropriate switching sequence to reach the optimal network from the original configuration. Detailed studies have been carried out on all three distribution systems.

6.1 Introduction

In previous chapters, the constant power load models have been considered during DSR. However, practically, significant part of distribution system loads, such as industrial, commercial and residential loads, are voltage dependent. In this chapter, first the optimal distribution system configurations are determined in the presence of voltage dependent loads and then appropriate switching sequence is determined to achieve this optimal configuration . Further, the results corresponding to constant-power loads and ZIP loads are compared considering the uncertain and correlated loads and RES based DGs.

6.2 Load combinations

In this study, the ZIP load models have been incorporated during DSR. This model consists of three components: a constant-power (P), a constant-current (I) and a constant impedance (Z). The load at any bus i is given by [97]

$$P_{Li} = P_{oi}\Big\{F_P + F_I(V_i/V_{oi}) + F_Z(V_i/V_{oi})^2\Big\} \tag{6.1}$$

$$Q_{Li} = Q_{oi}\Big\{F'_P + F'_I(V_i/V_{oi}) + F'_Z(V_i/V_{oi})^2\Big\} \tag{6.2}$$

where P_{oi}, Q_{oi} and V_{oi} are nominal real power, reactive power and bus voltage magnitude respectively, F and F' are constant parameters, and the subscripts P, I and Z denote the constant power, constant current and constant impedance contributions, respectively. The values for the coefficients

F and F' for the ZIP load model for various types of loads (industrial, residential and commercial loads) in real systems are given in Table 6.1.

Table 6.1: Parameters for different load composition[76]

	Load class	F_Z	F_I	F_P
Active power	Residential	0.24	0.64	0.13
	Commercial	0.16	0.80	0.04
	Industrial	-0.07	0.24	0.83
Reactive power	Residential	2.44	-1.94	0.50
	Commercial	3.26	-3.10	0.84
	Industrial	1	0	0

For all three test systems, the details of types of loads connected at various buses are listed in Table 6.2.

Table 6.2: Load characteristics at various buses

Test system	Residential ZIP model	Commercial ZIP model	Industrial ZIP model
33-bus system	9-16	18-22, 26-31	17,32,25
69 bus system	3-19,	36-46, 48-51	52,59,69
119 bus system	19-25, 30-42	67-75	45,78,114,120

To study the importance of considering voltage dependent loads in DSR problem, the presented formulation has been carried out on IEEE 33-bus, 69-bus and 119-bus distribution system considering uncertainties in loads and DG power outputs. All three types of DGs, namely SHPP-DGs, PV-DGs and DFIGs, are considered in this analysis. Details related to sizing and locations of SHPP-DGs, PV-DGs and DFIGs are same as given in Chapter 3, 4 and 5. In this study, the solar irradiation is assumed to follow Beta probability density function with mean and standard deviation as 721 W/m^2 and 200 W/m^2, respectively and wind speed is assumed to follow Weibull function

with the scale parameter of 9.0 m/s and the shape parameter of 3 m/s. Some loads are assumed to be correlated and the correlation between DG power outputs has also been considered. The same correlation matrices as given in the previous chapters, have been used in this case. The loads at other buses, are treated as constant power loads. The obtained results are shown in Tables 6.3, 6.4 and 6.5 for all three systems.

Table 6.3: Comparison of DSR results obtained with ZIP load model and constant power loads (for 33 bus system)

	Open switch	Power loss (kW)	Voltage stability index	Switching number	Participating DGs and associated states	$P\{\alpha_c < 0\}$	status
Initial network							
ZIP load model		61.018	0.16155	0	DFIG1 and e_{d1}, e_{q1}	0.82786	unstable
Constant power load model		86.31	0.207171	0	PV-DG1 and I_{pv1}, x_{pv11}, x_{pv31}	0.47133	unstable
Reconfigured network							
ZIP load model	s7,s9,s29,s34,s37	47.715	0.078354	6	DFIG1 and e_{d1}, e_{q1}	1	stable
Constant power load model	s11,s29,s33,s34,s37	69.340	0.159168	4	PV-DG1 and I_{pv1}, x_{pv11}, x_{pv31}	1	stable

These results show that for constant power load model, power losses are higher than those obtained for ZIP load model. This is due to the fact that the loads with constant power characteristics always draw rated power and increases the power loss. On the other hand, during normal operation, the power drawn by the voltage dependent loads are less than the rated power. This is due to the fact that under normal operation, the voltage magnitudes at all the buses are less than the rated value, and therefore, following equations (6.1) and (6.2), the power consumed by the voltage dependent load (VDL) will be less than the rated values resulting into less amount of loss in the system. Similarly, other objective function values also vary differently when ZIP loads are considered.

Table 6.4: Comparison of DSR results obtained with ZIP load model and constant power loads (for 69 bus system)

	Open switch	Power loss	Voltage stability index	Switching number	Participating DGs and associated states	$P\{\alpha_c < 0\}$	status
Initial network							
ZIP load model		51.80	0.05806	0	DFIG1 and e_{d1}, e_{q1}	0.40151	unstable
Constant power load model		55.128	0.06879	0	DFIG1 and e_{d1}, e_{q1}	0.32370	unstable
Reconfigured network							
ZIP load model	s18,s58,s69,s71,s73	40.972	0.047955	4	DFIG1 and e_{d1}, e_{q1}	1	stable
Constant power load model	s13,s52,s69,s71,s73	43.606	0.056926	4	DFIG1 and e_{d1}, e_{q1}	1	stable

Table 6.5: Comparison of DSR results obtained with ZIP load model and constant power loads (for 119 bus system)

	Open switch	Power loss	Voltage stability index	Switching number	Participating DGs and associated states	$P\{\alpha_c < 0\}$	status
119 bus system							
Initial network							
ZIP load model		601.90	0.29981	0	PV-DG1 and I_{pv1}, x_{pv11}, x_{pv31}	0.5240	unstable
Constant power load model		680.08	0.3020	0	DFIG2 and e_{d2}, e_{q2}	0.3912	unsable
Reconfigured network							
ZIP load model	s23,s39,s43,s51,s71 s74,s110,s121,s122 s123,s126,s127 s130,s131,s132	462.283	0.176722	14	PV-DG1 and I_{pv1}, x_{pv11}, x_{pv31}	1	stable
Constant power load model	s9,s23,s42,s49,s61 s69,s110,s121,s122 s126,s127,s129,s130 s131,s132	512.326	0.178515	14	DFIG2 and e_{d2}, e_{q2}	1	stable

From these tables, it is observed that the optimal topological structure of the network with ZIP loads are different from those obtained with constant power loads. This variation is because of the voltage dependent characteristic of different load combinations. Therefore, for reconfiguration, appropriate knowledge of type of load in a system is necessary.

The voltage profiles of the 119-bus system before and after reconfiguration are shown in Fig. 6.1, for constant power load and for ZIP load model.

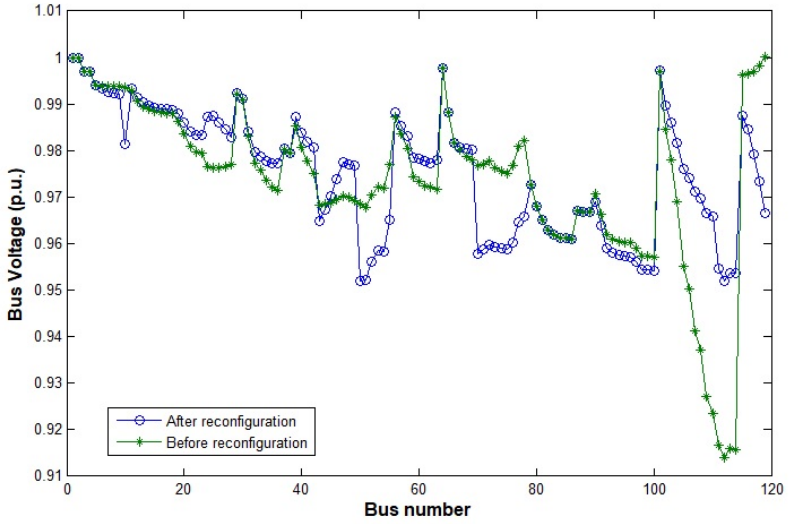

(a) For constant power loads

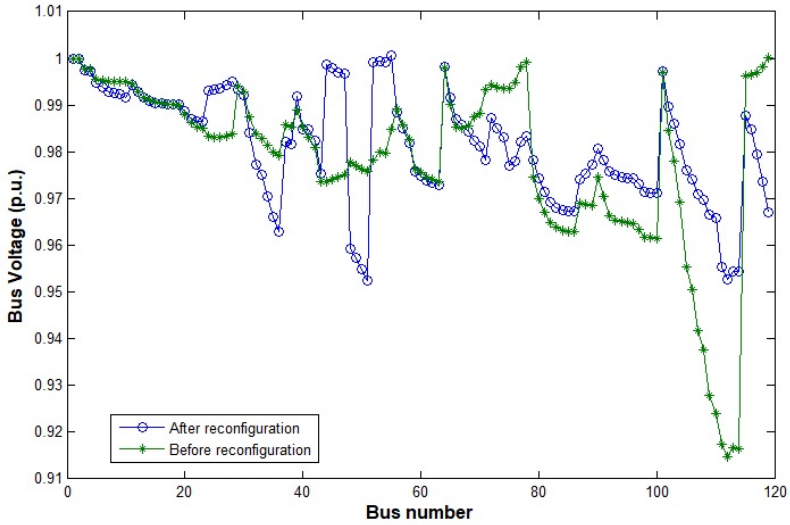

(b) For ZIP loads

Figure 6.1: Voltage profiles of 119-bus system.

The angles of voltages at various buses in the system are shown in Fig. 6.2, for constant power load and for ZIP load model. The improvement in bus voltages and angles after reconfiguration has been achieved.

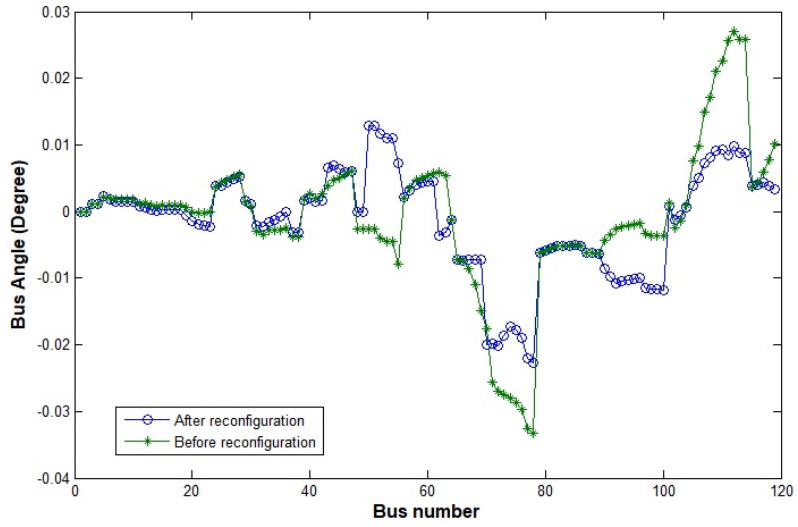

(a) For constant power loads

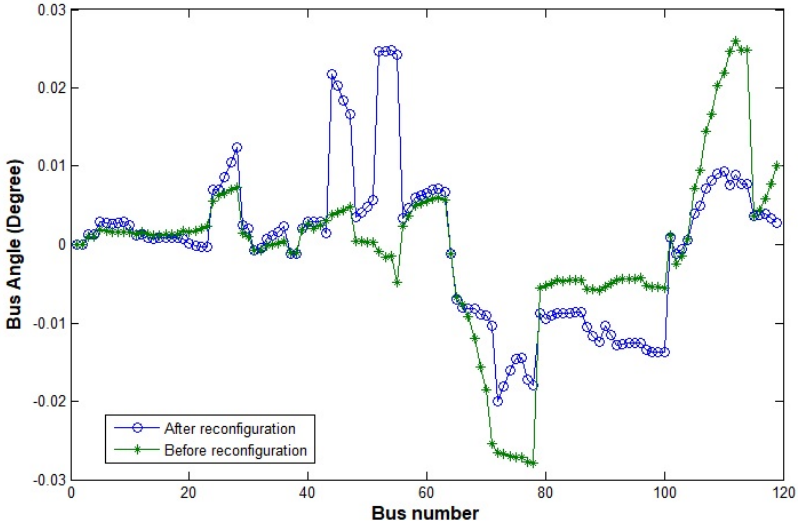

(b) For ZIP loads

Figure 6.2: Angles of voltages of at various buses in 119-bus system.

In addition, Eigen values of the 119-bus system are also shown in Table 6.6, for constant power load model and ZIP load model. From Table 6.6, it can be observed that the initial system (before

reconfiguration) is unstable (there is a pair of eigenvalues in the right hand side of the s-plane). For ZIP loads, the critical mean eigenvalues (which are the rightmost eigenvalues) -0.00144 ± 0.3920196 have probability of 0.5240 (listed in Table 6.5) for remaining in the left hand side of the complex plane which indicates that the initial system could become unstable. On the other hand, the reconfigured system is stable as all the eigenvalues lie in the left side of the s-plane.

Table 6.6: Eigenvalues of the 119-bus system

(a) for constant power loads

before reconfiguration	after reconfiguration
0.151452 ± 378.240i	-12.134±372.8021
-1.96617±377.547i	-37.047±356.309
-57.376±91.6612i	-30.262±125.097
-59.078±89.6377i	-55.083± 98.408
-40.964	-42.0322
-0.0601±36.1524757	-0.8973±40.3262
-0.810629 ±31.9616i	-0.06217±36.107953
-0.0423016 ± 33.8870i	-0.06231+33.508818
-0.2707± 27.561i	-0.0561±34.458
-18.6526	-17.8823
-18.8513	-17.221
-10.07022	-9.7952
-9.67584	-9.7442
-9.74357	-6.1275
-3.65651±5.79090i	-3.71760±5.55060
-3.61024 ±1.603414i	-3.8151± 1.89971i
- 3.815250±1.2236i	- 3.815250±1.2236i
-1.5402 ± 0.61367	1.51091 ±0.645359i
-1.51763 ±0.700867i	-1.49702±0.7579377i
-0.00316±0.401871	-0.0808±0.5182643i
-0.09392± 0.373110i	-0.1161±0.3640166i
-0.18436	-0.186639
-0.18287	-0.18239
-0.191969	-0.19031
-0.190260	-0.192013

(b) for ZIP loads

before reconfiguration	after reconfiguration
-0.44953±379.85727	-17.5595± 369.88i
-2.5977±379.08173	-37.67784± 358.41
-57.040±87.5788317	-28.28± 122.044
-55.284± 89.6520	-47.59 ±101.02
-40.5271	-40.519
-0.08102±35.61015	-0.05596± 35.75517
-0.264787±27.5755	-0.06230± 35.377
-0.36194±28.1626	-0.06153±33.526
-1.38761+18.199693	-3.8479±19.099
-18.97817	-18.5028
-19.20720	-17.6817
-8.6268	-9.93812
-9.72465	-9.81054
-9.91456	-3.17661
-3.473138±5.119	-3.6755± 4.91622
-3.615±1.6055	-3.534±2.443653
-3.879492±0.446080	-3.8157± 1.899
-1.543±0.6115	-1.513± 0.638553
-1.55304±0.673432	-1.5091± 0.7245
-0.00144±0.3920196	-0.0672± 0.512678
-0.08768±0.37263	-0.11352±0.36417
-0.1841286	-0.186544
-0.18237	-0.18215
-0.16872	-0.16871
-0.16720	-0.16723

So far, in all the above studies, the final configuration of the system is decided. However, for practical implementation, once a system configuration is decided, appropriate switching sequence to implement that configuration needs also to be determined. In the next Section, a methodology for determining the proper switching sequence is described.

6.3 DETERMINATION OF APPROPRIATE SWITCHING SEQUENCE

The determination of appropriate switching sequence consists of the following steps [63]:
(I) Randomly generate 's' number of strings using the switches of final optimal configuration. Each of these strings specifies the sequence of operation of the switches (vis-a-vis their status in the original configuration). For any string, the first element of the string represents the switch that should be closed and the second one represents the switch to be opened, so that the radiality of DS is maintained. All these generated strings are subsequently arranged in a matrix $\mathbf{X_{sw}}$ as follows:

$$\mathbf{X_{sw}} = \begin{bmatrix} sw_{c11} & sw_{o11} & sw_{c12} & sw_{o12} & \dots & sw_{c1N_{steps}} & sw_{o1N_{steps}} \\ sw_{c21} & sw_{o21} & \dots & \dots & \dots & sw_{c2N_{steps}} & sw_{o2N_{steps}} \\ \vdots & \vdots & \ddots & \ddots & & \ddots & \vdots \\ sw_{cs1} & sw_{os1} & \dots & \dots & \dots & sw_{csN_{steps}} & sw_{osN_{steps}} \end{bmatrix} \tag{6.3}$$

In equation (6.3), sw_{cs1} and sw_{os1} denote the closing and opening switch pair respectively of 1^{st} step in sequence s. Further, N_{steps} denotes the total number of steps in each sequence. It is to be noted that, each step consists of the pair of closing and opening operation. In $\mathbf{X_{sw}}$, the total number of steps in each sequence is same as the number of tie switches which are not in the same state after reconfiguration.
(II) Calculate the objective functions given in equations (3.2), (3.3) and damping ratio of critical eigenvalue [81] taking into consideration the topological and operational constraints given in equations (3.7), (3.8) based on the results of load studies and SSSA for every step of a sequence. For each sequence, the aggregate objective function is calculated as follows

$$F_M(\mathbf{X}_{sw}) = \sum_{i=1}^{N_{steps}} f_M(\mathbf{X}_{sw}), \qquad M = 1, 2, 3 \tag{6.4}$$

where M is the number of objectives and N_{steps} is the total number of steps in each sequence.
(III) Perform ENS and generate new set of strings (given by the matrix $\mathbf{Y_{sw}}$ having the same dimension as $\mathbf{X_{sw}}$) using mutation and crossover operations on the parent strings and form combined

population $\mathbf{R_{sw}} = \mathbf{X_{sw}} \cup \mathbf{Y_{sw}}$.

(IV) Rank the non dominated front using ENS and identify the knee points for combined population based on the procedure described in Section 3.3.2. Generate the parent population for next generation.

(V) Repeat the process from step (II) until termination criterion is met and obtain the best result following the procedure mentioned in Section 2.3.8 of Chapter 2. Table 6.7 shows the switching sequence obtained by the above-mentioned method for all three test systems. It is to be noted that for generating these sequences, the final configuration corresponding to ZIP load models and constant power load models given in Tables 6.3, 6.4 and 6.5 for all three system, have been used.

Table 6.7: Distribution system switching sequence results for ZIP load model results and constant power loads

test system	Switching sequence path
33 bus system	
ZIP load model	s36 s9 s35 s29 s33 s7
constant power load model	s36 s11 s35 s29
69 bus system	
ZIP load model	s72 s58 s70 s18
constant power load model	s72 s52 s70 s13
119 bus system	
ZIP load model	s129 s71 s120 s39 s128 s74 s133 s110 s125 s51 s119 s23 s124 s43
constant power load model	s119 s23 s128 s69 s123 s61 s124 s42 s120 s9 s133 s110 s125 s49

For 33 bus system, the optimal configuration obtained with ZIP load as shown in Table 6.3 is $s7, s9, s29, s34$ and $s37$ and the initial configuration is $s33, s34, s35, s36$ and $s37$. From switching sequence process, $s34$ and $s37$ switches are removed as they both have the same status after reconfiguration. Therefore, switches $s7, s9, s29, s33, s35$ and $s36$ participated in the switching process. As shown in Table 6.7, the obtained switching sequence is $s36, s9, s35, s29, s33, s7$ which leads to the following sequence of operation: (i) first close $s36$ and open $s9$ (ii) close $s35$ and open $s29$ and (iii) close $s33$ and open $s7$. Similarly, corresponding to constant power loads, the optimal configuration is $s11, s29, s33, s34$ and $s37$. Hence, switches $s33, s34$ and $s37$ should be removed

from the switching process and the final appropriate switching sequence obtained is: (i) close s36 - open s11 and (ii) close s35 - open s29. Similarly for 69 bus system, with ZIP load model, only four switches namely, $s18, s56, s72$ and $s74$ and with constant power load model switches $s13, s52, s72$ and $s74$ are utilized in switching sequence process. Remaining switches listed in Table 6.4 have same status after reconfiguration. Thus, the result presented in Table 6.7 indicates the following sequence of operation to obtain the optimal network: (i) close s72- open s58 and (ii) close 70 - open 18 (for ZIP load model); (i) close s72- open s52 and (ii) close 70 - open 13 (for constant power load model). The same analysis of the switching sequence path leads to the results shown in Table 6.7 with the both type of load model, for 119 bus distribution system.

6.4 CONCLUSION

In this chapter, DSR has been presented in the presence of voltage dependent load models for optimal operation using KnEA-PE method. From the results, it can be observed that the configuration obtained for composite load differs from the constant power loads. Therefore, it is necessary to find the exact model for the connected loads while reconfiguring the network. Further, this chapter also presented a methodology to determine the optimal switching sequence.

Chapter 7

Conclusion

This chapter summarizes the major findings of the work and suggests a number of possible directions for future works in the area of DSR.

7.1 Conclusions

The important contributions in the area of DSR in distribution system in the presence of distributed generation can be summarized as follows:

The DSR problem is posed as a constrained multi-objective optimization problem. The objective functions include minimization of power loss, switching operations as well as maximization of the voltage stability margin while maintaining the constraints of bus voltage, branch current carrying capacity and radiality of DS. Further, small signal stability of the system has also been considered in the formulated reconfiguration problem. A KnEA based optimization approach has been applied for DSR. The effectiveness of this method has been investigated on IEEE 33-bus, 69-bus and 119-bus radial DSs. Comparing the results obtained by KnEA method with NSGA-II method, the following conclusions can be drawn:

- Though reconfiguration, a dynamically unstable distribution system can be made stable with increased small signal stability margin. The proposed formulation and solution methodology ensure that the final configuration of the distribution system always remains dynamically stable in the presence of DGs.
- The performance of the KnEA technique is superior to that of NSGA-II algorithm for solving the multi-objective network reconfiguration problem.
- For ensuring stability of the system, the stability issue should be enforced as a constraint in the formulated problem.

For considering the uncertainties of loads and generations, probabilistic DSR problem has been formulated and KnEA-PE approach has been proposed to solve the formulated problem with the

acceptable confidence level. The performance indices (expected values of objective functions) have large values compared to deterministic results of DSR because in highly uncertain environment, DSR tries to find an optimum configuration in the face of uncertainties of loads and generation. From this study, the following conclusions have been drawn:

- The correlation among the uncertain load demands and among the uncertain DG power outputs have an influence on the final configuration of the system. Moreover, correlation among DGs has more pronounced effect on the final configuration than the correlation among the loads.

- Stability of dynamically unstable DS is achieved through reconfiguration with a desired confidence level. The proposed formulation and solution methodology ensure that the final system configuration always remains dynamically stable even with uncertainties and correlation in load and generation.

Further, in the small-signal stability constrained DSR, PV-DGs and DFIG have been integrated along with SHPP based DGs. The impact of different solar irradiance and wind power penetrations on the small signal stability constraint and subsequently, on reconfiguration has been assessed. The following conclusions can be drawn:

- Due to load and generation uncertainty and also growing deployment of RES-DGs in DS, the risk of system instability is increased.

- Depending on the system operating conditions, DFIGs, PV-DGs and SHPP-DGs can contribute to the system instability.

- At higher level of solar irradiance level, the impact of PV-DGs on the system instability is quite significant.

- This formulation considers stability risk with the increasing level of wind penetration in the reconfiguration problem and optimal configuration is selected based on improved performance indices with acceptable stability margin.

In addition, due to its simplicity or the lack of data, many works in the literature assume that all loads are constant-power loads. However, as significant part of loads, such as commercial and

residential loads, are voltage dependent, this thesis also considers this dependency and compares the results corresponding to constant-power loads and ZIP loads considering uncertainty in loads and generation. From those comparisons, the following conclusions can be drawn:

- A voltage-dependent load model provides more realistic results than a constant power model by more accurately representing the actual behavior of the loads in response to voltage variations.
- The optimal configuration for different load combination may differ from each other because of the voltage dependent characteristic of different load combinations.

7.2 Further Works

1. It is predicted that the number of electric vehicles (EVs) connected to the distribution network will be significant in the future. Therefore, the presence of EVs can be considered in the DSR problem.
2. Modelling of DGs as per operational limits and as per capability curve can be carried out during DSR.
3. DSR can be solved by some other MOEA which has good trade-off among convergence of algorithm, diversity in pareto optimal solution and computational time to get the accurate result in minimum time.

Bibliography

[1] R. J. Sarfi, M. Salama, and A. Chikhani, "A survey of the state of the art in distribution system reconfiguration for system loss reduction," *Electric Power Systems Research*, vol. 31, no. 1, pp. 61–70, 1994.

[2] H. Haghighat and B. Zeng, "Distribution system reconfiguration under uncertain load and renewable generation," *IEEE Transactions on Power Systems*, vol. 31, no. 4, pp. 2666–2675, July 2016.

[3] R. A. Jabr, R. Singh, and B. C. Pal, "Minimum loss network reconfiguration using mixed-integer convex programming," *IEEE Transactions on Power Systems*, vol. 27, no. 2, pp. 1106–1115, May 2012.

[4] J. F. Franco, M. J. Rider, M. Lavorato, and R. Romero, "A mixed-integer lp model for the reconfiguration of radial electric distribution systems considering distributed generation," *Electric Power Systems Research*, vol. 97, pp. 51–60, Apr 2013.

[5] A. Borghetti, "A mixed-integer linear programming approach for the computation of the minimum-losses radial configuration of electrical distribution networks," *IEEE Transactions on Power Systems*, vol. 27, no. 3, pp. 1264–1273, Aug 2012.

[6] G. J. Rosseti, E. J. de Oliveira, L. W. de Oliveira, I. C. Silva, and W. Peres, "Optimal allocation of distributed generation with reconfiguration in electric distribution systems," *Electric Power Systems Research*, vol. 103, pp. 178–183, Oct 2013.

[7] P. Pavani and S. Singh, "Placement of dg for reliability improvement and loss minimization with reconfiguration of radial distribution systems," *International Journal of Energy Sector Management*, vol. 8, no. 3, pp. 312–329, 2014.

[8] G. V. Raju and P. Bijwe, "An efficient algorithm for minimum loss reconfiguration of distribution system based on sensitivity and heuristics," *IEEE transactions on power systems*, vol. 23, no. 3, pp. 1280–1287, 2008.

[9] G. K. V. Raju and P. R. Bijwe, "Efficient reconfiguration of balanced and unbalanced distribution systems for loss minimisation," *IET Generation, Transmission Distribution*, vol. 2, no. 1, pp. 7–12, January 2008.

[10] E. J. de Oliveira, G. J. Rosseti, L. W. de Oliveira, F. V. Gomes, and W. Peres, "New algorithm for reconfiguration and operating procedures in electric distribution systems," *International Journal of Electrical Power & Energy Systems*, vol. 57, pp. 129–134, 2014.

[11] R. J. Sarfi, M. M. A. Salama, and A. Y. Chikhani, "Distribution system reconfiguration for loss reduction: an algorithm based on network partitioning theory," *IEEE Transactions on Power Systems*, vol. 11, no. 1, pp. 504–510, Feb 1996.

[12] D. Bernardon, A. Mello, L. Pfitscher, L. Canha, A. Abaide, and A. Ferreira, "Real-time reconfiguration of distribution network with distributed generation," *Electric Power Systems Research*, vol. 107, pp. 59 – 67, 2014.

[13] R. Rao, K. Ravindra, K. Satish, and S. Narasimham, "Power loss minimization in distribution system using network reconfiguration in the presence of distributed generation," *Power Systems, IEEE Transactions on*, vol. 28, no. 1, pp. 317–325, Feb 2013.

[14] A. Tyagi, A. Verma, and P. Bijwe, "Reconfiguration for loadability limit enhancement of distribution systems," *IET Generation, Transmission & Distribution*, vol. 12, no. 1, pp. 88–93, 2017.

[15] Y.-K. Wu, C.-Y. Lee, L.-C. Liu, and S.-H. Tsai, "Study of reconfiguration for the distribution system with distributed generators," *IEEE Trans. Power Delivery*, vol. 25, no. 3, pp. 1678–1685, Jul 2010.

[16] S. S. Souza, R. Romero, J. Pereira, and J. T. Saraiva, "Artificial immune algorithm applied to distribution system reconfiguration with variable demand," *International Journal of Electrical Power & Energy Systems*, vol. 82, pp. 561–568, 2016.

[17] S. S. Souza, R. Romero, and J. F. Franco, "Artificial immune networks copt-ainet and opt-ainet applied to the reconfiguration problem of radial electrical distribution systems," *Electric Power Systems Research*, vol. 119, pp. 304–312, 2015.

[18] M. A. N. Guimaraes, C. A. Castro, and R. Romero, "Distribution systems operation optimisation through reconfiguration and capacitor allocation by a dedicated genetic algorithm," *IET Generation, Transmission Distribution*, vol. 4, no. 11, pp. 1213–1222, November 2010.

[19] T. T. Nguyen, A. V. Truong, and T. A. Phung, "A novel method based on adaptive cuckoo search for optimal network reconfiguration and distributed generation allocation in distribu-

tion network," *International Journal of Electrical Power & Energy Systems*, vol. 78, pp. 801 – 815, 2016.

[20] M. R. Andervazh, J. Olamaei, and M. R. Haghifam, "Adaptive multi-objective distribution network reconfiguration using multi-objective discrete particles swarm optimisation algorithm and graph theory," *IET Generation, Transmission Distribution*, vol. 7, no. 12, pp. 1367–1382, December 2013.

[21] W. Guan, Y. Tan, H. Zhang, and J. Song, "Distribution system feeder reconfiguration considering different model of dg sources," *International Journal of Electrical Power & Energy Systems*, vol. 68, pp. 210 – 221, 2015.

[22] B. Amanulla, S. Chakrabarti, and S. Singh, "Reconfiguration of power distribution systems considering reliability and power loss," *IEEE transactions on power delivery*, vol. 27, no. 2, pp. 918–926, 2012.

[23] M. R. Narimani, A. A. Vahed, R. Azizipanah-Abarghooee, and M. Javidsharifi, "Enhanced gravitational search algorithm for multi-objective distribution feeder reconfiguration considering reliability, loss and operational cost," *IET Generation, Transmission Distribution*, vol. 8, no. 1, pp. 55–69, Jan 2014.

[24] A. Mohamed Imran, M. Kowsalya, and D. Kothari, "A novel integration technique for optimal network reconfiguration and distributed generation placement in power distribution networks," *International Journal of Electrical Power & Energy Systems*, vol. 63, pp. 461–472, Dec 2014.

[25] L. W. de Oliveira, F. da S. Seta, and E. J. de Oliveira, "Optimal reconfiguration of distribution systems with representation of uncertainties through interval analysis," *International Journal of Electrical Power & Energy Systems*, vol. 83, pp. 382 – 391, 2016.

[26] A. Kavousi-Fard, T. Niknam, and M. H. Khooban, "Intelligent stochastic framework to solve the reconfiguration problem from the reliability view," *IET Science, Measurement Technology*, vol. 8, no. 5, pp. 245–259, Sept 2014.

[27] T. Niknam, A. K. Fard, and A. Baziar, "Multi-objective stochastic distribution feeder reconfiguration problem considering hydrogen and thermal energy production by fuel cell power

plants," *Energy*, vol. 42, no. 1, pp. 563 – 573, 2012, 8th World Energy System Conference, {WESC} 2010.

[28] A. Kavousi-Fard and T. Niknam, "Multi-objective stochastic distribution feeder reconfiguration from the reliability point of view," *Energy*, vol. 64, pp. 342 – 354, 2014.

[29] T. Niknam and A. Kavousifard, "Impact of thermal recovery and hydrogen production of fuel cell power plants on distribution feeder reconfiguration," *IET Generation, Transmission Distribution*, vol. 6, no. 9, pp. 831–843, September 2012.

[30] S. M. M. Larimi, M. R. Haghifam, and A. Moradkhani, "Risk-based reconfiguration of active electric distribution networks," *IET Generation, Transmission Distribution*, vol. 10, no. 4, pp. 1006–1015, 2016.

[31] T. Niknam, A. Kavousifard, and J. Aghaei, "Scenario-based multiobjective distribution feeder reconfiguration considering wind power using adaptive modified particle swarm optimisation," *IET Renewable Power Generation*, vol. 6, no. 4, pp. 236–247, July 2012.

[32] A. Zidan and E. F. El-Saadany, "Distribution system reconfiguration for energy loss reduction considering the variability of load and local renewable generation," *Energy*, vol. 59, pp. 698 – 707, 2013.

[33] A. R. Malekpour, T. Niknam, A. Pahwa, and A. K. Fard, "Multi-objective stochastic distribution feeder reconfiguration in systems with wind power generators and fuel cells using the point estimate method," *IEEE Transactions on Power Systems*, vol. 28, no. 2, pp. 1483–1492, May 2013.

[34] I. B. Hamida, S. B. Salah, F. Msahli, and M. F. Mimouni, "Optimal network reconfiguration and renewable dg integration considering time sequence variation in load and dgs," *Renewable Energy*, vol. 121, pp. 66 – 80, 2018.

[35] H. B. Tolabi, M. H. Ali, and M. Rizwan, "Simultaneous reconfiguration, optimal placement of dstatcom, and photovoltaic array in a distribution system based on fuzzy-aco approach," *IEEE Transactions on Sustainable Energy*, vol. 6, no. 1, pp. 210–218, Jan 2015.

[36] I. Ali, M. S. Thomas, and P. Kumar, "Energy efficient reconfiguration for practical load combinations in distribution systems," *IET Generation, Transmission Distribution*, vol. 9, no. 11, pp. 1051–1060, 2015.

[37] H. B. Tolabi, M. H. Ali, S. B. M. Ayob, and M. Rizwan, "Novel hybrid fuzzy-bees algorithm for optimal feeder multi-objective reconfiguration by considering multiple-distributed generation," *Energy*, vol. 71, pp. 507–515, Jul 2014.

[38] A. Kavousi-Fard, T. Niknam, and A. khosravi, "Multi-objective probabilistic distribution feeder reconfiguration considering wind power plants," *International Journal of Electrical Power & Energy Systems*, vol. 55, no. 0, pp. 680 – 691, 2014.

[39] D. Das, "A fuzzy multiobjective approach for network reconfiguration of distribution systems," *IEEE Transactions on Power Delivery*, vol. 21, no. 1, pp. 202–209, Jan 2006.

[40] S. Banerjee, C. Chanda, and D. Das, "Reconfiguration of distribution networks based on fuzzy multiobjective approach by considering loads of different types," *Journal of The Institution of Engineers (India): Series B*, vol. 94, no. 1, pp. 29–42, 2013.

[41] J. Savier and D. Das, "Impact of network reconfiguration on loss allocation of radial distribution systems," *IEEE Transactions on Power Delivery*, vol. 22, no. 4, pp. 2473–2480, 2007.

[42] R. K. Mishra and K. S. Swarup, "Adaptive weight-based self reconfiguration of smart distribution network with intelligent agents," *IEEE Transactions on Emerging Topics in Computational Intelligence*, vol. 2, no. 6, pp. 464–472, Dec 2018.

[43] M. P. Selvan and K. S. Swarup, "Dynamic topology processing in a radial distribution system," *IEE Proceedings - Generation, Transmission and Distribution*, vol. 153, no. 2, pp. 155–163, March 2006.

[44] T. Niknam, A. K. Fard, and A. Seifi, "Distribution feeder reconfiguration considering fuel cell/wind/photovoltaic power plants," *Renewable Energy*, vol. 37, no. 1, pp. 213 – 225, 2012.

[45] M. Sedighizadeh, M. Esmaili, and M. Esmaeili, "Application of the hybrid big bang-big crunch algorithm to optimal reconfiguration and distributed generation power allocation in distribution systems," *Energy*, vol. 76, pp. 920 – 930, 2014.

[46] M. Kashem, G. Jasmon, A. Mohamed, and M. Moghavvemi, "Artificial neural network approach to network reconfiguration for loss minimization in distribution networks," *International Journal of Electrical Power & Energy Systems*, vol. 20, no. 4, pp. 247–258, 1998.

[47] M. Kashem, M. Moghawemi, A. Mohamed, and G. Jasmon, "Loss reduction in distribution networks using new network reconfiguration algorithm," *Electric Machines and power systems*, vol. 26, no. 8, pp. 815–829, 1998.

[48] D. Singh and R. K. Misra, "Load type impact on distribution system reconfiguration," *International Journal of Electrical Power & Energy Systems*, vol. 42, no. 1, pp. 583–592, 2012.

[49] F. de Leon and B.-T. Ooi, "Damping power system oscillations by unidirectional control of alternative power generation plants," in *Power Engineering Society Winter Meeting, 2001. IEEE*, vol. 2, 2001, pp. 747–752 vol.2.

[50] Z. W. Wang, C. Shen, and F. Liu, "Probabilistic analysis of small signal stability for power systems with high penetration of wind generation," *IEEE Transactions on Sustainable Energy*, vol. 7, no. 3, pp. 1182–1193, July 2016.

[51] R. V. de Oliveira, J. A. Zamadei, and C. H. Hossi, "Impact of distributed synchronous and doubly-fed induction generators on small-signal stability of a distribution network," in *Power and Energy Society General Meeting, 2011 IEEE*, July 2011, pp. 1–8.

[52] S. Liu, P. X. Liu, and X. Wang, "Stochastic small-signal stability analysis of grid-connected photovoltaic systems," *IEEE Transactions on Industrial Electronics*, vol. 63, no. 2, pp. 1027–1038, Feb 2016.

[53] S. Liu, P. X. Liu, and X. Wang, "Stability analysis of grid-interfacing inverter control in distribution systems with multiple photovoltaic-based distributed generators," *IEEE Transactions on Industrial Electronics*, vol. 63, no. 12, pp. 7339–7348, Dec 2016.

[54] S. Mishra and D. Ramasubramanian, "Improving the small signal stability of a pv-de-dynamic load-based microgrid using an auxiliary signal in the pv control loop," *IEEE Transactions on Power Systems*, vol. 30, no. 1, pp. 166–176, Jan 2015.

[55] J. Ma, Z. Song, Y. Zhang, Y. Zhao, and J. S. Thorp, "Robust stochastic stability analysis method of dfig integration on power system considering virtual inertia control," *IEEE Transactions on Power Systems*, vol. 32, no. 5, pp. 4069–4079, Sept 2017.

[56] S. Q. Bu, W. Du, and H. F. Wang, "Probabilistic analysis of small-signal rotor angle/voltage stability of large-scale ac/dc power systems as affected by grid-connected offshore wind

generation," *IEEE Transactions on Power Systems*, vol. 28, no. 4, pp. 3712–3719, Nov 2013.

[57] S. Q. Bu, W. Du, H. F. Wang, Z. Chen, L. Y. Xiao, and H. F. Li, "Probabilistic analysis of small-signal stability of large-scale power systems as affected by penetration of wind generation," *IEEE Transactions on Power Systems*, vol. 27, no. 2, pp. 762–770, May 2012.

[58] W. Du, H. Wang, and L.-Y. Xiao, "Power system small-signal stability as affected by grid-connected photovoltaic generation," *European Transactions on Electrical Power*, vol. 22, no. 5, pp. 688–703, 2012.

[59] S. Y. Ruan, G. J. Li, B. T. Ooi, and Y. Z. Sun, "Power system damping from real and reactive power modulations of voltage-source-converter station," *IET Generation, Transmission Distribution*, vol. 2, no. 3, pp. 311–320, May 2008.

[60] S. Eftekharnejad, V. Vittal, G. T. Heydt, B. Keel, and J. Loehr, "Small signal stability assessment of power systems with increased penetration of photovoltaic generation: A case study," *IEEE Transactions on Sustainable Energy*, vol. 4, no. 4, pp. 960–967, Oct 2013.

[61] Y. M. Atwa, E. F. El-Saadany, M. M. A. Salama, and R. Seethapathy, "Optimal renewable resources mix for distribution system energy loss minimization," *IEEE Transactions on Power Systems*, vol. 25, no. 1, pp. 360–370, Feb 2010.

[62] D. Singh and R. K. Misra, "Multi-objective feeder reconfiguration in different tariff structures," *IET Generation, Transmission Distribution*, vol. 4, no. 8, pp. 974–988, August 2010.

[63] O. Badran, S. Mekhilef, H. Mokhlis, and W. Dahalan, "Optimal switching sequence path for distribution network reconfiguration considering different types of distributed generation," *IEEJ Transactions on Electrical and Electronic Engineering*, vol. 12, no. 6, pp. 874–882, 2017.

[64] C. H. N. de Resende Barbosa, M. H. S. Mendes, and J. A. de Vasconcelos, "Robust feeder reconfiguration in radial distribution networks," *International Journal of Electrical Power & Energy Systems*, vol. 54, pp. 619 – 630, 2014.

[65] P. W. Sauer and M. A. Pai, *Power system dynamics and stability*. Prentice Hall Engineering, 1998.

[66] X. Zhang, Y. Tian, and Y. Jin, "A knee point-driven evolutionary algorithm for many-objective optimization," *IEEE Transactions on Evolutionary Computation*, vol. 19, no. 6, pp. 761–776, Dec 2015.

[67] Y. Kumar, B. Das, and J. Sharma, "Multiobjective, multiconstraint service restoration of electric power distribution system with priority customers," *IEEE Trans. Power Delivery*, vol. 23, no. 1, pp. 261–270, Jan 2008.

[68] X. Zhang, Y. Tian, R. Cheng, and Y. Jin, "An efficient approach to nondominated sorting for evolutionary multiobjective optimization," *IEEE Transactions on Evolutionary Computation*, vol. 19, no. 2, pp. 201–213, April 2015.

[69] A. M. Eldurssi and R. M. O'Connell, "A fast nondominated sorting guided genetic algorithm for multi-objective power distribution system reconfiguration problem," *IEEE Transactions on Power Systems*, vol. 30, no. 2, pp. 593–601, March 2015.

[70] *Matlab, Mathworks Inc., Massachusetts, USA, Version r2012a.*

[71] W. Freitas, J. C. M. Vieira, A. Morelato, L. C. P. da Silva, V. F. da Costa, and F. A. B. Lemos, "Comparative analysis between synchronous and induction machines for distributed generation applications," *IEEE Transactions on Power Systems*, vol. 21, no. 1, pp. 301–311, Feb 2006.

[72] H.-D. Chiang and R. Jean-Jumeau, "Optimal network reconfigurations in distribution systems. ii. solution algorithms and numerical results," *Power Delivery, IEEE Transactions on*, vol. 5, no. 3, pp. 1568–1574, Jul 1990.

[73] A. Zidan, M. F. Shaaban, and E. F. El-Saadany, "Long-term multi-objective distribution network planning by {DG} allocation and feeders reconfiguration," *Electric Power Systems Research*, vol. 105, pp. 95 – 104, 2013.

[74] S. Chandramohan, N. Atturulu, R. K. Devi, and B. Venkatesh, "Operating cost minimization of a radial distribution system in a deregulated electricity market through reconfiguration using {NSGA} method," *International Journal of Electrical Power & Energy Systems*, vol. 32, no. 2, pp. 126 – 132, 2010.

[75] S. Xia, X. Luo, K. W. Chan, M. Zhou, and G. Li, "Probabilistic transient stability constrained optimal power flow for power systems with multiple correlated uncertain wind

generations," *IEEE Transactions on Sustainable Energy*, vol. 7, no. 3, pp. 1133–1144, July 2016.

[76] C. L. T. Borges and R. J. Pinto, "Small hydro power plants energy availability modeling for generation reliability evaluation," *IEEE Transactions on Power Systems*, vol. 23, no. 3, pp. 1125–1135, Aug 2008.

[77] J. M. Morales and J. Perez-Ruiz, "Point estimate schemes to solve the probabilistic power flow," *IEEE Transactions on Power Systems*, vol. 22, no. 4, pp. 1594–1601, Nov 2007.

[78] P. Zhang and S. T. Lee, "Probabilistic load flow computation using the method of combined cumulants and gram-charlier expansion," *IEEE Transactions on Power Systems*, vol. 19, no. 1, pp. 676–682, Feb 2004.

[79] J. M. Morales, L. Baringo, A. J. Conejo, and R. Minguez, "Probabilistic power flow with correlated wind sources," *IET Generation, Transmission Distribution*, vol. 4, no. 5, pp. 641–651, May 2010.

[80] Q. Xiao, "Evaluating correlation coefficient for nataf transformation," *Probabilistic Engineering Mechanics*, vol. 37, pp. 1 – 6, 2014. [Online]. Available: http://www.sciencedirect.com/science/article/pii/S0266892014000241

[81] J. Shukla, B. Das, and V. Pant, "Consideration of small signal stability in multi-objective ds reconfiguration in the presence of distributed generation," *IET Generation, Transmission Distribution*, vol. 11, no. 1, pp. 236–245, 2017.

[82] M. Fan, V. Vittal, G. T. Heydt, and R. Ayyanar, "Probabilistic power flow studies for transmission systems with photovoltaic generation using cumulants," *IEEE Transactions on Power Systems*, vol. 27, no. 4, pp. 2251–2261, 2012.

[83] N. Gupta, V. Pant, and B. Das, "Probabilistic load flow incorporating generator reactive power limit violations with spline based reconstruction method," *Electric Power Systems Research*, vol. 106, pp. 203–213, 2014.

[84] M. Aien, M. Fotuhi-Firuzabad, and M. Rashidinejad, "Probabilistic optimal power flow in correlated hybrid wind and photovoltaic power systems," *IEEE Transactions on Smart Grid*, vol. 5, no. 1, pp. 130–138, Jan 2014.

[85] P. Kayal and C. Chanda, "Optimal mix of solar and wind distributed generations considering performance improvement of electrical distribution network," *Renewable energy*, vol. 75, pp. 173–186, 2015.

[86] H. Huang and C. Chung, "Coordinated damping control design for dfig-based wind generation considering power output variation," *IEEE Transactions on Power Systems*, vol. 27, no. 4, pp. 1916–1925, 2012.

[87] L. Holdsworth, X. G. Wu, J. B. Ekanayake, and N. Jenkins, "Comparison of fixed speed and doubly-fed induction wind turbines during power system disturbances," *IEE Proceedings - Generation, Transmission and Distribution*, vol. 150, no. 3, pp. 343–352, May 2003.

[88] B. C. Pal and F. Mei, "Modelling adequacy of the doubly fed induction generator for small-signal stability studies in power systems," *IET Renewable Power Generation*, vol. 2, no. 3, pp. 181–190, September 2008.

[89] S. Ahmed-Zaid and M. Taleb, "Structural modeling of small and large induction machines using integral manifolds," *IEEE Transactions on Energy Conversion*, vol. 6, no. 3, pp. 529–535, Sep 1991.

[90] P. C. Krause, O. Wasynczuk, and S. D. Sudhoff, "Analysis of electrical machinery and drives system," *IEEE Press Power Eng. Series*, 2002.

[91] M. Yamamoto and O. Motoyoshi, "Active and reactive power control for doubly-fed wound rotor induction generator," *IEEE Transactions on Power Electronics*, vol. 6, no. 4, pp. 624–629, Oct 1991.

[92] A. Luna, F. K. A. Lima, D. Santos, P. Rodriguez, E. H. Watanabe, and S. Arnaltes, "Simplified modeling of a dfig for transient studies in wind power applications," *IEEE Transactions on Industrial Electronics*, vol. 58, no. 1, pp. 9–20, Jan 2011.

[93] D. Song, J. Yang, M. Su, A. Liu, Y. Liu, and Y. H. Joo, "A comparison study between two mppt control methods for a large variable-speed wind turbine under different wind speed characteristics," *Energies*, vol. 10, no. 5, p. 613, 2017.

[94] H. A. Pulgar-Painemal and P. W. Sauer, "Towards a wind farm reduced-order model," *Electric Power Systems Research*, vol. 81, no. 8, pp. 1688 – 1695, 2011.

[95] J. He, T. Zhao, X. Jing, and N. A. Demerdash, "Application of wide bandgap devices in renewable energy systems-benefits and challenges," in *Renewable Energy Research and Application (ICRERA), 2014 International Conference on*. IEEE, 2014, pp. 749–754.

[96] P. Ledesma and J. Usaola, "Doubly fed induction generator model for transient stability analysis," *IEEE transactions on energy conversion*, vol. 20, no. 2, pp. 388–397, 2005.

[97] J. R. Marti, H. Ahmadi, and L. Bashualdo, "Linear power-flow formulation based on a voltage-dependent load model," *IEEE Transactions on Power Delivery*, vol. 28, no. 3, pp. 1682–1690, July 2013.

[98] A. G. Endegnanew, "Distributed generation in future distribution systems: Dynamic aspects," Master's thesis, Institutt for elkraftteknikk, 2010.

[99] T. Shintai, Y. Miura, and T. Ise, "Oscillation damping of a distributed generator using a virtual synchronous generator," *IEEE Transactions on Power Delivery*, vol. 29, no. 2, pp. 668–676, April 2014.

[100] D. Milosevic and Z. Djurisic, "A new technique for improving stability of distributed synchronous generators during temporary faults in a distribution network," *International Journal of Electrical Power & Energy Systems*, vol. 100, pp. 299 – 308, 2018.

Appendix A

System data

The relevent data for 12.66 kV, 33-bus distribution system is given in Table A.1.

Table A.1: Branch data for 12.666 kV, 33-bus distribution system

Branch Number	Sending end bus number	Receiving end bus number	Resistance	Reactance
1	1	2	0.092200	0.047000
2	2	3	0.493000	0.251200
3	3	4	0.366000	0.186400
4	4	5	0.381100	0.194100
5	5	6	0.819000	0.707000
6	6	7	0.187200	0.618800
7	7	8	0.711400	0.235100
8	8	9	1.030000	0.740000
9	9	10	1.044000	0.740000
10	10	11	0.196000	0.065100
11	11	12	0.374400	0.129800
12	12	13	1.468000	1.155000
13	13	14	0.542000	0.713000
14	14	15	0.591000	0.526000
15	15	16	0.746300	0.545000
16	16	17	1.289000	1.721000
17	17	18	0.732000	0.574000
18	2	19	0.164000	0.156500
19	19	20	1.504200	1.355400
20	20	21	0.409500	0.478400

Continued on next page

Table A.1 – *Continued from previous page*

Branch Number	**Sending end bus number**	**Receiving end bus number**	**Resistance**	**Reactance**
21	21	22	0.708900	0.937300
22	3	23	0.451200	0.308300
23	23	24	0.898000	0.709100
23	23	24	0.898000	0.709100
24	24	25	0.896000	0.701100
25	6	26	0.203000	0.103400
26	26	27	0.284200	0.144700
27	27	28	1.059000	0.933700
28	28	29	0.804200	0.700600
29	29	30	0.507500	0.258500
30	30	31	0.974400	0.963000
31	31	32	0.310500	0.361900
32	32	33	0.341000	0.530200
33	8	21	2.000000	2.000000
34	9	15	2.000000	2.000000
35	12	22	2.000000	2.000000
36	18	33	0.500000	0.500000
37	25	29	0.500000	0.5000000

Table A.2: Bus data for 12.666 kV, 33-bus distribution system

Bus Number	P (kW)	Q(kVAR)	Bus Number	P (kW)	Q(kVAR)
1	0.000	0.000	27	0.060	0.025
2	0.100	0.060	28	0.060	0.020
3	0.090	0.040	29	0.120	0.070
4	0.120	0.080	30	0.200	0.600
5	0.060	0.030	31	0.150	0.070
6	0.060	0.020	32	0.210	0.100
7	0.200	0.100	33	0.060	0.040
8	0.200	0.100			
9	0.060	0.020			
10	0.060	0.020			
11	0.045	0.030			
12	0.060	0.035			
13	0.060	0.035			
14	0.120	0.080			
15	0.060	0.010			
16	0.060	0.020			
17	0.060	0.020			
18	0.090	0.040			
19	0.090	0.040			
20	0.090	0.040			
21	0.090	0.040			
22	0.090	0.040			
23	0.090	0.050			
24	0.420	0.200			
25	0.420	0.200			
26	0.060	0.025			

The relevent data for 12.66 kV, 69-bus distribution system is given in Table A.2.

Table A.3: Branch data for 12.666 kV, 69-bus distribution system.

Branch Number	**Sending end bus number**	**Receiving end bus number**	**Resistance**	**Reactance**
1	1	2	0.0005	0.0012
2	2	3	0.0005	0.0012
3	3	4	0.0015	0.0036
4	4	5	0.0251	0.0294
5	5	6	0.366	0.1864
6	6	7	0.3811	0.1941
7	7	8	0.0922	0.047
8	8	9	0.0493	0.0251
9	9	10	0.819	0.2707
10	10	11	0.1872	0.0619
11	11	12	0.7114	0.2351
12	12	13	1.03	0.34
13	13	14	1.044	0.345
14	14	15	1.058	0.3496
15	15	16	0.1966	0.065
16	16	17	0.3744	0.1238
17	17	18	0.0047	0.0016
18	18	19	0.3276	0.1083
19	19	20	0.2106	0.0696
20	20	21	0.3416	0.1129
21	21	22	0.014	0.0046
22	22	23	0.1591	0.0526
23	23	24	0.3463	0.1145
24	24	25	0.7488	0.2475
25	25	26	0.3089	0.1021

Continued on next page

Table A.3 – *Continued from previous page*

Branch Number	Sending end bus number	Receiving end bus number	Resistance	Reactance
26	26	27	0.1732	0.0572
27	3	28	0.0044	0.0108
28	28	29	0.064	0.1565
29	29	30	0.3978	0.1315
30	30	31	0.0702	0.0232
31	31	32	0.351	0.116
32	32	33	0.839	0.2816
33	33	34	1.708	0.5646
34	34	35	1.474	0.4873
35	3	36	0.0044	0.0108
36	36	37	0.064	0.1565
37	37	38	0.1053	0.123
38	38	39	0.0304	0.0355
39	39	40	0.0018	0.0021
40	40	41	0.7283	0.8509
41	41	42	0.31	0.3623
42	42	43	0.041	0.0478
43	43	44	0.0092	0.0116
44	44	45	0.1089	0.1373
45	45	46	0.0009	0.0012
46	4	47	0.0034	0.0084
47	47	48	0.0851	0.2083
48	48	49	0.2898	0.7091
49	49	50	0.0822	0.2011
50	8	51	0.0928	0.0473
51	51	52	0.3319	0.1114
52	9	53	0.174	0.0886

Continued on next page

Table A.3 – *Continued from previous page*

Branch Number	**Sending end bus number**	**Receiving end bus number**	**Resistance**	**Reactance**
53	53	54	0.203	0.1034
54	54	55	0.2842	0.1447
55	55	56	0.2813	0.1433
56	56	57	1.59	0.5337
57	57	58	0.7837	0.263
58	58	59	0.3042	0.1006
59	59	60	0.3861	0.1172
60	60	61	0.5075	0.2585
61	61	62	0.0974	0.0496
62	62	63	0.145	0.0738
63	63	64	0.7105	0.3619
64	64	65	1.041	0.5302
65	11	66	0.2012	0.0611
66	66	67	0.0047	0.0014
67	12	68	0.7394	0.2444
68	68	69	0.0047	0.0016
69	11	43	0.5000	0.500
70	13	21	0.5	0.5
71	15	46	1.0	1.0
72	50	59	2.0	2.0
73	27	65	1.0	1.0

Table A.4: Bus data for 12.666 kV, 69-bus distribution system

Bus Number	P (kW)	Q(kVAR)	Bus Number	P (kW)	Q(kVAR)
1.0000	0	0	27.0000	0.0140	0.0100
2.0000	0	0	28.0000	0.0260	0.0186
3.0000	0	0	29.0000	0.0260	0.0186
4.0000	0	0	30.0000	0	0
5.0000	0	0	31.0000	0	0
6.0000	0.0026	0.0022	32.0000	0	0
7.0000	0.0404	0.0300	33.0000	0.0140	0.0100
8.0000	0.0750	0.0540	34.0000	0.0195	0.0140
9.0000	0.0300	0.0220	35.0000	0.0060	0.0040
10.0000	0.0280	0.0190	36.0000	0.0260	0.0186
11.0000	0.1450	0.1040	37.0000	0.0260	0.0186
12.0000	0.1450	0.1040	38.0000	0	0
13.0000	0.0080	0.0055	39.0000	0.0240	0.0170
14.0000	0.0080	0.0055	40.0000	0.0240	0.0170
15.0000	0	0	41.0000	0.0012	0.0010
16.0000	0.0455	0.0300	42.0000	0	0
17.0000	0.0600	0.0350	43.0000	0.0060	0.0043
18.0000	0.0600	0.0350	44.0000	0	0
19.0000	0	0	45.0000	0.0392	0.0263
20.0000	0.0010	0.0006	46.0000	0.0392	0.0263
21.0000	0.1140	0.0810	47.0000	0	0
22.0000	0.0053	0.0035	48.0000	0.0790	0.0564
23.0000	0	0	49.0000	0.3847	0.2745
24.0000	0.0280	0.0200	50.0000	0.3847	0.2745
25.0000	0	0	51.0000	0.0405	0.0283
26.0000	0.0140	0.0100	52.0000	0.0036	0.0027

Continued on next page

Table A.4 – *Continued from previous page*

Bus Number	**P (kW)**	**Q(kVAR)**	**Bus Number**	**P (kW)**	**Q(kVAR)**
53.0000	0.0043	0.0035	62.0000	0.0320	0.0230
54.0000	0.0264	0.0190	63.0000	0	0
55.0000	0.0240	0.0172	64.0000	0.2270	0.1620
56.0000	0	0	65.0000	0.0590	0.0420
57.0000	0	0	66.0000	0.0180	0.0130
58.0000	0	0	67.0000	0.0180	0.0130
59.0000	0.1000	0.0720	68.0000	0.0280	0.0200
60.0000	0	0	69.0000	0.0280	0.0200
61.0000	1.2440	0.8880			

Table A.5: Branch data for 11 kV, 119-bus distribution system

Branch Number	Sending end bus number	Receiving end bus number	Resistance	Reactance
1.0000	0	1.0000	0	0.0001
2.0000	1.0000	2.0000	0.0360	0.0130
3.0000	2.0000	3.0000	0.0330	0.0119
4.0000	2.0000	4.0000	0.0450	0.0162
5.0000	4.0000	5.0000	0.0150	0.0540
6.0000	5.0000	6.0000	0.0150	0.0540
7.0000	6.0000	7.0000	0.0150	0.0125
8.0000	7.0000	8.0000	0.0180	0.0140
9.0000	8.0000	9.0000	0.0210	0.0630
10.0000	2.0000	10.0000	0.1660	0.1344
11.0000	10.0000	11.0000	0.1120	0.0789
12.0000	11.0000	12.0000	0.1870	0.3130
13.0000	12.0000	13.0000	0.1420	0.1512
14.0000	13.0000	14.0000	0.1800	0.1180
15.0000	14.0000	15.0000	0.1500	0.0450
16.0000	15.0000	16.0000	0.1600	0.1800
17.0000	16.0000	17.0000	0.1570	0.1710
18.0000	11.0000	18.0000	0.2180	0.2850
19.0000	18.0000	19.0000	0.1180	0.1850
20.0000	19.0000	20.0000	0.1600	0.1960
21.0000	20.0000	21.0000	0.1200	0.1890
22.0000	21.0000	22.0000	0.1200	0.0789
23.0000	22.0000	23.0000	1.4100	0.7230
24.0000	23.0000	24.0000	0.2930	0.1348
25.0000	24.0000	25.0000	0.1330	0.1040
26.0000	25.0000	26.0000	0.1780	0.1340

Continued on next page

Table A.5 – *Continued from previous page*

Branch Number	Sending end bus number	Receiving end bus number	Resistance	Reactance
27.0000	26.0000	27.0000	0.1780	0.1340
28.0000	4.0000	28.0000	0.0150	0.0296
29.0000	28.0000	29.0000	0.0120	0.0276
30.0000	29.0000	30.0000	0.1200	0.2766
31.0000	30.0000	31.0000	0.2100	0.2430
32.0000	31.0000	32.0000	0.1200	0.0540
33.0000	32.0000	33.0000	0.1780	0.2340
34.0000	33.0000	34.0000	0.1780	0.2340
35.0000	34.0000	35.0000	0.1540	0.1620
36.0000	30.0000	36.0000	0.1870	0.2610
37.0000	36.0000	37.0000	0.1330	0.0990
38.0000	29.0000	38.0000	0.3300	0.1940
39.0000	38.0000	39.0000	0.3100	0.1940
40.0000	39.0000	40.0000	0.1300	0.1940
41.0000	40.0000	41.0000	0.2800	0.1500
42.0000	41.0000	42.0000	1.1800	0.8500
43.0000	42.0000	43.0000	0.4200	0.2436
44.0000	43.0000	44.0000	0.2700	0.0972
45.0000	44.0000	45.0000	0.3390	0.1221
46.0000	45.0000	46.0000	0.2700	0.1779
47.0000	35.0000	47.0000	0.2100	0.1383
48.0000	47.0000	48.0000	0.1200	0.0789
49.0000	48.0000	49.0000	0.1500	0.0987
50.0000	49.0000	50.0000	0.1500	0.0987
51.0000	50.0000	51.0000	0.2400	0.1581
52.0000	51.0000	52.0000	0.1200	0.0789
53.0000	52.0000	53.0000	0.4050	0.1458

Continued on next page

Table A.5 – *Continued from previous page*

Branch Number	Sending end bus number	Receiving end bus number	Resistance	Reactance
54.0000	52.0000	54.0000	0.4050	0.1458
55.0000	29.0000	55.0000	0.3910	0.1410
56.0000	55.0000	56.0000	0.4060	0.1461
57.0000	56.0000	57.0000	0.4060	0.1461
58.0000	57.0000	58.0000	0.7060	0.5461
59.0000	58.0000	59.0000	0.3380	0.1218
60.0000	59.0000	60.0000	0.3380	0.1218
61.0000	60.0000	61.0000	0.2070	0.0747
62.0000	61.0000	62.0000	0.2470	0.8922
63.0000	1	63.0000	0.0280	0.0418
64.0000	63.0000	64.0000	0.1170	0.2016
65.0000	64.0000	65.0000	0.2550	0.0918
66.0000	65.0000	66.0000	0.2100	0.0759
67.0000	66.0000	67.0000	0.3830	0.1380
68.0000	67.0000	68.0000	0.5040	0.3303
69.0000	68.0000	69.0000	0.4060	0.1461
70.0000	69.0000	70.0000	0.9620	0.7610
71.0000	70.0000	71.0000	0.1650	0.0600
72.0000	71.0000	72.0000	0.3030	0.1092
73.0000	72.0000	73.0000	0.3030	0.1092
74.0000	73.0000	74.0000	0.2060	0.1440
75.0000	74.0000	75.0000	0.2330	0.0840
76.0000	75.0000	76.0000	0.5910	0.1773
77.0000	76.0000	77.0000	0.1260	0.0453
78.0000	64.0000	78.0000	0.5590	0.3687
79.0000	78.0000	79.0000	0.1860	0.1227
80.0000	79.0000	80.0000	0.1860	0.1227

Continued on next page

Table A.5 – *Continued from previous page*

Branch Number	Sending end bus number	Receiving end bus number	Resistance	Reactance
81.0000	80.0000	81.0000	0.2600	0.1390
82.0000	81.0000	82.0000	0.1540	0.1480
83.0000	82.0000	83.0000	0.2300	0.1280
84.0000	83.0000	84.0000	0.2520	0.1060
85.0000	84.0000	85.0000	0.1800	0.1480
86.0000	79.0000	86.0000	0.1600	0.1820
87.0000	86.0000	87.0000	0.2000	0.2300
88.0000	87.0000	88.0000	0.1600	0.3930
89.0000	65.0000	89.0000	0.6690	0.2412
90.0000	89.0000	90.0000	0.2660	0.1227
91.0000	90.0000	91.0000	0.2660	0.1227
92.0000	91.0000	92.0000	0.2660	0.1227
93.0000	92.0000	93.0000	0.2660	0.1227
94.0000	93.0000	94.0000	0.2330	0.1150
95.0000	94.0000	95.0000	0.4960	0.1380
96.0000	91.0000	96.0000	0.1960	0.1800
97.0000	96.0000	97.0000	0.1960	0.1800
98.0000	97.0000	98.0000	0.1866	0.1220
99.0000	98.0000	99.0000	0.0746	0.3180
100.0000	1	100.0000	0.0625	0.0265
101.0000	100.0000	101.0000	0.1501	0.2340
102.0000	101.0000	102.0000	0.1347	0.0888
103.0000	102.0000	103.0000	0.2307	0.1203
104.0000	103.0000	104.0000	0.4470	0.1608
105.0000	104.0000	105.0000	0.1632	0.0588
106.0000	105.0000	106.0000	0.3300	0.0990
107.0000	106.0000	107.0000	0.1560	0.0561

Continued on next page

Table A.5 – *Continued from previous page*

Branch Number	Sending end bus number	Receiving end bus number	Resistance	Reactance
108.0000	107.0000	108.0000	0.3819	0.1374
109.0000	108.0000	109.0000	0.1626	0.0585
110.0000	109.0000	110.0000	0.3819	0.1374
111.0000	110.0000	111.0000	0.2445	0.0879
112.0000	110.0000	112.0000	0.2088	0.0753
113.0000	112.0000	113.0000	0.2301	0.0828
114.0000	100.0000	114.0000	0.6102	0.2196
115.0000	114.0000	115.0000	0.1866	0.1270
116.0000	115.0000	116.0000	0.3732	0.2460
117.0000	116.0000	117.0000	0.4050	0.3670
118.0000	117.0000	118.0000	0.4890	0.4380
119.0000	8.0000	24.0000	0.4272	0.1539
120.0000	9.0000	40.0000	0.5300	0.3348
121.0000	17.0000	27.0000	0.5258	0.2916
122.0000	25.0000	35.0000	0.5000	0.5000
123.0000	37.0000	62.0000	0.5700	0.5720
124.0000	46.0000	27.0000	0.5258	0.2925
125.0000	54.0000	43.0000	0.4800	0.1728
126.0000	58.0000	91.0000	0.3957	0.1425
127.0000	62.0000	54.0000	0.3600	0.1296
128.0000	73.0000	91.0000	0.6800	0.6480
129.0000	88.0000	75.0000	0.4062	0.1464
130.0000	99.0000	77.0000	0.4626	0.1674
131.0000	108.0000	83.0000	0.6510	0.2340
132.0000	105.0000	86.0000	0.8125	0.2925
133.0000	110.0000	118.0000	0.7089	0.2553

Table A.6: Bus data for 12.666 kV, 69-bus distribution system

Bus Number	P (kW)	Q(kVAR)	Bus Number	P (kW)	Q(kVAR)
1	0	0	27	16.03	24.62
2	0	0	28	26.03	24.62
3	133.84	101.14	29	594.56	522.62
4	16.214	11.292	30	120.62	59.117
5	34.315	21.845	31	102.38	99.554
6	73.016	63.602	32	513.4	318.5
7	144.2	68.604	33	475.25	456.14
8	104.47	61.725	34	151.43	136.79
9	28.547	11.503	35	205.38	83.302
10	87.56	51.073	36	131.6	93.082
11	198.2	106.77	37	448.4	369.79
12	146.8	75.995	38	440.52	321.64
13	26.04	18.687	39	112.54	55.134
14	52.1	23.22	40	53.963	38.998
15	141.9	117.5	41	393.05	342.6
16	21.87	28.79	42	326.74	278.56
17	33.37	26.45	43	536.26	240.24
18	32.43	25.23	44	76.247	66.562
19	20.234	11.906	45	53.52	39.76
20	156.94	78.523	46	40.328	31.964
21	546.29	351.4	47	39.653	20.758
22	180.31	164.2	48	66.195	42.361
23	93.167	54.594	49	73.904	51.653
24	85.18	39.65	50	114.77	57.965
25	168.1	95.178	51	918.37	1205.1
26	125.11	150.22	52	210.3	146.66

Continued on next page

Table A.6 – *Continued from previous page*

Bus Number	P (kW)	Q(kVAR)	Bus Number	P (kW)	Q(kVAR)
53	66.68	56.608	79	238.15	223.22
54	42.207	40.184	80	294.55	162.47
55	433.74	283.41	81	485.57	437.92
56	62.1	26.86	82	243.53	183.03
57	92.46	88.38	83	243.53	183.03
58	85.188	55.436	84	134.25	119.29
59	345.3	332.4	85	22.71	27.96
60	22.5	16.83	86	49.513	26.515
61	80.551	49.156	87	383.78	257.16
62	95.86	90.758	88	49.64	20.6
63	62.92	47.7	89	22.473	11.806
64	478.8	463.74	90	62.93	42.96
65	120.94	52.006	91	30.67	34.93
66	139.11	100.34	92	62.53	66.79
67	391.78	193.5	93	114.57	81.748
68	27.741	26.713	94	81.292	66.526
69	52.814	25.257	95	31.733	15.96
70	66.89	38.713	96	33.32	60.48
71	467.5	395.14	97	531.28	224.85
72	594.85	239.74	98	507.03	367.42
73	132.5	84.363	99	26.39	11.7
74	52.699	22.482	100	45.99	30.392
75	869.79	614.775	101	100.66	47.572
76	31.349	29.817	102	456.48	350.3
77	192.39	122.43	103	522.56	449.29
78	65.75	45.37	104	408.43	168.46
105	141.48	134.25	113	305.08	215.37

Continued on next page

Table A.6 – *Continued from previous page*

Bus Number	**P (kW)**	**Q(kVAR)**	**Bus Number**	**P (kW)**	**Q(kVAR)**
106	104.43	66.024	114	54.38	40.97
107	96.793	83.647	115	211.14	192.9
108	493.92	419.34	116	67.009	53.336
109	225.38	135.88	117	162.07	90.321
110	509.21	387.21	118	48.785	29.156
111	188.5	173.46	119	33.9	18.98
112	918.03	898.55			

Appendix B

Generator data

SHPP-DGs's parameters are presented in Tables B.1, Tables B.2 and Tables B.3. Data for SHPP-DGs are obtained from [71], [98], [99], [100]. All values are given in pu on base of machine rating.

33 bus system:

Table B.1

parameters	SHPP-DG1	SHPP-DG2	SHPP-DG3
X_{di}	2.656	2.656	1.85
X'_{di}	0.136	0.136	0.277
R_{si}	0.088	0.088	0.088
T'_{doi}	3.7	3.7	3.7
X_{qi}	2.52	2.52	1.11
H	1.5	1.5	1.5
T_{Ai}	0.2	0.20	0.2
K_{Ai}	50	50	50

69 bus system:

Table B.2

parameters	SHPP-DG1	SHPP-DG2	SHPP-DG3
X_{di}	2.656	2.656	1.85
X'_{di}	0.136	0.136	0.277
R_{si}	0.088	0.088	0.088
T'_{doi}	3.7	3.7	3.7
X_{qi}	2.52	2.52	1.11
H	1.5	1.5	1.5
T_{Ai}	0.2	0.20	0.2
K_{Ai}	50	50	50

for 119 bus system:

Table B.3

parameters	SHPP-DG1	SHPP-DG2	SHPP-DG3	SHPP-DG4
X_{di}	1.4	1.4	1.192	1.85
X'_{di}	0.236	0.236	0.185	0.277
R_{si}	0.088	0.088	0.088	0.088
T'_{doi}	3.7	3.7	3.7	3.7
X_{qi}	1.37	1.37	1.16	1.11
H	3.15	2.21	1.57	1.5
T_{Ai}	0.20	0.2	0.20	0.2
K_{Ai}	40	40	40	40

For 33-bus and 69-bus system: DFIG parameters [95]

$P = 250kW$, $L_m = 2.18p.u.$, $L_{ss} = 2.20p.u.$, $L_{rr} = 2.216p.u.$, $R_s = 0.0053pu$, $R_r = 0.0053$, $H = 4s$

control parameter: $k_{p1} = k_{p2} = k_{p3} = k_{p4} = .01, k_{l1} = k_{l2} = k_{l3} = k_{l4} = 10$

For 119-bus system: DFIG parameters [96]

$P = 660kW$, $L_m = 2.1p.u.$, $L_{ss} = 2.13p.u.$, $L_{rr} = 2.135p.u.$, $R_s = 0.007pu$, $R_r = 0.007$, $H = 4s$

control parameter: $k_{p1} = k_{p2} = k_{p3} = k_{p4} = .01, k_{l1} = k_{l2} = k_{l3} = k_{l4} = 10$

For all three systems, PV-DG parameters are taken from [58] and [52].

S_{ref}=1000 w/m^2; $I_o = 1.175e^{-8}A$;$I_o = 1.175e^{-8}$,$I_{phref} = 5.96A$, $T = 298K$, $T_{ref} = 298K$, $\rho = 0.00023$; $n = 2.15$ L_{dc}=1.5 p.u.; C_{dc}=1 p.u. ;V_{dc0}=1 p.u.;K_{dc}=0.3;K_{ac}=0.3; K_{pv}=5; K_{dci}=0.5;K_{aci}=0.5;K_{pvi}=10;